A New Approach for Compaction of HVDC Transmission Lines and the Assessment of the Electrical Aspects

By

Maryam Salimi

A thesis submitted to the Faculty of Graduate Studies
in partial fulfillment of the requirements for the degree of
Doctor of Philosophy

Department of Electrical and Computer Engineering
Faculty of Graduate Studies
University of Manitoba
Winnipeg, Manitoba

February 2017

Abstract

This thesis proposes a novel consolidated approach for substantial compaction of HVDC lines that includes both new tower geometries as well as novel control concepts. This is based on a thorough discussion on the basic overhead line design parameters and their impact on the right of way width and tower height. Then the electrical aspects of the new approach such as dc overvoltage assessment and lightning performance are investigated.

The required horizontal clearances between pole conductors and tower members, as a component of the right of way width, depend on the maximum expected overvoltages. Detailed electromagnetic transient models for the point to point MMC HVDC with different transmission configurations, all including the proposed dc overhead line, are developed for this thesis. The models are used to assess fault contingencies that result in the most significant overvoltage stresses on the HVDC transmission line for finding minimum air clearances and for the design of overvoltage limiting devices, such as surge arresters. New control approaches are proposed that significantly reduce the dc side overvoltage and consequently minimize the required air clearances for maximum compaction of the HVDC overhead lines and also reduce the required surge arrester size for line insulation.

Because power transmission lines are the most exposed component within a power system, they are subject to lightning strikes which, in turn, are the main cause of disruption to power flows. This thesis will include an analysis of lightning occurrence on the proposed compact transmission line in order to assess the risk of pole faults. The focus of this analysis is mainly on evaluation of the critical lightning currents that cause fast front overvoltage stresses that may result in insulation failure.

Acknowledgments

I heard the first 'YES' from Dr. Gole and Dennis Woodford about three years ago when I had got used to hearing 'NO' from anywhere. Actually I just won a PhD lottery to be their student and really enjoyed this experience with two very smart, kind and fun supervisors.

I appreciate the generous financial support and the warm and friendly environment of the Electranix Corporation. I am also very grateful to have all these kind collogues there. Special thanks to Francisco Gomez, Xiuyu Chen, Garth Irwin and Jeremy Sneath for their technical support.

I would like to thank Lionel Barthold from iMod and David Swatek and Zibby Kieloch from Manitoba Hydro for their enthusiastic guidance throughout this research. I also would like to thank my committee members, Dr. Swatek, and Dr. Anderson for their valuable time and feedbacks. I am truly honored that this thesis was also reviewed by Dr. Nigel Shore who is one of the world most competent experts in the HVDC transmission industry.

Now I just want to write to all who I deeply love. This was not a normal four years in my life, but all these people helped me to stand up again and live life fully and wholeheartedly. Dennis and Janet, my second parents! The only thing that I can say about you two is that if I can ever make such an impact in someone's life, the way that you made in mine, I truly achieved my mission in life. Thank you for making me feel like home here.

-To all who stayed in my heart-

Contents

5. **Slow Front Overvoltage Analysis of MMC HVDC Systems under Fault Condition**

List of Tables

List of Figures

List of Abbreviations

ac	alternating current
dc	direct current
FDMM	Frequency Dependent Mode Model
FDPM	Frequency Dependent Phase Model
HTLS	High-Temperature, Low Sag
HVDC	High Voltage Direct Current
LCC	Line Commuted Converters
MMC	Modular Multi-level Converter
OHL	Overhead Line
ROW	Right of Way
SM	Sub-Module
VSC	Voltage Sourced Converter
XLPE	Cross Linked Polyethylene

List of Appendices

Chapter 1

Introduction

1.1   History of Electricity Transmission System

Early in the development of electric power, the importance of economies of scale in power generation was recognized by its proponents and developers. They realized that larger centralized generation facilities could provide power at much lower cost to a broader customer base [1]. The first electric generators supplied direct current which was distributed to loads by dc distribution lines. However despite the initial dominance of dc and a chaotic search for industry structure at that time, the debate was ended by introduction of the ac magnetic transformer, a device that could assign different voltage levels for transmission, distribution and consumption of electric power [2].

Efficient transformation of energy between ac voltage levels led to an energy generation and transmission pattern that lasted more than sixty years. That period was characterized by vertically-integrated supply companies, steady increases in generator size from 5 megawatts (MW) to a thousand megawatts, plants sited near fuel and/or cooling water and

progressively higher ac transmission voltages, ultimately reaching 765 kV in North America. The primary challenge in system expansion was finding suitable locations for power plants - the problem of the power transmission being of secondary importance. With the help of eminent domain laws, transmission lines could be built almost anywhere [3].

The interconnection of generating stations that started in the early years of the industry continued as capacity grew, eventually evolving into a sophisticated electricity transmission grid which, at that time, was not intended for long-term transfer of large amounts of power between different regions or utilities [4]. Utilities expanded their own generating capacity to achieve self-sufficiency – even for supply of peak electrical demands. Imports from or exports to other utilities through interconnections were short-term solutions to maintain reliability during outages or other unexpected conditions. The use of interties for long-term inter-utility power transfers started to grow in the 1970s because of regional imbalances in generating capacity and power demand. The growing economic incentive for non-utility generation of power also promoted the need for increased transfer capability. As a result, the transmission infrastructure began to expand and transmission line loading increased [4].

As transmission voltage levels increased, transmission loading increased accordingly. However, in addition to the thermal transmission limit, i.e., maximum current, long ac lines transmission capacity is also limited by transient stability and reliability considerations [4]. The role of dc in transmission again began in the 1950s using the technology developed extensively in the 1930s in Sweden and Germany [5]. Early commercial installations included a modest commercial link between Moscow and Kashira in the Soviet Union in 1951 [6], and a 100 kV, 20 MW system between Gotland and mainland Sweden in 1954

[5] both using mercury arc technology. Later on, dc was recognized as being well adapted for bulk transfer of power over long distances [7]. The longest HVDC link in the world is the 2,350 km Rio Madeira link in Brazil, consisting of two bipoles of ±600 kV, 3150 MW each and connecting Porto Velho in the state of Rondônia to the São Paulo area [8].

Since its first commercial application in the 1950s, HVDC transmission has matured, continuing technological innovations that have made HVDC both more efficient and more cost-effective [9], [10], [11]. Those advances have served to expand the range of HVDC applications and made it more suitable to overcome some limitations in the expansion of ac networks [12]. Specifically:

- HVDC provides higher power transmission capacity in a narrower right-of-way while also reducing costs by carrying more power for the same conductor size.

- HVDC has lower losses per MW than does HVAC of similar length and rating, that advantage, taken together with the above point made it an ideal solution for long-haul, bulk power transmission both from environmental and industrial points of view.

- HVDC has strong economic and functional advantages for underwater and underground cable transmission. The high capacitance of ac cables requires considerable charging current which, in turn, increases losses and demands sources of reactive power supply. Therefore, ac cables are mostly used for a limited length.

- HVDC is capable of interconnecting to ac systems asynchronously.

1.2   The Expanding Role of HVDC Transmission and the Vision of a Future DC Grid

Growth in power demand and in the types and location of power generation has produced changes in load flow patterns that are now difficult to accommodate, especially in mature networks such as those in Europe and North America. This shift in generation pattern, in significant measure to wind and solar sources, has been caused mainly by the search for sources of safe and clean energy to reduce carbon emission by displacing coal-fired generators, and even in some cases nuclear power plants. This shift to sources of renewable energy has now intensified in many nations. Widespread interest in feeding large amounts of renewable energy into the ac transmission grid, principally from wind and solar generation, revealed serious shortcomings in the existing transmission infrastructure. In Europe the major wind resources are in North West locations remote from the major load centers. The existing grid infrastructure in areas is relatively weak and unable to carry the power potential offered by local wind power plants. A similar situation exists in the South of Europe and North Africa which offer the potential for extremely large amounts of solar power generation, but no transmission system to deliver that power to the market. In the USA and Canada there is abundant wind power generation capability in the Mid-West and solar power in the Southwest, but again at sites remote from the major load centers [13], [14], [15], [16], [17], [18].

The need to increase the flexibility and reliability of transmission infrastructure so as to share resources and carry power to market at a lower cost is now very obvious. However the starting point for this effort is a large and complex system that has suffered some major

and widespread blackouts in the recent two decades (e.g. North America 2003, the North-east and Italy blackouts in 2003 and India 2012 [19]). These rare but significant events increase concerns for the stable and secure operation of power systems which will be still further stretched by accommodating remote renewable resources. The main challenges for secure operation of future power systems include complex modes of instability (angle, voltage and frequency), vulnerability to propagation of disturbances across ac grids and vulnerability to sabotage strategies (cyber-terrorism) [20].

Grid operators and transmission owners, faced with future demands on transmission infra-structure, are now well aware of the benefits that HVDC can offer [12], [17]. HVDC is not only a cost-effective solution for moving remotely located renewable energies to the load centers but also provides a higher level of controllability than is currently possible with ac technology [21]. This precise ability to control power can prevent the overall system from entering an unsafe operating condition, and therefore also offers a significant reliability benefit for the new power grid. Because both the amount and direction of power flows can be controlled, operators can address issues such as thermal overloads and voltage control to help maintain the stability of the ac system [21]. An overlaying HVDC transmission system ("Supergrid") will help the development of a new smart grid to enhance reliability and resilience against both natural and man-made threats [22], [23].

1.3   Problem Definition and the Thesis Motivation

Until now HVDC has been used primarily for point to point transmission between just two terminals although a few three terminal systems have been built and successfully operated [24], [25]. HVDC transmission lines with a few intermediate terminals can now be realized

for both Line Commutated Converter (LCC) and Voltage Sourced Converter (VSC) HVDC transmission technologies. VSC HVDC transmission (or Modular Multi-level Converter (MMC) HVDC as a modern form of it) is well suited to dc grids and their interconnection with weak ac systems, since it has black start capability, the ability to control active and reactive power independently, and can change direction of power without change of voltage polarity as is required for thyristor-based LCC HVDC technology [26], [27].

While the need for HVDC links within or overlaying existing ac systems becomes more widely recognized, a significant amount of research has been carried out to make a new dc transmission grid feasible [28]. Power flow control, fast protection, practical dc breakers, and power electronic based dc transformers are prominent in these researches [29], [30], [31], [32], [33]. However there remain many challenges with HVDC grid implementation including methods for building new converter stations and transmission lines in populated commercial or residential areas [34].

Almost all existing overhead HVDC lines use LCC technology while MMC HVDC has a lack of experience with overhead lines to this date [35]. Moreover, underground cables cost four to fifteen times more than an overhead line depending on the voltage level and the line route [36]. This is due to time, materials, process and other issues such as going under a road, highway, or river and also avoiding other underground installations such as water, gas, and sewer lines [36], [37]. Virtually all overhead transmission lines have been located on the rights-of-ways for which ownership or easements have been acquired by the transmission owner. Approval of new dc transmission rights-of-way has become increasingly difficult and must now consider and minimize such environmental issues as [4], [38]:

- Potential ground-level annoyance due to electric and magnetic fields

- Aggravation of those fields by the flow of corona-generation ions from overhead conductors through the air to the ground or to grounded objects including people

- Corona based power losses (CL)

- Corona based interference to radio signals (RI)

- Audible noise resulting from corona discharge (AN)

- Allocation of land to transmission line and substation facilities;

- Visual impacts.

New rights-of-way now require what is considered a "social license" [39]. Public opposition and the high cost and long delays of land acquisition, coupled with very high developing cost makes the acquisition of such a license very challenging and in some jurisdiction impossible to obtain. Thus power system planners the world over, especially in Europe, face the dilemma of how to expand networks to meet increasing power transfer needs in the face of strong public opposition to new lines [40].

The vast majority of existing transmission towers are of the lattice type – a design concept that has changed little over the past hundred years. This is significant since opposition to additional power transmission lines across the globe seems to relate much more to appearance than to function. Thus, rightly or wrongly, it is now firmly established that the conventional lattice tower has become a symbol of the blemish that overhead lines are presumed to impose on natural landscapes. That suggests that alternative, more aesthetically pleasing structures will significantly increase the chances of public acceptance – a conclusion verified by experience in many cases [40]. Irrespective of tower design, reducing the height and width of transmission corridor requirements for a prospective new line of a given voltage and conductor array both improves the prospect of public acceptance and

increases the likelihood that new circuits can share rights-of-way with transportation cor-
ridors. It is therefore appropriate to undertake studies leading to greater compaction of dc
lines, seeking ways to reduce their visual and environmental impact, making regulatory
approval easier, and to allow their construction on narrower rights of way – possibly shared
with public transport routes.

1.4   Research Objectives

Recognizing that compaction of the dc overhead lines facilitates construction of new trans-
mission lines both by gaining public acceptance through use of aesthetic pylons [40], [41]
and by allowing their construction on narrower a rights-of-way (ROW), the aim of this
thesis is to first propose a new approach that results in greater compaction of HVDC lines
and then to investigate the electrical aspects of that approach to assess its effectiveness and
its limitations.

 "Compaction", as considered in this thesis, refers to reductions in tower height and re-
quired ROW width. The variables effecting HVDC tower height and ROW width are com-
plex and interdependent [42]. ROW width is driven mainly by pole-to-pole spacing, con-
ductor out-swing and lateral safety clearances.

It will be shown that conductor sag is the principal factor affecting tower height for a given
voltage and minimum ground clearance and therefore also the major factor in conductor
blow-out, which is the magnitude of the horizontal displacement of a conductor, at high
winds and the corresponding ROW width requirement. Principal recourses for reducing
sag are (1) shortening spans and/or (2) high-temperature, low sag (HTLS) conductors
which reduce sag for a given thermal loading [42]. The influence of conductor blow-out,

due to wind forces, on right-of-way width can also be minimized by using conductors with compact stranding and/or conductor bundling that minimizes wind force. The new dc transmission line structure should have a low profile design that focuses on shortening spans to the point where decreases in tower height, conductor out-swing, wind and weight loading of structures and footings significantly diminish cross section requirements. Modern pre-manufactured towers are considered for the studies since they have a number of advantages in compaction including slimmer appearance, lower installation cost, and somewhat lower profile for a given conductor suspension point while maintaining the required ground clearance at mid-span [43].

Unique to ground clearance limits for HVDC is the prospect of annoyance from ground-level field effects; specifically ground-level electric fields and the density of ions flowing to ground below and in proximity to conductors. Criteria suggested for ground-level electric fields and the ion current density, based on annoyance histories, are cited [38], [44]. In minimizing conductor spacing and height, compacting HVDC lines requires a much more careful assessment of acceptable field and corona and ground field effects than for conventional construction. Therefore, the main factors that have a significant impact on the field effect of transmission line, which are the conductor diameter and minimum conductor height above the ground, are assumed to be the same for the proposed design as a conventional design of which Bipole III in Manitoba is a typical example.

Tower top geometry, which determines insulator configuration as well as pole-to-pole spacing, is a particularly important aspect of compaction. Tower top geometry is governed in large measure by clearance requirements and the number, type and configuration of in-

sulators used [45]. In this study, first the insulation options for achieving maximum com-
paction, such as V-string insulators and insulated cross-arms, will be documented and eval-
uated. Horizontal clearances between pole conductors and tower members or, where there
is no intervening structure, between pole conductors themselves, depend on the maximum
expected overvoltages. The latter results from lightning strokes, switching operations or
pole-to-ground faults. For air clearances, switching or pole-to-ground fault overvoltages
are usually the limiting criterion.

Most HVDC projects use either symmetrical monopoles or grounded bipole configurations
– now combined with voltage source conversion terminal architecture [10], [46]. LCC
HVDC is a mature technology and all dc overvoltages associated with it are well known
[47]. However there is no corresponding experience base for the modern Modular Multi-
level Converters (MMC) HVDC used in overhead line dc transmission. MMC HVDC with
full-bridge and half-bridge modules offers significant benefits over older VSC technologies
[48]. The use of surge arresters together with the proper design of controllers for MMCs,
especially with full-bridge converters, can reduce the overvoltage levels and thereby reduce
clearance requirements and facilitate compaction.

 To demonstrate that advantage in specific cases, first the detailed electromagnetic transient
models of the MMC HVDC systems are required. PSCAD/EMTDC, a powerful electro-
magnetic transient simulation tool, is the recommended tool for performing a comprehen-
sive overvoltage assessment of the MMC HVDC transmission line [29]. In conjunction
with those studies, novel control methods that can reduce the dc side overvoltages will be
proposed.

Because power transmission lines are the most exposed component within a power system from a geographical point of view, they are subject to lightning strokes which, in turn, are the main cause of disruption to power flows [4]. On one hand, lightning performance is not of primary importance in the economics of line design compared to factors such as line length, ROW costs, construction costs, material costs and losses. On the other hand, the reliability of transmission lines and substations is also of critical importance to the utility and its customers. Therefore, the designer should always balance the costs of higher insulation levels, improved grounding, better shielding, or line relocation against the benefits of improved reliability [49]. To minimize vulnerability to lightning strokes, HVDC lines generally include one or two shield wires in the right location to avoid direct strokes to the conductors. However strokes that hit the shield wire will induce an overvoltage on the pole conductors and transmission tower that may or may not be sufficient to cause a pole-to-ground flashover [50].

This thesis will include an analysis of lightning occurrence on transmission lines in order to assess the risk of pole faults. The focus of this analysis is mainly on evaluation of the critical lightning currents that may cause insulation failure and the fast front overvoltage stresses. The study results for the proposed compact design and also a typical dc line will be presented.

1.5   Thesis Outline

This chapter started with an overview of the HVDC history and the benefits of a future overlaying HVDC grid, and then explained the motivation of this research.

Chapter 2 provides a background of existing technologies germane to the main components of the HVDC transmission system, including the converter stations, underground/undersea cables and overhead transmission lines.

In Chapter 3, the overall HVDC transmission line design parameters are considered, with a focus mainly on the variables that impact the compaction of the dc lines. Then the proposed compact structure will be introduced, the main electrical aspects of it being analyzed in the following chapters.

As a prerequisite step for dc fault overvoltage evaluations, details associated with the HVDC system modeling, including both components and controller systems for the steady state operation of the system, are provided in Chapter 4.

Chapter 5 first shows results considering all the fault contingencies and associated overvoltages on a MMC HVDC system with both symmetrical monopole and bipole transmission configurations. It also considers the dc systems that have purely overhead lines as well as the systems that have both overhead lines and underground cables in the same circuit. The worst case scenario will be determined for the insulation coordination of the dc line. In this chapter novel controlling schemes will be also proposed that, together with surge arrestor, result in significant dc overvoltage reduction and consequently minimize insulator length and air clearances for maximum compaction.

Once the design is finalized and the feasibility studies have been carried out, Chapter 6 presents the lightning performance analysis of the proposed compact design as well as a conventional design for comparison. This chapter also evaluates the fast front lightning overvoltage stresses on the dc line.

Chapter 7 presents the concluding remarks of this thesis and suggestions for the future works that can enhance this research.

Chapter 2

Overview of HVDC Converters, Cables and Overhead Transmission Lines

Since the objective of this thesis is to propose a compact dc overhead line and investigate its electrical aspects, it is important first to understand the basic concepts and essential components in HVDC transmission technology, including those pertaining to dc overhead lines now in operation. The fundamental process in any HVDC transmission system, as demonstrated in Figure 2-1, is the conversion of electrical power from ac to dc at the transmitting end (rectifier station), and from dc back to ac (inverter station) at the receiving end. The major components of an HVDC system are: the converter station at each end, the electrodes or earth return path and the transmission line itself [51]. The following sections present an overview of each component, and the options available for these components according to the current technology.
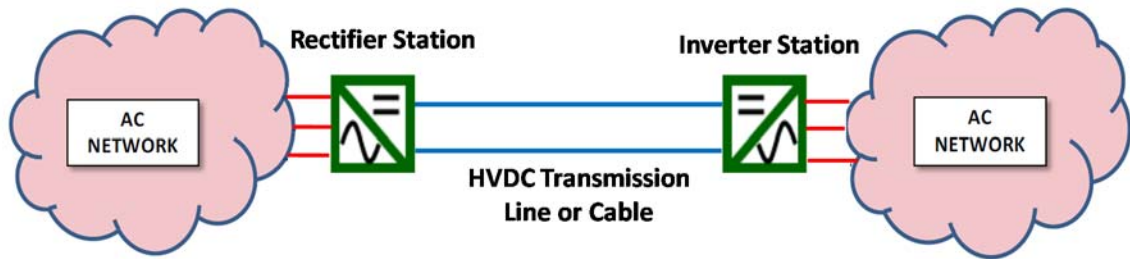
Figure 2-1 A General Diagram of HVDC Transmission

2.1   The Converter Station

The converter stations at each end usually have the same structure. Each consists of all the required equipment for ac to dc conversion or vice versa since their roles must often be interchangeable. The main components of a converter station are [51]:

- Converter valves

- Transformer

- Ac filters and capacitor banks

- Dc filter

2.1.1   Converter Technologies

HVDC transmission is generally classified according to the HVDC converter technologies used. Conversion from ac to dc and vice versa is achieved by means of semiconductor switches. Three converter technologies have been used in all HVDC transmission system to date; each based on the capabilities and switching functions of the switches used [10]. These converter technologies are:

1. Line Commutated Converters (LCC)

   Line commutated converters, also referred to as "conventional" or "classic" HVDC, are the most common converter technology in the HVDC systems as of today (as of 2016) [52], [35]. As shown in Figure 2-2, thyristor valves, built up by a group of thyristor switches in series, are the main elements of these converters and can carry very high currents (4 kA) and operate up to 800kV [10] with 1,100 kV under construction. An LCC converter is modular in design; each "module" consisting of a six pulse bridge. Two six pulse bridges are connected in series to create a twelve pulse bridge. In a twelve pulse bridge, a 30˚ phase shift between each six pulse bridge is achieved by using a star/star connected converter transformer for one six pulse bridge and a star/delta connected converter transformer for the other six pulse bridge. Using six pulse bridges, each with a 30˚ phase shift, helps reducing ac harmonic currents [53].

   Thyristors are half-controllable semiconductors that have only turn-on controllability. LCC technology requires a synchronous ac voltage source in order to operate and the ac network's short circuit capacity has to be relatively strong compared to the dc power transfer [53]. As the thyristor valve is operated at net frequency (50 Hz or 60 Hz), it is possible to change the dc voltage level of the bridge by means of a firing control angle. This ability allows the transmitted power to be controlled rapidly and efficiently [53].
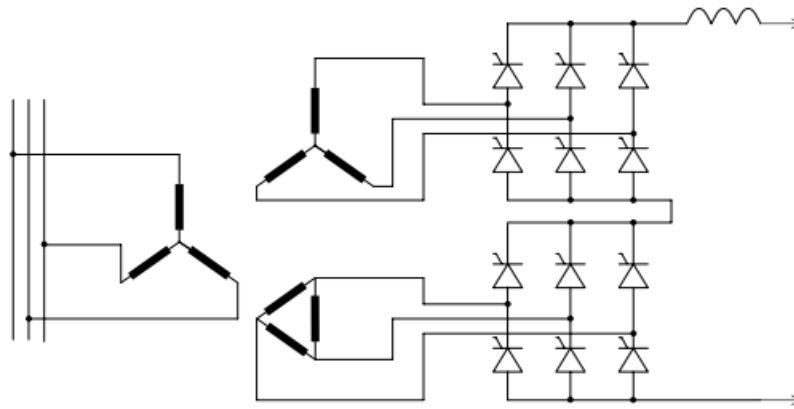
Figure 2-2 A twelve pulse LCC Configuration

2. Capacitor Commutated Converters (CCC)

Capacitive commutated converters are a variation of the LCC and use the same thyristor configuration. However, additional commutation capacitors are inserted in series between the converter transformers and the thyristor valves in order to improve the thyristor-based commutation performance of the converters when connected to weak ac networks [54].

The series capacitors develop a voltage which aids in the commutation process. The converter is capable of operating at close to unity power factor, and even slightly leading power factors. It is also far more immune against commutation failures compared to the traditional LCC. This technology is limited by the additional dc voltage stress it places on the valves. Because of that additional stress, CCC technology has to date been used only for back to back HVDC schemes, where the dc voltages are much lower than for point to point HVDC transmission [55].

3. Voltage Sourced Converters (VSC):

VSC technology converts an ac voltage to dc voltage by means of IGBT (Insulated Gate Bipolar Transistors) or the GTO (Gate Turn-Off Thyristor) switches which are fully controllable over the turn-on and turn-off status of the switch. This switch off capability enables the VSC converters to operate without the need for a synchronous voltage for commutation as in the LCC converters [46].

VSC HVDC transmission systems are expanding and improving rapidly. Initially VSC valves were built just of series connected IGBT switches with a common capacitive dc link, and based on the different structures, were categorized as two level [56] (Figure 2-3 (a)), three level [56] (Figure 2-3 (b)) and multi-level topologies [57]. Because VSCs can commutate at high frequency, independent of the network frequency, converter switching operations can be achieved by a Pulse Width Modulation (PWM) technique [58] that makes it possible to create the voltage waveform of the desired fundamental frequency component with any angle and/or magnitude (within a certain limit) almost instantly. Thus, it allows control of both active and reactive power independently [59]. However, high switching frequency and consequently high losses were the main disadvantages of PWM based converters [46].

A more recent topology, Modular Multilevel Converters (MMC) offers significant benefits over the previous VSC technologies [10]. The MMC is able to generate a large number of voltage levels by connecting a number of identical power electronic building blocks, called full-bridge/half-bridge sub-modules, in series [48]. Instead of using a common capacitive dc link as with PWM-based converters, each sub-module comprising the MMC has a physically smaller capacitor which can be

bypassed or inserted directly or with reverse polarity in case of a full-bridge con-

figuration. Figure 2-4 illustrates the MMC topology. Its modular structure allows

adding modules and thus introducing redundancy and higher reliability for the en-

tire system.
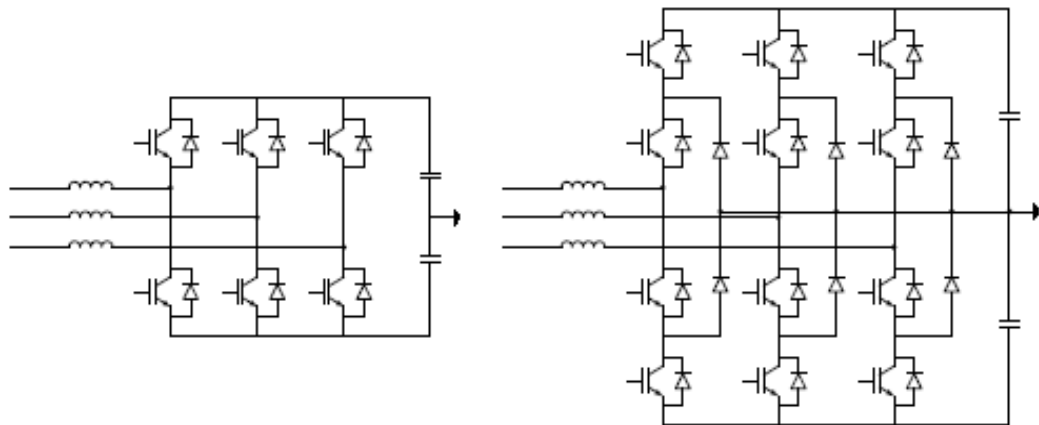
Figure 2-3 (a) Two-Level and (b) Three-Level topologies of voltage sourced converters
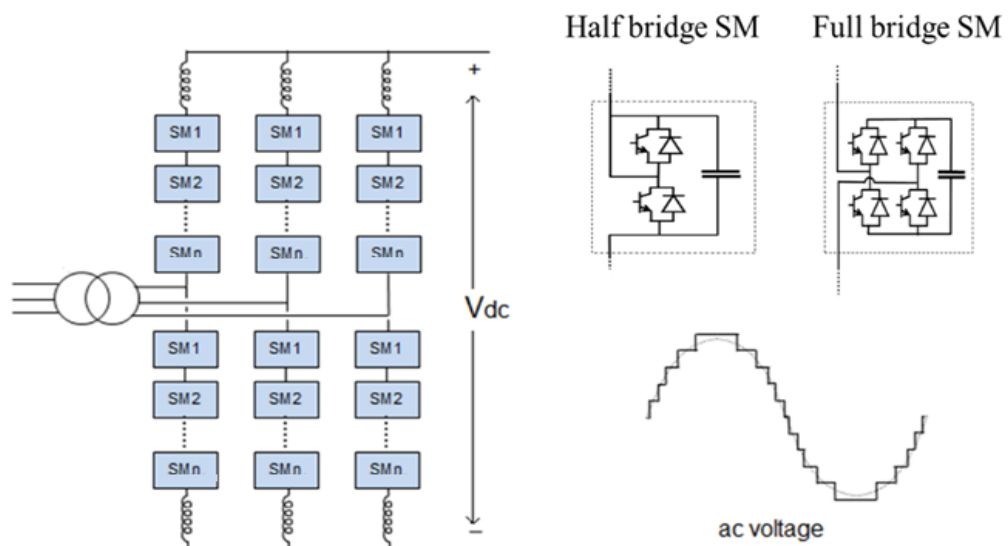
Figure 2-4 Modular Multi-level voltage sourced converter

MMC HVDC technology is particularly suitable for renewable energy integration and the HVDC grids development due to its higher controllability and its ability to be connected to weak ac systems [10]. The operation and control methods of MMC HVDC will be explained in detail in Chapter 4.

2.1.2   Transformer

In all HVDC systems the transformer connecting the converter station to the ac system adapts the existing ac voltage level to the required dc voltage level. In LCC converter technology, they are called "converter transformers" and are characterized by a higher leakage reactance than conventional ac transformers [53]. This leakage reactance is necessary to buffer the transformer from the shock of the line to line short circuit that happens 6 times a cycle (for 6 pulse converters) during the commutation process. Although the basic operating principles are the same as a normal ac transformer, converter transformers are subjected to additional stresses, including ac and dc voltage stresses. DC pre-magnetization of the transformer core requires additional core steel to prevent magnetic saturation and high harmonic currents, the latter resulting in additional losses and consequently heating the transformer [53].

To differentiate the VSC transformers from LCC converter transformers, the term "interface transformer" is often used with VSC systems. Although VSC interface transformers are also subjected to a higher level of harmonic currents than normal ac transformers, the harmonic level is significantly lower than for LCC converter transformers, particularly for MMC type topologies. For symmetrical VSC designs, explained later in this chapter, the interface transformers see no dc voltage stress, thus resulting in a transformer design very

similar to a normal ac transformer. However transformers used in bipole or asymmetrical configurations will be subjected to a dc offset and stress on the valve side ac winding [46].

2.1.3   AC Filters and Capacitor Banks

Converter operation generates harmonic currents and voltages on the ac and dc sides. On the ac side of a twelve-pulse LCC HVDC converter, current harmonics of the order of 11, 13, 23, 25 and higher ($2n\pm1$, where n=12) are generated. Ac filters are installed to absorb those harmonic components and to reduce voltage distortion to levels below a certain threshold required by the network. Moreover, in the LCC conversion process the converter consumes reactive power equal to about 60% of the active power which is compensated partly by the filter banks and the rest by capacitor banks. To assure a satisfactory power factor on the ac side of an LCC HVDC converter over various load levels, ac filters and shunt capacitors are normally subdivided and switched by circuit breakers as the dc power varies. The ac filters and shunt capacitors for LCC converter stations require a significant amount of space due to the number and magnitude of the current harmonics produced by a LCC converter [53].

For the CCC configuration, the converter operates close to unity power factor and hence does not require significant VAR supply at the ac bus. The elimination of switched reactive power compensation equipment simplifies the ac switchyard and minimizes the number of circuit-breakers needed– thus also reducing the area required for a CCC HVDC station [54].

Likewise, there is no need to compensate for reactive power consumed using VSC schemes as there is with LCC schemes. VSC systems require much less filter equipment than is the

case with LCC configurations. The level and frequency of current harmonics on the ac side of any ac/dc converter system depend mainly to the converter topology; PWM VSC schemes produce high frequency harmonics of larger magnitudes than do MMC VSC schemes. The permissible voltage distortion and the harmonic impedance of the connected ac system may determine whether or not filtering is required. Filtering is generally not used with MMC VSC converters [10], [60]. Some MMC converters may generate very high frequency currents that can travel through the ac network interfering with signals that use the ac transmission lines for a communication path. High frequency filtering may be required in such cases.

2.1.4   DC Filters

Because harmonic currents flowing in a dc transmission line can adversely influence the equipment and telecommunication systems located in the vicinity of the transmission line, dc filters, along with dc smoothing reactors are used to mitigate the problem [61]. This problem is an issue principally with dc overhead lines or a combination of dc cable and dc overhead line. Harmonics in pure cable transmissions or the Back-to-Back schemes do not require dc filtering [61].

DC side filters are usually significantly smaller and less expensive than the filters on the ac side. Some dc filters are partially "active" in design and as such are very effective. In these filters the passive part is reduced to a minimum while modern power electronics also measure, invert and re-inject harmonics to smooth net harmonic currents in the line.

DC series reactors help smooth dc current while also providing harmonic voltage reduction on the dc line. These reactors also help limit crest current during short-circuit faults on the dc line [47].

2.2   Transmission Configurations

Existing HVDC schemes fall into two basic groups: back-to-back schemes and point-to-point transmission schemes [11]. In back-to-back schemes, the rectifier and inverter are located in the same station with no interconnecting transmission line. In point-to-point transmission schemes, converters at different geographical locations are interconnected by a dc transmission system. The two systems may have differing and incompatible electrical parameters, e.g. frequency, voltage level and short circuit power level. DC transmission was first mostly via underground/undersea cables, and later adapted for bulk power long transmission using overhead lines [9].   HVDC transmission systems can be configured in different ways to suit operational requirements. Symmetrical monopoles and Asymmetrical monopoles or bipoles, as shown in Figure 2-5, are the most popular configurations that have been successfully applied in many HVDC transmission systems throughout the world [10].

- Monopolar configurations connect single converter modules at the rectifier and inverter stations. Depending on the grounding system, the monopolar configuration can be either symmetrical or asymmetrical. Asymmetrical Monopolar HVDC uses a single high-voltage conductor, positive or negative, along with a return path via either earth/sea electrode or a metallic low-voltage conductor, explained more in the following section. In contrast a symmetrical monopolar HVDC requires a line

with both positive and negative high-voltage conductors. Symmetrical monopole configuration is well adapted to VSC-based HVDC applications. They are usually provided with a high resistance grounded on the dc side [10].

- Bipolar configurations connect two converter modules at each end using two high-voltage conductor lines while the middle point is either the earth, the sea or a metallic low-voltage conductor as a dedicated metallic return conductor. A bipolar system is essentially two asymmetrical monopoles having opposite polarity [10].
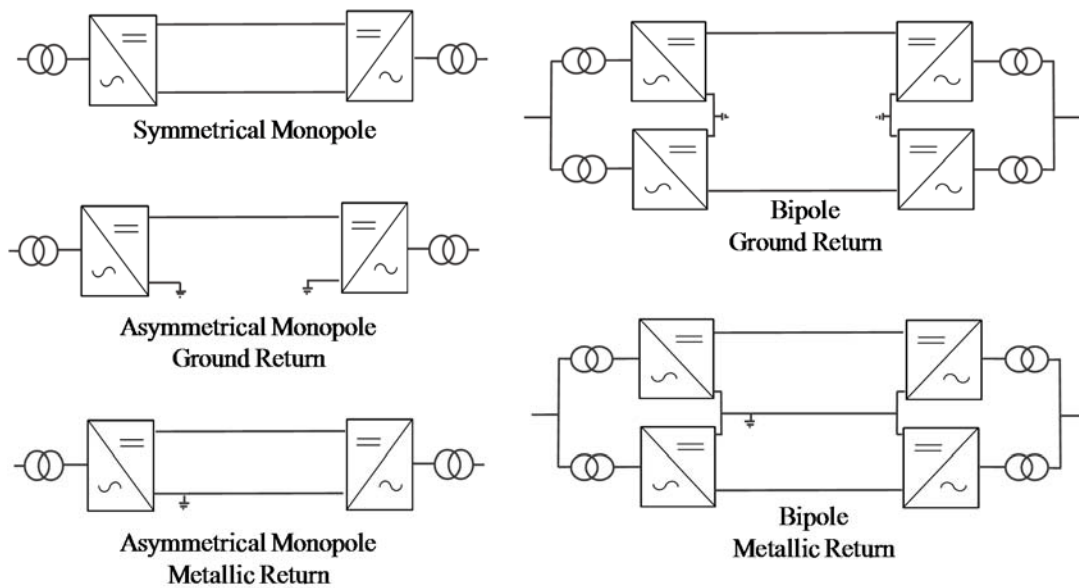
Figure 2-5 HVDC transmission configurations

Each configuration has its own advantages and disadvantages. For example, the symmetrical monopole using two conductors does not require firm earth connection as does a conventional bipole with three conductors, one of which is the metallic return [10]. It is also capable of operating at reduced power in case of a single line to ground fault, which is the most common type of fault. However the single symmetrical monopole has no redundancy. All power is lost with a permanent line or cable fault unless two independent monopoles

with a total of four conductors are used [62]. With bipole configuration, it is possible to avoid the unbalanced pole voltage and overvoltage problem of a symmetrical monopole configuration when there is one pole to ground fault. The main advantage is the high availability with redundant transmission system, e.g. the fault in one pole does not affect the operation of other pole [10].

The optimal transmission configuration for a given application depends on many factors. Consideration must be given to design criteria to be used as well as the cost and overall economic factors versus reliability and security factors for the project [47].

2.2.1   System Grounding

Unlike the grounding systems of HVAC systems, which are designed only for a fault condition, HVDC grounding systems are designed for normal, emergency and fault conditions [11]. In bipolar HVDC transmission systems, the grounding system is used as a means to improve the reliability of the entire system. Should one of the poles in the bipolar system be faulted, the current path will switch to ground return, thus allowing the system to continue operating at about half capacity, thus avoiding a total bipolar outage. During normal operation of a bipolar system this return path will carry only a small unbalanced current. In asymmetrical monopolar systems, the ground path continuously carries the same current as the high-voltage conductor. A ground return path for HVDC systems can be achieved either through a ground electrode, thus using the earth or sea itself as a return path, or by use of a low voltage metallic return conductor [11].

A ground electrode is typically a large metal ring (about 300 - 800 meters in diameter) buried in the earth/sea and surrounded by a highly conductive bed of soil [63]. Ground

electrodes must be located on a site of about one square mile far away from the converter station in order to avoid possible problems such as saturation of HVDC converter transformers or corrosion in the converter station grounding system. A low voltage electrode line connects the ground electrode to the converter station. The electrode line can be an underground/undersea cable, an overhead line, or a combination of the two [63].

Alternatively, metallic return uses a low voltage dc conductor to carry the returning dc current. The conductor is grounded at one end to maintain a low dc potential along the metallic return. All of the return current flows in the metallic return conductor, and there is no dc current in the ground. In some HVDC overhead transmission line systems, the metallic return function is served by insulated lightning shield wires.

Metallic return schemes have two key disadvantages compared with ground electrodes; higher initial capital costs, particularly for long distance power transmission lines, and increased operational power losses. In the ground electrode return option, dc return current will spread over a large cross-sectional area within the earth/sea and therefore has a very low effective resistance, whereas the resistance of the metallic return path is similar to the resistance of the high voltage conductor [64]. However despite the ground electrode system's advantages it is now seldom used due to issues associated with high dc ground currents in the earth or sea, such as environmental opposition and erosion in buried metallic pipes and structures associated with high dc ground currents in the earth or sea [64].

Unlike bipolar and asymmetrical monopolar systems, VSC HVDC with symmetrical monopole configuration has high resistance grounding on the dc side. For such systems the grounding options are [65]:

- High resistance grounding at transformer secondary winding Y point

- High resistance grounding through a zig-zag grounding transformer

- High resistance grounding at a shunt reactor neutral point

High resistance grounding for zero sequence voltages can achieved with a bank of MOV surge arresters which may be rated to limit the voltage displacement of a single pole to ground line or cable fault to an acceptable level [65].

2.3   HVDC Cables

A high voltage dc cable is a high voltage conductor surrounded concentrically by the appropriate layers of insulation, screening, water blocking and mechanical protection layers sufficient to allow cable burial underground or laying on the sea bed. The key components of a typical XLPE land and submarine dc cable, as illustrated in Figure 2-6, are [10]:
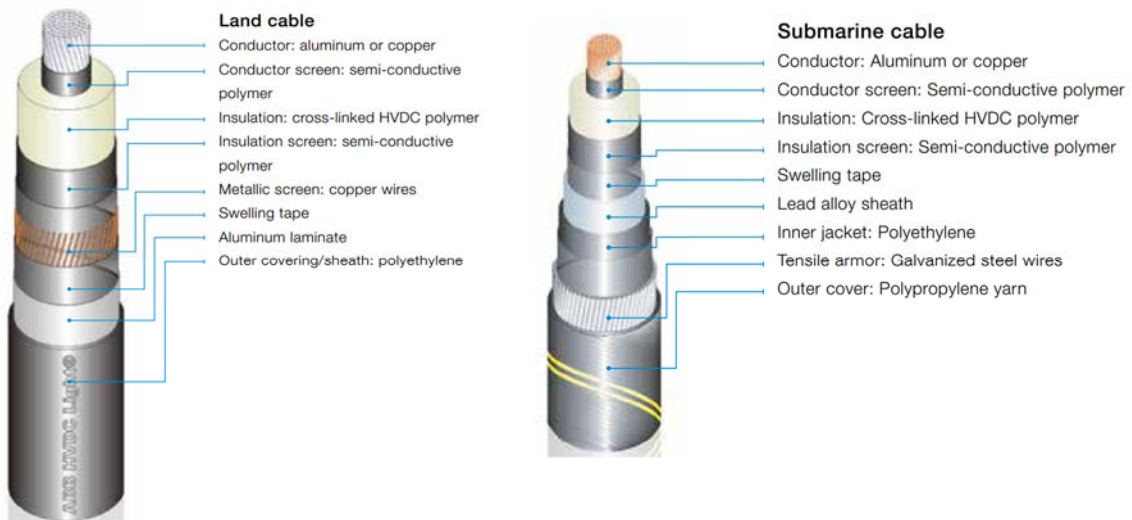
Figure 2-6 Typical Land and Submarine cable layer arrangement (courtesy of ABB)

1. Conductor: The cable conductor consists of aluminum or copper. The cross-section shape is round and built up of compacted stranded round wires or concentric layers of keystone-shaped wires for large cross-sections.

2. Insulation system: The dc polymeric or thermoplastic elastomer insulation system consists of the conductor screen, the insulation and the insulation screen. The insulation layer insulates the high voltage conductor from the outer mechanical protection layers and therefore from the "earth". The conductor and insulation screens are semi-conductor layers providing a smooth surface between the conductor, the insulation and the outer layers of the cable and managing the electrical stresses.

3. Water barrier: Aluminum or copper laminate is used as the water barrier for underground cables, whereas the lead alloy sheath is used for undersea cables.

4. Armoring: Submarine cables can be equipped with single or double layer of galvanized steel wires twisted around the cable. It provides effective corrosion protection as well as mechanical strength to protect the cable during handling, transportation and laying of the cable in the sea.

5. Outer sheath/Outer serving: Underground cables are sheathed with two layers of polypropylene providing appropriate mechanical and chemical stability protecting against most chemical agents.

The two particular parts of a cable that plays a crucial role in the final design, as well as the transportation and installation requirements for any underground/undersea HVDC transmission link are [10], [11]:

1. Conductor material and size

   The conductor material and size depends on the required dc voltage, power transfer, losses, installation method and mechanical environment. Aluminum is lighter and cheaper than copper but has poorer mechanical properties and lower conductivity. For this reason, it is common to use aluminum conductors for land cables and copper for submarine applications, the latter requiring higher tensile strength during installation. However even for large, high power-rated land cables copper conductors can provide much smaller diameter cables for equal losses [10].

   The size of the conductor required to transmit a given current is also determined by the conductor material's thermal characteristics and the cable's ability to dissipate heat away from the cable.

2. Cable insulation

   The most popular dc cable types in terms of the choice of insulation materials are mass impregnated (MI) cable and cross linked polyethylene (XLPE) cables.

   MI cable insulation consists of layers of lapped paper tape impregnated with a mineral oil-based, high viscosity compound. The MI cable is a proven technology used for dc voltages up to 500kV. It can accommodate voltage polarity reversal, as is required for power flow reversal with LCC HVDC transmission schemes. However, MI cables tend to be larger, heavier and more expensive than the polymer alternative [11].

   The insulation within XLPE cables consists of cross linked polyethylene layers extruded over the conductor and the conductor screen. Polyethylene (PE) has low di-

electric loss characteristics which makes it attractive for extra high voltage appli-

cations. These cables are much lighter than the equivalent MI cables and less ex-

pensive. XLPE cables have been used for HVDC applications since the 1990s and

are presently available up to 525 kV [66]. A new solid thermoplastic elastomer

insulated dc cable with less weight than XLPE has been developed with the capa-

bility for voltage reversal and is called "P-laser" [67].

2.4   HVDC Overhead Line Transmission Structure

The essential components of HVDC overhead transmission lines are conductors, insulators,

towers and right of way (ROW) [47]. The towers support the conductors, and along with

the insulators, provide physical and electrical isolation between energized lines and ground

as well as from one another. The real estate corridor accommodating transmission lines are

called rights-of-way. Their width requirements are discussed in a Chapter 3.

2.4.1   Tower Structure

Tower requirements for a given HVDC line are generally defined by the construction ma-

terial, type or geometry, capacity to withstand wind loading (horizontal) and weight load-

ing, span between towers, tower weight, footing design, number of circuits, and circuit

configuration. Most high voltage towers, ac or dc, are constructed of steel though alumi-

num and hybrid steel and aluminum construction has also been used. Tower configuration

or basic tower geometry is very site-dependent. For high voltage application, the options

are lattice, monopole, H-frame, guyed-V, or guyed-Y [4]. The most widely used options

for HVDC transmission are self-supporting and guyed suspension lattice towers, as shown

in Figure 2-7 [68]. Monopole towers have been also used in a few HVDC projects [47].

The span is commonly expressed as an average based on the number of towers per mile -

normally from three to six towers for most HVDC voltages [4]. Towers normally accom-

modate just one circuit but may accommodate two or three, including the metallic return

in some cases. Circuit configuration refers to the relative positioning of conductors for each

of the poles, e.g. horizontal, vertical. Vertical orientations allow for a more compact ROW

but require a taller tower [4]. Tower structures include cross-arm sections, from which the

conductors are suspended by means of the insulators.

Self-Supporting Suspension Tower   Guyed Suspension Tower
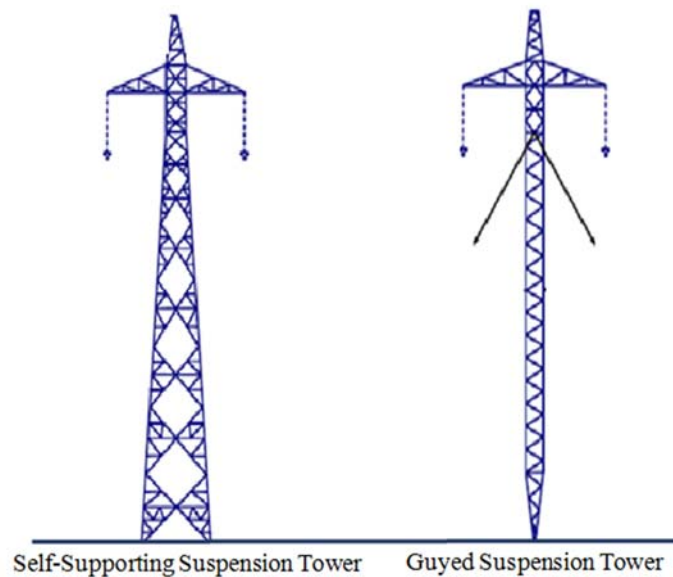
Figure 2-7 Typical HVDC lattice towers (Courtesy of Manitoba Hydro [68].)

2.4.2   Insulators

Insulators serve two critical functions: They provide a means by which power line conduc-

tors are suspended and they insulate energized poles from the suspension point, i.e. the

grounded tower. Proper insulation design of an HVDC transmission lines is essential for a

reliable operation over the lifetime of the circuit [4]. Dc voltage subjects insulators to much more unfavorable conditions than does ac voltage. This is due, in part, to a higher collection of insulation surface contamination with unidirectional electric fields. Moreover, dc and ac arc propagation across the insulator surface is different due to the natural zero crossing of the ac arc [69]. Selection of insulator type, material, and string configuration for HVDC is complex and site-dependent. This issue is explained in greater detail in Chapter 3.

Insulators for high voltage power transmission may be made from ceramics (glass or porcelain) or of polymer composite configurations [11]. Two basic insulator configurations have proven useful for HVDC: One of which is comprised of individual cap and pin "discs" which are used in sufficient number to accommodate the voltage for which they are selected; the other being "long rod" insulators consisting of a central glass core for mechanical support surrounded by a molded polymer core with "skirts" to accommodate contamination [11]. The schematic of cap and pin and long rod insulators are shown in Figure 2-8.
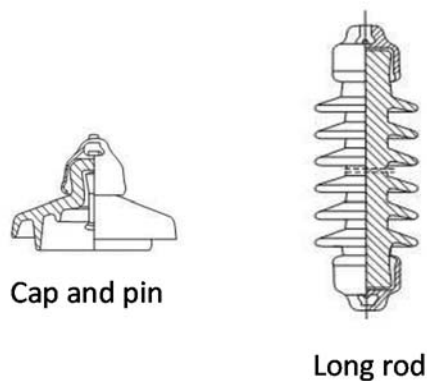
Cap and pin

Long rod

Figure 2-8 Schematic of typical cap and pin and long rod insulator [70]

Cap and pin insulators consist of a ceramic shell to which metal cap and pin components are cemented to provide a means of attaching insulators to each other and to the tower and the line hardware. This configuration provides flexibility within the insulator string. Cap and pin insulators have good mechanical strength and a long term track record. However, they are heavy and expensive [11]. Long-rod insulators can be adapted in length to the applied voltage or connected in series for higher dc voltage applications. There are two popular long-rod insulator options:

- Long-rod ceramic insulators are one-piece units of varying length made of glass or porcelain. They have a long term track record of almost 40 years and have demonstrated moderately satisfactory performance [11].

- A newer insulator technology consists of an interior rod for mechanical strength, surrounded by a molded polymer outer surface with skirts optimally contoured for dc applications. They are significantly lighter and their performance in contaminated environments is considerably better than ceramic insulators of equal length. Furthermore the hydrophobic property of the exterior surface material discourages wetting, thus increasing electrical withstand strength per unit length in comparison with disc insulators. However, this is relatively a new technology with a limited experience base on which to base life expectancy [11].

2.4.3   Conductors

The most commonly used conductor material options for overhead transmission lines, as with cables, are copper and aluminum. Although copper has higher conductivity, aluminum is more popular for overhead lines due to its lower costs and higher strength-to-weight

ratio, the latter causing less conductor sag and thereby allowing for greater span lengths. Aluminum Conductor Steel Reinforced (ACSR), Aluminum Conductor Composite Reinforced (ACCR), Aluminum Conductor Composite Core (ACCC) and All Aluminum Alloy Conductor (AAAC) are different available conductor technologies that achieve higher strength to weight ration while maintaining the electrical performance of aluminum [4]. Corona effects on high voltage power transmission, explained in Chapter 3, cause limited environmental issues as well as some degree of power loss and interference with communication circuits. In order to reduce this corona effect, more than one conductor per pole is normally used at the higher dc voltages. "Bundled" conductors consist of several parallel conductors, often in a cylindrical configuration, connected at intervals by spacers. The optimum number of conductors depends on both the current rating and the voltage level. For HVDC applications, normally the number of the conductors in a bundle is between two and six conductors [38].

2.4.4   Right of Way
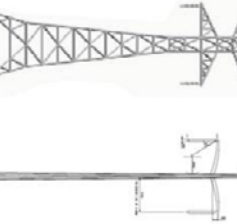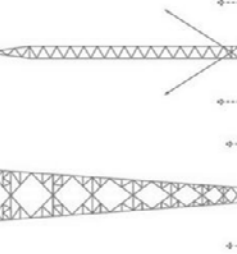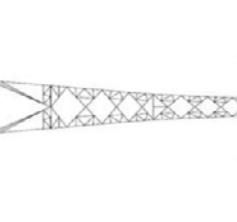
In today's world, where real estate cost, agricultural and ecological impacts are of very high significance, the right of way has become a critical component of a transmission line. It must provide adequate width to eliminate the risk of having the transmission line interfere with use or safety of adjacent properties and managed to minimize the risk of flashovers of the line due to vegetation adjacent to energized conductors. Failure to preserve a ROW adequately can result in dangerous situations, including ground faults. The ROW must also be adequate for line construction and access to transmission towers and other line components for ground-based inspections and maintenance. In some cases, access

roads constitute a portion of the ROW, providing more convenient access for repair and

inspection vehicles [4]. In Chapter 3, the main issues relating rights-of-way to transmission

line design will be explained.

2.4.5   General Specifications of the Existing HVDC Overhead Lines

Typical example configurations and dimensions of HVDC transmission lines already op-

erating in many parts of the world are presented in Table 2-1 [47], [69], [70]. This table

will be used as a basis for assessing the advantage of a proposed new compact design which

is proposed in this thesis.

Table 2-1 Configurations and dimensions of typical existing HVDC transmission lines

Description	Nominal DC Voltage			
	± 300 kV	± 400 kV	± 500 kV	± 800 kV
Power Rating [MW]	600-1000	1000 - 2000	1500 - 3000	3000 - 7500
System Configuration	Monopole/Bipole	Monopole/Bipole	Monopole/Bipole	Bipole
No. Of conductors in a bundle per pole	2, 3, 4	2, 3, 4	2, 3, 4, 6	6, 8
Required Right of Way [m]	40	45-50	55-70	85-90
Typical suspension tower				
Minimum Ground clearance [m] (Subject to local Regulations)	8.5	10-11	11-13	16
Range of tower height [m]	25 – 40	36 – 51	31 – 51	39 – 93
Typical insulator length [m]	4.34 (Porcelain Cap & Pin) 3.60 (Composite)	6.18 (Porcelain) 5.06 (Composite)	6.00 (Porcelain)	12.94 (Cap & pin)

Chapter 3

A New Approach for Compaction of HVDC Transmission Line Design

Chapter 2 described the essential components of modern HVDC systems including the ac-dc converter, dc overhead transmission lines and underground cables and related elements. Underground cables have the advantage of low visibility and minimal right of way (ROW) over transmission lines. However, an underground cable can be four to fifteen times more expensive than an overhead line depending on the voltage level and the line route [36]. This is due to time, materials, process and other issues such as going under a road, highway, or river and also avoiding other underground installations such as water, gas, and sewer lines [36], [37]. An important contribution of this thesis is the investigation of whether the ROW and tower height of overhead lines can be significantly reduced so that they might be more acceptable to the public. This would result in a significant cost saving over employing underground cables. The converter topology in this thesis is assumed to be voltage sourced converter based, as this is the most modern configuration.

This chapter first discusses basic overhead line design parameters and their impact on the ROW width and tower height. Then, based on this discussion, a new compact dc overhead transmission line is proposed; one which results in a much smaller ROW so that it not only lessens the visible impact of new lines but adapts them to ROWs too narrow for conventional construction, e.g. road- or rail-side routes. In later chapters, electrical aspects of the compact design, such as overvoltages and lightning performance will be considered.

3.1   Overview of the Line Design Parameters

This effort began with a comprehensive literature review to investigate line design parameters and their interdependence, as summarized in Figure 2-1 [4], [38], [45], [47], [69], [70], [71], [72]. As shown in this figure, the variables effecting HVDC tower height and ROW width are very complex and interrelated. While this figure has little to do with design *procedures*, it illustrates that virtually every design variable affects either tower height or ROW width, or both, and is therefore germane to the compaction issue.
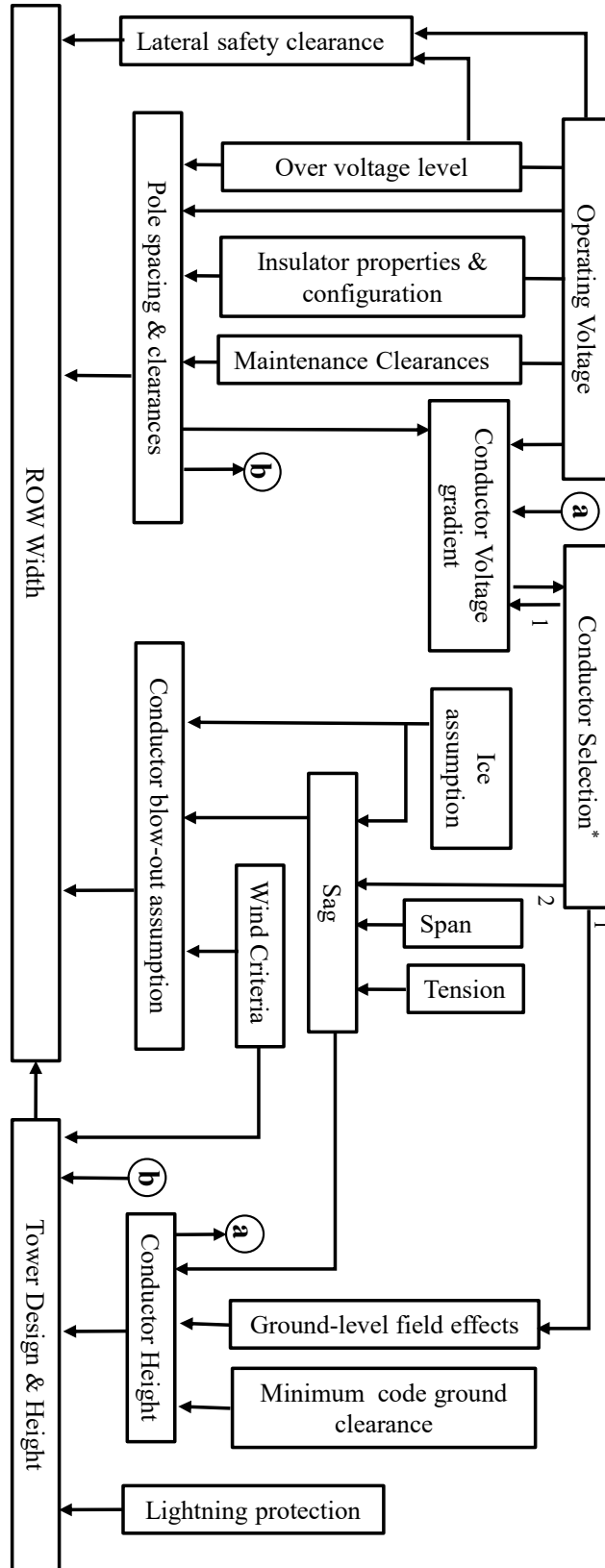
Figure 3-1 Functional relationships affecting tower height and ROW width

HVDC transmission line design must be based on power transfer requirements and voltage options. After this, the transmission line electrical configurations (e.g. monopole or bipole) are considered, as are alternative tower-top geometries, conductor type and configuration, and pole spacing – the latter all subject to studies of electric field effects, corona effects, as well as overvoltages and their impact on insulation coordination. The foregoing establishes the width of the required ROW. On that basis the mechanical design of the towers and foundations can be considered, and the mechanical stresses on conductors and shield wires can be determined. Finally the economics including direct costs, cost of losses, operation and maintenance cost over anticipated line life, is evaluated. This design process is iterative as the design criteria can be satisfied by multiple parameter solutions [47], [70].

This chapter will discuss those variables having the greatest impact on the vertical and/or horizontal ROW requirement to demonstrate viability of the proposed designs. It should be realized that the final design will require interaction between planners and designers and can only be reached when electrical, mechanical, civil and environmental aspects are all taken into account, considering both performance and costs [47]. The electrical aspects related to compact dc transmission line design will be investigated in the following chapters.

Throughout this research, Manitoba Hydro's Bipole III transmission line [68], illustrated in Figure 3-2 and with parameters as listed in Table 3-1, is used as the example of a conventional overhead dc line for comparison with the proposed innovative designs.

Table 3-1 Bipole III conductor and insulator parameters

Pole Conductor	Type	806-A4-61 AAAC (equivalent to 1,590 MCM ACSR)
	Total bundled sub-conductor	3
	Diameter	38.01 mm (1.50 in.)
	Sub-conductor spacing	457 mm (18 in)
	Pole to pole spacing	15.5
	Conductor mass	2.354 kg/m
Shield Wires	Total bundled sub-conductor	1
	Diameter	18 mm (0.7 in.)
Insulator	Suspension configuration	I-string
	Number of discs	25
	Diameter	380 mm
	Weight per disc	15.4 kg
	Insulator length	5 m
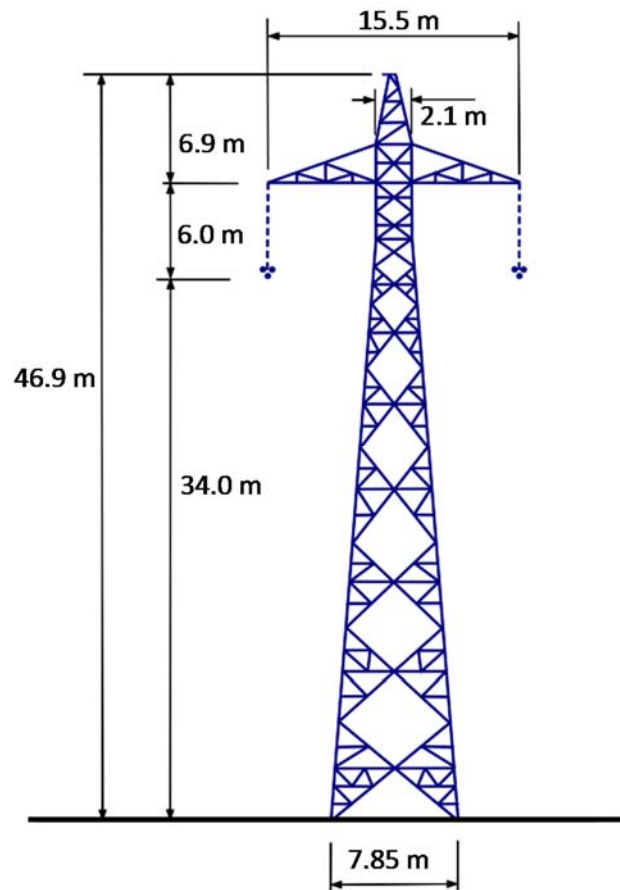
Figure 3-2 Lattice tower design for Bipole III in Manitoba [68]

3.2   Right of Way Width Components

As shown in Figure 3-3, ROW width is comprised mainly of the pole-to-pole spacing, conductor outswings and lateral safety clearances that can be formulated as follows [47], [73].

$$ROW = [(L + S)\sin\theta + R + d_{min}] \times 2 + PS \qquad 3.1$$

where:

d_{min} = lateral clearance for operating voltage and safety

R = bundle radius (m)

L = insulator string length if I- string (L is zero in this formula for V-string insulators)

S = conductor sag

θ = maximum swing angle due to maximum wind (e.g. 50 year return)

PS = pole to pole spacing of the conductors
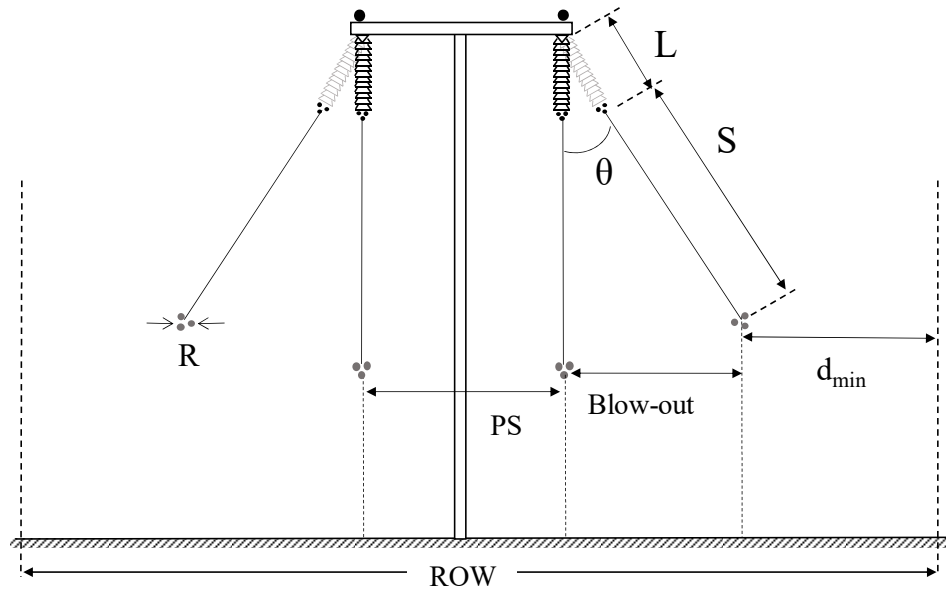
Figure 3-3 ROW width determinants

- Pole to pole spacing, *PS*, controlled by tower top geometry, must ensure adequate electric clearances both between the high voltage conductors and tower structures as well as between conductors along the span. Minimum pole spacing must also limit the maximum surface gradient of pole conductors to a reasonable level [45].

- Conductor mid-span outswing depends on insulator configuration, conductor sag and the assumed wind-dependent swing angle, θ [74].

- Lateral clearances, d_{min}, are based on safety standards between the conductor and the ROW edge under maximum assumed swing. They are a function of operating voltage, overvoltage levels and the proximity of any neighboring structures [73].

3.3   Overview of Compact Design Criteria

Compacting can be viewed in two different ways:

- A means to maximize transmitted power on a given ROW [75] or inversely,

- A means to minimize the ROW for a given power transfer requirement.

This thesis considers the latter, i.e., compaction refers to minimizing both tower height and right of way width requirements for a given voltage and MW rating for HVDC transmission systems with overhead lines. The elements that influence the tower top geometry and the conductor sag as well as their interrelationship with pole to pole spacing and conductor blow out, are considered in the following sections.

3.4   Tower Top Geometry Consideration

Tower top geometry is governed by clearance requirements and the number, type and configuration of insulators used. The number of dc disc insulators or the length of long-rod insulators is based on dc voltage withstands under the pollution conditions prevailing on the ROW. Service experience has shown that the most critical factor affecting the performance of dc systems is the behavior of the insulators under normal operating voltage [69]. HVDC operating experience has shown that insulator flashovers due to contamination and/or wet weather conditions occur under normal operating voltage. Altitude and other environmental factors, such as fog or salt spray, also need to be considered [69]. The resulting withstand is then adjusted, if necessary to accommodate anticipated switching overvoltages under normal weather conditions [76].

Horizontal clearances between pole conductors and tower members or, in the absence of an intervening structure, between pole conductors themselves, depend on the maximum expected overvoltage [47]. Adequacy of clearances to tower and guy wires must be also verified considering insulator swing due to wind, explained in Section 3.4.4.

3.4.1   Insulator Properties

Pollution such as salt or industrial waste is attracted to the surface of dc insulators. When subject to atmospheric moisture, this can form a conductive path causing leakage currents and eventual flashovers [69]. Thus pollution severity will directly impact the withstand strength of insulators or, conversely, the insulator string length required for satisfactory

performance. The appropriate insulator design for dc lines can be obtained through a statistical determination of pollution severity as well as knowledge of insulator performance under specific pollution conditions [76]. A large number of test results [77], [78], [79], show that the relationship between the pollution severity and the flashover voltage can be described as

$$U = A\gamma^{-\alpha}$$ 3.2

where U is the flashover or withstands voltage, γ is the pollution severity, and A and α are empirically determined constants related to the shape and material of insulator. Because the nature of pollutants varies quite widely, industry has used salt contamination as a standard for gauging pollution performance of various insulator types and lengths. Thus the pollution severity in equation 3.2 is usually defined in terms of the Equivalent Salt Deposit Density (ESDD) for field measurements and as Salt Deposit Density (SDD) for the clean-fog (or solid layer) laboratory tests in mg/cm^2 [79], [76].

High voltage insulators for outdoor use are shaped to maximize the length of the leakage path along the surface from one end to the other, called the creepage length, thereby minimizing leakage currents [76]. The creepage distance of an insulator, often identified as the Unified Specific Creepage Distance (USCD) is used to determine the insulator dimension for pollution performance. It is expressed by the leakage distance (or creepage distance) of the insulator in mm divided by the flashover or withstand voltage in kV as:

$$USCD = B\gamma^{\alpha}$$ 3.3

where B and α are an empirically determined constants. Research based on uniform artificial pollution tests for dc insulators, shows that there is a nearly linear relation between the dc pollution flashover voltage and the disc type insulator string length [77]. [80].

3.4.2   Impact of the Insulator Options on Compaction

The constants used in the above empirical formulae (Equations 3.2 and 3.3) show that the insulator material, shed shapes and suspension string configuration will impact the effectiveness of the creepage distance and as a result, the critical flashover voltage.

Typical insulators used for HVDC overhead transmission line applications were discussed in Chapter 2. The fundamental design details of both material and strings (overall length, creepage distance, maximum shed diameter etc.) are governed by requirements specific to the project to which they are applied. For a given project the design process steps are [81]:

1) identify candidate insulators (material, profile)

2) assess the environmental and system stresses

3) determine specific characteristics and dimensions of insulator options

4) verify the selection(s) made.

The detailed theory of insulator design, while based on well-established practices is beyond the scope of this thesis. However factors such as materials, insulator types and suspension configurations which are particularly germane to compaction of the line will be addressed in succeeding paragraphs.

For a given length, insulator types and materials differ over a range of roughly 1.3 to 1 in their ability to sustain dc voltage under pollution conditions [69]. Recent studies [77], based on artificial pollution and field tests, show that glass insulators have better antipollution

performances than porcelain insulators with the same profile. However the effectiveness

of leakage distance as well as the pollution flashover withstand of composite long-rod in-

sulators is much superior to either porcelain or glass disc insulators [77], [83]. Moreover,

as salt deposit density increases, the effectiveness of leakage distances of the composite

insulators will increase and that of the porcelain and glass insulators will decrease [77].

Schematics of different insulator suspension strings are shown in Figure 3-4. Selection of

insulators for compaction of dc lines requires careful attention, since the length of suspen-

sion string configurations will impact pole-to-pole spacing, tower height, and ROW width.

For example a 30% gain in pollution withstand per meter of string length, combined with

a shift from tangent strings to 90º V-strings could, for typical 500 kV line dimensions,

shorten the suspension distance (and the tower) by about 1.3 m [82].
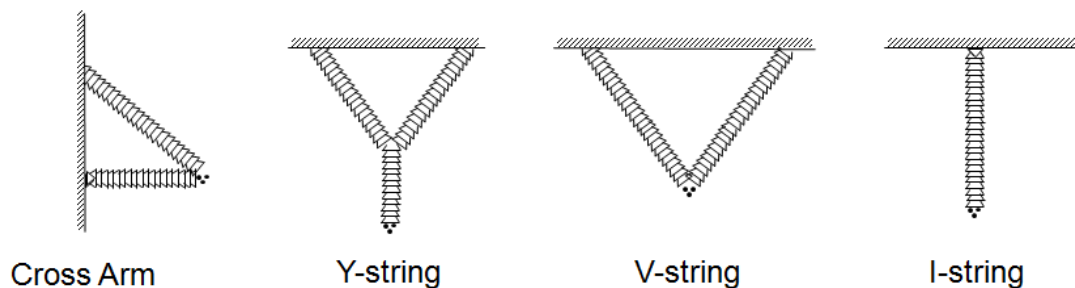
Figure 3-4 Schematics of different insulator suspension strings

The insulator suspension angle at the tower not only defines the tower top geometry, but

also impacts the arcing process and the leakage currents and consequently the insulator

withstand voltage level [47]. Both insulator cross arms and V-string configurations main-

tain the conductor at a fixed location from the tower, thus preventing insulator movement

from conductor outswing caused by wind. However V-strings require a wider cross arm

section at the tower than do I-strings [47]. The Y-string has partly the benefit of both V-string and I-string in terms of a more compact tower top geometry and minimum conductor outswing at the tower. However, this design is usually not recommended for ultra-high voltage transmission dc lines, since the flashover voltage of the Y-string is much lower than the I-strings or V-strings for the same number of insulator units due largely to the fact that unequal leakage current per path distorts voltage distribution [80].

Bell-type and tri-shed are two common insulator shed types, as shown in Figure 3-5. Disc insulators for HVDC applications most commonly have bell-type (or anti-fog) profiles with a relatively high creepage distance per unit. Typical shed profiles utilized on long-rod insulators are of tri-shed type [80].

Tests on the bell-type V-string insulators showed, for angles of 60° or 90°, arcs easily levitate from the insulator surface, dropping the flashover voltage compared to I-strings. However, when the V-string angle is 120°, part of the arc develops along the insulator surface, so the withstand voltage is much higher than the I-strings or the V-strings with an angle of 60° or 90° [80], [84].

For tri-shed V-string insulators, the flashover voltage for 60° is much lower than for I-strings since, in the former case, arcs easily levitate from the insulator surface. However, when the V-string angle is equal to or greater than 90°, the flashover performance is similar or better than the same strings at 60°, partly because the arc propagates along the insulator surface while most of the arc levitates from the insulator string. The flashover voltage of the V-strings at 90° and 120° are slightly higher than the I-string [80], [84].
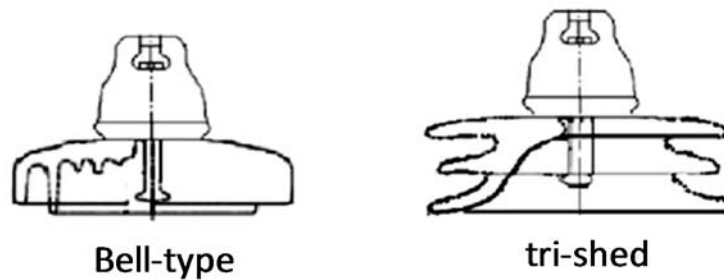
Figure 3-5 Bell-type and tri-shed insulator configurations [80], [84]

Because arc levitation on the surface of the tri-shed insulators is much more significant than on bell-type insulators, the flashover performance of bell-type insulators (I-, Y- and V-strings) is better than the tri-shed insulators [80].

3.4.3   Overvoltages in dc Transmission Lines

Horizontal clearances between pole conductors and tower members are governed mainly by the maximum expected overvoltage [45]. Overvoltages in overhead transmission lines are mainly categorized into temporary, slow-front and fast-front overvoltages according to the rise time and duration of the overvoltage [47], [85].

Temporary overvoltages may occur due to mal-operation of the controller system in the HVDC converter station, line energization and reclosing. However, normally for line energization, the dc voltage is ramped up smoothly from zero, and for the line reclosing, the trapped charge will be eliminated through the line de-energization process to limit the overvoltages [47].

Slow-front overvoltages on dc transmission lines generally happen due to ac or dc side fault occurrence and clearing process [47]. However, the most significant slow-front overvoltages come from single pole to ground faults and occur on the un-faulted conductor.

The magnitude and duration of the slow-front overvoltages depends on converter technology, system configuration, line length, fault location, and smoothing reactor.

Fast front overvoltages are mainly caused by lightning surges directly striking the conductor, or the tower and shield wires that may result in insulator back flashover. The crest times of the fast front overvoltages are from 0.1–20 µs. The overvoltages caused by lightning depend also on the tower geometry and footing resistance of the towers [85], [86].

In order to determine the tower top minimum air clearances for HVDC voltage levels, continuous operating voltage and temporary overvoltages have negligible impact because the required voltage withstand strength is mainly affected by slow front and fast front overvoltages [87].

As mentioned earlier, most VSC HVDC projects use either symmetrical monopoles or grounded bipole configurations. LCC HVDC is a mature technology and all dc overvoltages associated with it are well known [47]; studies show that lightning and fault overvoltages on the dc side of LCC systems are generally in the range of 1.8 to 2.3 pu, when the maximum overvoltage happens for an earth fault in the middle of the line [47]. Faults in other locations produce smaller overvoltages.

 However there is no corresponding experience base for dc overhead lines which use modern Modular Multilevel Converters (MMC). The proper design of controllers for MMCs, especially with full-bridge converters, can reduce the slow front overvoltage levels formerly associated with LCC cases, thus reducing clearance requirements and facilitating compaction. A comprehensive slow front overvoltage assessment of MMC HVDC is presented in Chapter 5. The lightning performance and fast front overvoltage analysis of the compact and conventional dc overhead lines are also presented in Chapter 6. Moreover, the

application of a properly designed line surge arrester, which can limit these overvoltages based the design criteria, is discussed in these chapters.

3.4.4   Wind Loads on the Insulator Strings and Insulator Swing Angle

Wind force may cause conductor swing and thus reduce clearances to grounded tower members. Thus when I-type suspension strings are used, lateral wind loads are important in defining the tower top geometry [45]. In this case, conductor position depends both on wind action, which varies with time and location, and line parameters such as conductor type, ratio of the wind span to weight span, etc. The mean swing angle of an insulator set can be derived as a function of the wind loads on the conductors and the insulators and expressed as [88]:

$$\phi_{ins} = \tan^{-1}\left[(\rho/2)\cdot V_z^2 \cdot \frac{C_{xc}\cdot G_c\cdot G_L\cdot d\cdot n\cdot L_w + C_{xi}\cdot G_t\cdot S_i/2}{m_c\cdot g\cdot n\cdot L_c + M_{ins}\cdot g/2} \right] \qquad 3.4$$

Where:

ρ air density corrected for temperature and altitude;

V_z mean wind velocity (e.g. 50 year return) at the height z above ground;

C_{xc} drag coefficient of conductor which is 1.0 for the generally considered stranded conductors and wind velocities;

G_C combined wind factor for the conductors, which is a function of the height z and the terrain categories listed in Table 3-2, as shown in Figure 3-6;

G_L span factor shown in Figure 3-7 as a function of the height;

d conductor diameter [m];

n number of sub-conductors;

L_W wind span of the conductor [m];

C_{xi} drag coefficient of the insulator set, $C_{xi} = 1.2$;

G_t combined wind factor for insulators, which is a function of the height z and the

                    terrain categories listed in Table 3-2, as shown in Figure 3-8;

S_i insulator set area exposed to wind [m^2];

m_C linear mass of the conductor [kg/m];

L_C weight span of the conductor [m];

g gravitational acceleration, $g = 9.81$ [m/s^2];

M_{ins} mass of the insulator set [kg];

Terrain categories are classified as shown in Table 3-2 [88]:

Table 3-2 Terrain categories

A	Large stretch of water upwind, flat coastal areas
B	Open country with very few obstacles, airports or cultivated fields with few trees or buildings
C	Terrain with numerous small obstacles of low height (e.g. trees, buildings)
D	Urban areas or terrain with many tall trees
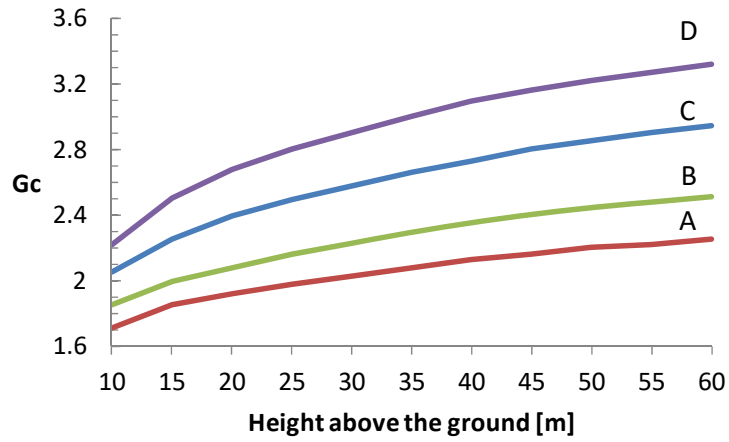
Figure 3-6 Combined wind factor Gc for conductors [IEC 2167/03]
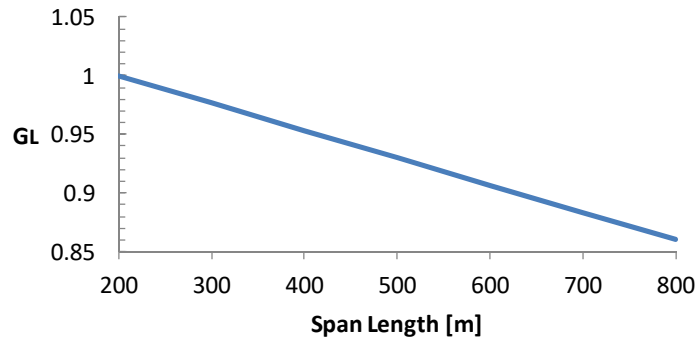
Figure 3-7 Span factor G_L [IEC 2168/03]
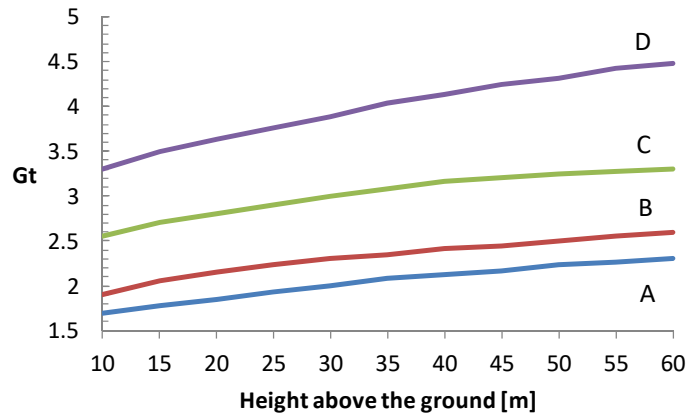
Figure 3-8 Combined wind factor G_t for insulators and supports [IEC 2169/03]

To determine the average swing angle of a conductor and insulator, one need only consider the *mean* value of wind velocity over a sufficient long period of time. Wind action is evaluated on the basis of a reference wind V_R, usually defined as the mean value of wind during a 10 min period at a level of 10 m above the ground [45]. Wind velocities increase with the height above ground level and the relationship between the mean wind velocities, V_z, and the wind at a height above the ground, z, can be calculated by the so called "power law" [45] which is expressed as:

$$V_z = V_R (z/z_R)^{\alpha} \qquad\qquad 3.5$$

where V_R is the reference mean wind velocity for the reference height Z_R and α is the roughness exponent depending on the terrain category (α is $0.1 - 0.12, 0.16, 0.22, 0.28$ for terrain category A, B, C and D respectively [45])

As cited previously, most of the parameters in equation 3.4 are affected by insulator height. The following section will consider the impact of sag and span on the tower height. Assume, for example, that the average insulator height for conventional design with span length 488 m is 37 m and for a low profile design with the span length of 258 m that height is 22 m (issues explained more in the following section). Assume further that the reference wind is $V_{R\,(10m/10min)}$ =20 m/s., using 3.4, for I-string insulators in terrain type B, the mean swing angle (ϕ_{ins2}=44.71^0) for low profile designs is slightly smaller than that for a conventional design (ϕ_{ins1}=51.78^0).

3.5   Influence of Span and Sag on ROW Width Reduction

The conductor profile within a particular transmission line span conforms to a set of hyperbolic functions which describe catenary curves [89]. For a cable with a span length l, the maximum sag S in meter, i.e. the vertical distance between the point of attachment and the cable at the lowest point in the span, is described by the hyperbolic function:

$$S = \frac{H}{w}[\cosh(\frac{wl}{2H}) - 1] \qquad\qquad 3.6$$

where H is the horizontal tension at each end in kg, w is weight per unit length in kg/m, and l is the span length in meter. This function is nonlinear and is not simple to work with for lines with multiple spans. For this reason, it is often simplified by linearizing around l= 0 as follows [71]:

$$S = \frac{wl^2}{8T} \qquad\qquad 3.7$$

Thus in a flat terrain, for a given conductor choice, stringing tension, electrical loading and weather context, sag is approximately proportional to the square of the span length [71]. Therefore reducing the spacing between towers has a significant effect in reducing sag, and consequently tower height and conspicuousness. In the general range of spans used for HVDC lines, cutting span length in half will reduce the sag by 75%, a reduction translating directly into reduction in tower height for a given ground clearance requirement. Such a gain obviously requires more towers per km, though each with proportionately less wind and weight loading. Although it could be argued that more towers per km give a poorer visual impact from close by, overall, they are more likely to be visually acceptable as their

lower height makes them blend into the background especially when viewed from a dis-

tance. With foreground trees, they may even not be visible at all.

Figure 3-9 shows an example of a 500 kV dc tower with a typical span length of $l_1 = 488$

meters, conductor height at the tower of 34 meters, and a mid-span clearance of 13.2 meters

[68]. It also shows a hypothetical low-profile tower of equal voltage and MW capability

with identical conductors and tension, but with span length of l_2=258 meters and, as a re-

sult, sag reduced from $S_1 = 20.8$ meters to $S_2 = 5.8$ meters. As shown in Figure 3-9 the

minimum clearance established either by safety codes or ground level field effects, dis-

cussed later, must be maintained for both structures.
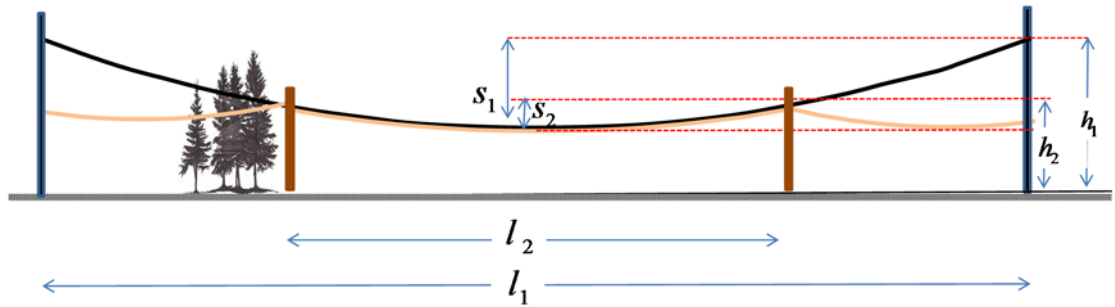
Figure 3-9 Comparison of longitudinal profiles

3.5.1   Wind Loads on the Conductors and Conductor Swing Angle

The wind load F_{WC} on the conductors with the wind span of L_W due to the effect of the

perpendicular wind pressure is expressed in equation 3.8 [88]. The parameters are as ex-

plained for equation 3.4.

$$F_{WC} = (\rho/2) \cdot V_z^2 \cdot C_{xc} \cdot G_c \cdot G_L \cdot d \cdot n \cdot L_w \qquad\qquad 3.8$$

From Equation 3.8, the mean swing angle ϕ_c of a conductor in a horizontal span, when the wind and weight spans are equal can be derived as:

$$\phi_c = \tan^{-1}[(\rho/2) \cdot V_z^2 \cdot C_{xc} \cdot G_c \cdot G_L \cdot d/(m_c \cdot g)]\qquad\qquad 3.9$$

The average height of the conventional design with span length 488m is 20.13 m, whereas the average height of the low profile design with the span length of 258m is 15.13 m. Assuming the reference wind is $V_{R\ 10m/10min}$ =20 m/s, therefore, using 3.9, the mean swing angle in terrain type B, for conventional and low profile designs, ϕ_{c1} and ϕ_{c2} respectively, are:

$$\phi_{c1} = \tan^{-1}[0.5 \times 1.225 \times ((20.13/10)^{0.16}20)^2 \times 1.0 \times 0.92 \times 2.2 \times 0.038/(2.354 \cdot 9.8)] = 45.6^o$$

$$\phi_{c1} = \tan^{-1}[0.5 \times 1.225 \times ((15.13/10)^{0.16}20)^2 \times 1.0 \times 0.975 \times 2.1 \times 0.038/(2.354 \cdot 9.8)] = 43.2^o$$

Figure 3-10 shows further the influence of sag on both tower height and ROW requirements which are based on a wind blow-out angle of 45° for each structure. It should be noted that the actual angle is governed not only by conductor configuration and wind assumptions, but also by ice-loading which influences sag itself and which is assumed to be the same for both structures [88]. In this example, assuming an insulator length of 6m for a 500kV transmission line, the blow-out distance for the conventional structures, referring to Figure 3-9, is almost $2 \times (L + S) \sin(\phi_c) = 37.9$ m, and will be reduced to less than half, i.e., to 16.7m for the low profile compact design illustrated in Figure 3-9. Note that using a V-string insulator can reduce the blow-out distance further to 8.2m for the low profile structure with the same swing angle.
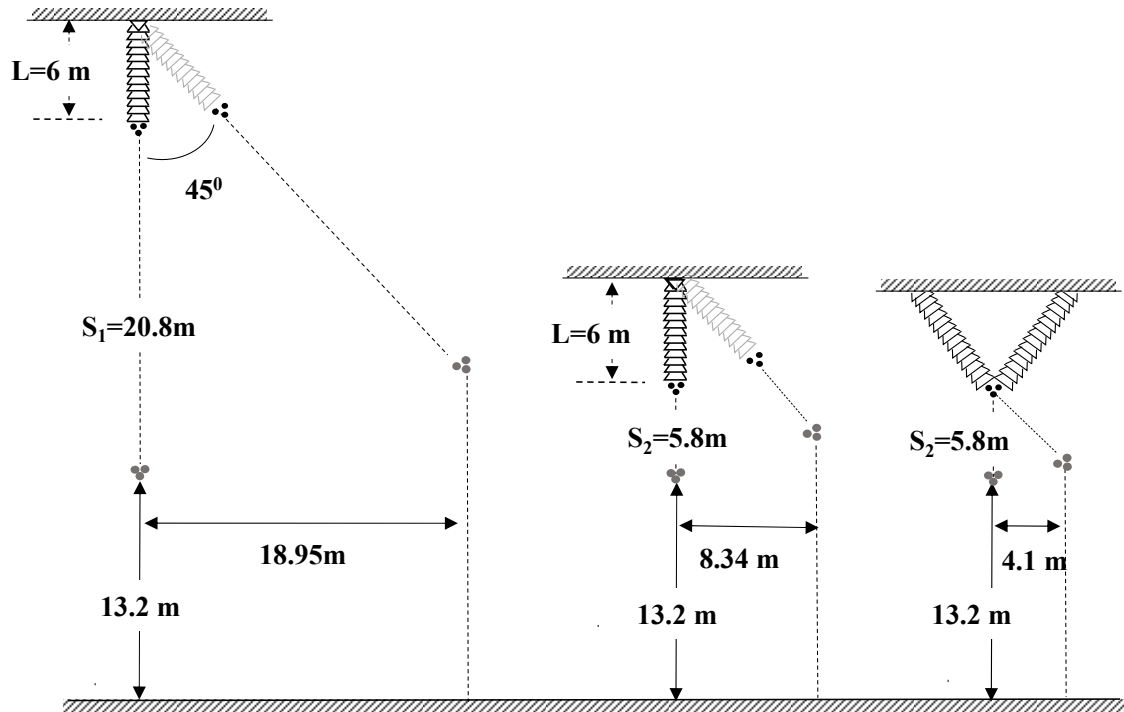
Figure 3-10 Sag's effect on tower height and ROW width

Without a concern for compaction, the economic optimization of HVAC and HVDC transmission lines simply minimizes the aggregate cost of structures, conductors, including future losses, and foundations per kilometer, ignoring ROW width [70], [90]. Compaction adds an additional ROW width constraint. In some cases, additional (but sometimes less tangible) cost advantages could be considered in the optimization such as a time cost to obtaining ROW permission.

In forested areas shorter spans and reduced conductor blow-out require fewer trees to be cut, and therefore more carbon dioxide (CO_2) to be sequestered from the atmosphere. It also saves maintenance costs related to regular cutting under the lines. In such areas, the cost of footing increases less rapidly with height, particularly if the average conductor height is at tree level or lower [88]. In agricultural areas, smaller corridors reduce the losses

due to land future value, land income and harvest losses and the time and cost of cleaning out weeds [34]. An objective function for finding the optimum span considering the material, labor cost as well as ROW width is described in Appendix A.

3.6   Conductor Selection

For a given span length, conductor selection can have an important bearing on both sag and conductor blow out. For example, for equal aluminum cross section area, flat stranded conductor can reduce both diameter and wind loading by 8% - 11% with corresponding reductions in conductor blow out and ROW requirement [91]. This reduction in wind loading would be roughly equivalent to a span reduction of 16% - 21% with the approximation that sag $\approx$ span^2 [71]. Flat stranding also reduces ice loading and ice-burdened sag, where applicable [91].

Conductors with solid aluminum alloy and aluminum strands or with aluminum strand and small carbon fiber center for strength are increasingly popular. Both are lighter than ACSR and can have less sag for equal tension [4].

Bundling of conductors, while having obvious advantages in voltage gradient control, also increases lateral wind-loading and the consequent ROW width component associated with conductor blow-out [91]. For a fixed total cross-section area per pole, the sum of conductor diameters against which wind force will be felt is, neglecting shielding effects, proportional to $\sqrt{n}$ where n is the number of conductors per bundle. Thus going from one to four conductors, for the same total area, will approximately double the wind surface exposure and blow-out force [91].

High Temperature Low Sag (HTLS) conductors can, in the limit, reduce sag by the difference between low and high temperature operation of a normal conductor [92]. As an example 795 kcmil 54/7 ACSR conductor, the difference in sag over a temperature range from 120º F (49º C) and -20º F (-29º C) is approximately 3 meters over a wide range of span lengths [92], [93]. Completely eliminating that sag difference for such cases would lower tower height by 3 meters while keeping equal ground clearance. It would also reduce ROW width required by $2\times3\sin(\phi_c)$ meters where ϕ_c is the conductor blow-out angle.

3.7   Tower Design

HVDC lines use a wide variety of both lattice and steel pole tower designs [4], [69]. Figure 3-11 illustrates their suspension principles only. The simplest T tower configurations in Figure 3-11a and Figure 3-11b may use either I or V insulator systems. The inverted U tower configurations as in Figure 3-11c and Figure 3-11d, allow closer pole-to-pole spacing, which could result in smaller ROW. On the other hand, a variety of free standing support systems, as one of them is shown in Figure 3-11e, can be used either for bipolar systems or (singly) for monopolar systems. As explained before, constrained suspension configurations such as the V string can reduce both tower height and blow-out related ROW width. Configurations which interpose no metallic structure between poles eliminate structure width as a component of minimum ROW requirement. The table in Figure 3-11 indicates the factors to be considered in assessing the contribution of the tower itself to ROW width requirements assuming (a) the insulator configuration itself is adequate for both steady-state operation under representative pollution conditions and overvoltages to

ground; and (b) pole spacing does not result in excessive conductor surface gradient. Tower

material is minimized with options "a" and "b" in Figure 3-11 and increased in *c, d* and *e*

of that figure.

Max. Overvoltage & Gap withstand	Pole-to-Ground	✔		✔		
	Pole-to-Pole			✔	✔	✔
Tower Thickness		✔	✔			
Insulator contribution to Blow-out		✔		✔		
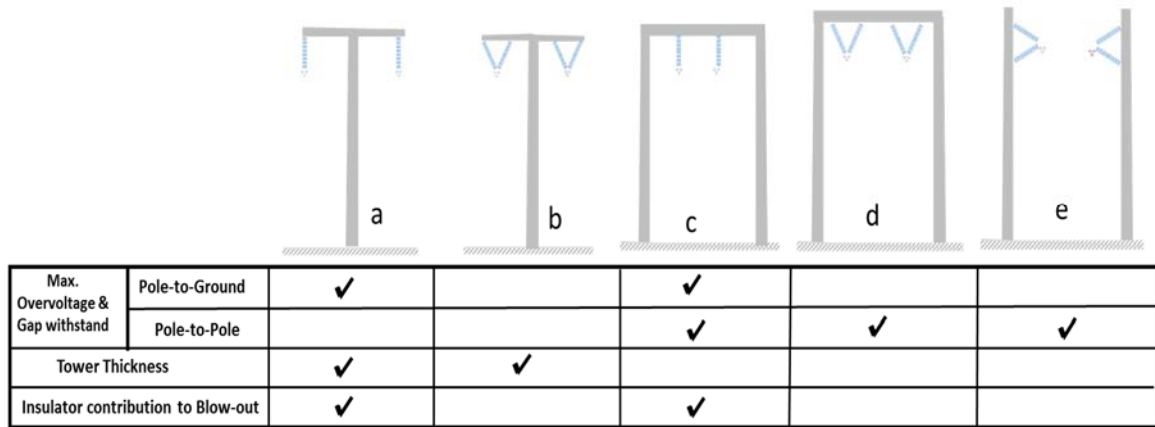
Figure 3-11 Basic tower configurations and configuration-related factors affecting poles spacing

Figure 3-12 compares a conventional lattice tower with a low profile pole tower, both con-

figured as type 'a' illustrated in Figure 3-11 [43], [68]. Public acceptance of new HVDC

lines can be enhanced by both compaction and aesthetically pleasing design as shown in

Figure 3-13. For example, a documented study from the United Kingdom, focused on pub-

lic acceptance of the T-pylon design, asked 2500 people what type of tower they preferred;

39% were in favor of the lattice tower, 56% in favor of the T-Pylon [41]. As for tower

land use, the T-pylon is approximately 1.8 meters in diameter at ground level, requires 2.6

m^2 of total footing area uses no guys whereas the self-supporting lattice tower (7.85 ×7.85

m) requires a footprint of 61 m^2.
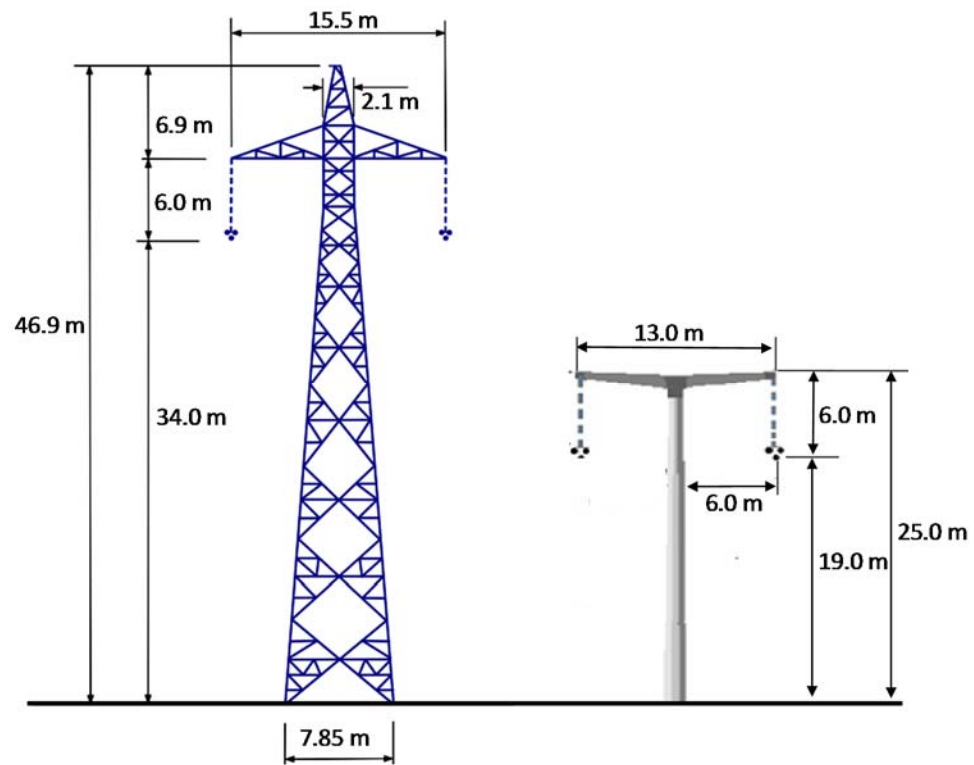
Figure 3-12 Comparison of HVDC Tower Options with equal mid-span ground clearance and thermal loading of 3800 MW at 500 kV [9], [13]

Figure 3-13 Modern pole tower structure for HVDC Transmission (courtesy of Bystrup)

3.8   Conductor Surface Voltage Gradient

The corona performance is an important considerations in designing high voltage transmission lines. It is usually defined by the resulting effects such as corona losses (CL), audible noise (AN), radio interference (RI), etc. The corona discharge phenomenon is mainly influenced by the electric field, or voltage gradient, at the surface of the conductor [38]. The appropriate electromagnetic model to calculate the conductor surface voltage gradient is the quasi static model, in which the electric field distribution is determined directly from the physical parameters of the line configuration and the voltages applied to the conductors [38]. The main physical parameters of the line consist of the conductor diameter, number for the conductors in a bundle, spacing between the conductors and the conductor average height above the ground plane of the conductors.

Calculating the conductor surface gradient is quite simple for a transmission line using a single conductor, but becomes more complicated for bundled conductors, especially as the number of conductors in the bundle increases. Various methods have been developed to calculate the conductor gradient. An easy to use method is the Markt and Mengele's method [94], whereas the method of successive images [95], the method of moments [96] and the charge simulation method [97] are more accurate calculation methods that can be used when there are a large number of sub-conductors in the conductor.

However, irrespective of the method of calculation, this is still inherently a complex problem due to the practical aspects of transmission line configurations, such as variation in conductor sag due to changes in the conductor temperature, proximity of transmission towers, uneven ground surface, finite ground conductivity, non-uniformity of the conductor

surface resulting from conductor stranding and other surface irregularities such as nicks, scratches, material deposits, etc. [98]. Thus there is always a degree of uncertainty in the values of the physical parameters used for the calculations and eventually in the value of the calculated voltage gradient [98].

Hence a number of assumptions [38], [98] which are used in each of the methods are: 1) an equivalent height above the ground (*H-2/3S*), also known as average height, is assumed for each conductor where *H* is the conductor height at the tower and *S* is the conductor sag; 2) the horizontal spacing between the conductors remains constant at a specified value; 3) the conductors are assumed to be smooth cylinders with diameters equal to the outside diameters of the actual stranded conductors, so the calculated gradients are nominal values; 4) ground is assumed to be an infinite horizontal conducting plane surface and the conductors are assumed to be infinitely long circular cylinders parallel to each other and to the ground plane; 5) the proximity effect on electric field distributions of individual conductors in a bundle is ignored, and a uniform field density is assumed.

A broad survey of methods for calculating transmission line conductor surface gradient indicates that errors due to the method of calculation of up to ±2% are acceptable for conductor surface voltage gradients [98]. Due to this fact, Markt and Mengele's method gives sufficiently accurate results for practical transmission line configurations with up to four sub-conductors in the bundle [98]. For line configurations using more than four sub-conductors in the bundle, more complex methods such as the method of successive images are required to achieve results of acceptable accuracy [98]. Hence Markt and Mengele's method is used in this thesis to calculate the voltage gradient of the proposed compact transmission line. The results from this method were deemed adequate for this initial study

of the phenomena and could be improved with a more accurate consideration of the proximity effect between conductors. This is left for future work. The details of the derivation of this method is explained in [38] and also summarized in Appendix B.

Note that for dc voltages, the electric field at any point remains constant, however, it is not uniform around the periphery of a conductor and has points with the defined maximum and minimum values. Experiments have shown that corona effects can be most conveniently characterized by the maximum conductor gradients [69]. In the bundle of two or more sub-conductors, the values of maximum gradient of each can be different. In this regard, the maximum bundle gradient is defined as the highest value among the gradients of individual conductors and the average-maximum bundle gradient is defined as the arithmetic mean of the maximum gradients of the individual sub-conductors. Since in most practical cases, the difference between maximum and the average-maximum values is only around 1-4%, it is common practice to use the average-maximum value and refer to it as the maximum gradient [69].

The maximum gradients of the proposed compact line as well as the conventional line described in Section 3.1, calculated based on Markt and Mengele's method, are presented in Table 3-3. Note that the two shield wires that are used in compact line slightly increase the voltage gradient on the conductors from 23.15 kV/cm to 23.41 kV/cm.

Table 3-3 Conductor surface voltage gradient of the compact and conventional line

	PS	H_{avg}	BS	N	D	Max surf gradient with shield wires
	[m]	[m]	[cm]		[mm]	[kV/cm]
Conventional DC line	15.5	20.13	45.7	3	38.01	22.18
Compact DC line	13	15.13	45.7	3	38.01	23.41

In practical cases, it is recommended that the resulting effects of corona discharge of the transmission lines can be limited to acceptable levels by limiting the conductor surface gradients to about 25 kV/cm [38]. The voltage gradient of a number of HVDC lines from all around the world are given in [44]. In the analysis presented in [44], it is shown that the line parameters that have a major impact on the value of the conductor surface voltage gradients are the number and diameter of sub conductors in the bundle. Thus in high voltage transmission applications, the overall conductor size is often established by corona performance rather than current-carrying capacity [69]. In this case, the conductor diameter can be increased from 38.01 mm to about 40.7 mm for the compact line to compensate the additional voltage gradient on the conductors compared to the conventional line.

It is also shown in [44] that pole to pole spacing and average conductor height has minor impact on the conductor surface voltage gradient. For example in this case, the conductor surface gradient of the compact line will be only reduced to 22.76 kV/cm, if the pole to pole spacing of the line is maintained the same as the conventional line, i.e. 15.5 m.

3.9   Ground Level Field Effects

Another important impact of corona discharge on HVDC lines is the generation of ions of the positive or negative polarities filling the space between the conductors and the ground below and in proximity of the conductors. Human perception of this phenomena, such as hair stimulation and tingling sensations, is due both to the perception of the highly variable flow of ions to the ground, J, and the electrical gradient at ground level, E, which is enhanced by the ion flow [38].

Hence the design of HVDC transmission lines also requires the ability to predict ground-level electric field and ion current distributions. The space charge fields are influenced, in addition to the line voltage and geometry, by ambient weather conditions such as temperature, pressure, humidity, precipitation and wind velocity as well as by the presence of any aerosols and atmospheric pollution [38]. Therefore, prediction methods should be based on a combination of analytical techniques to calculate the space charge fields and accurate long-term measurements under experimental as well as operating HVDC transmission lines to validate the analytical technique and justify their assumptions for the calculations [44]. It was shown in [38], [44] that the ground-level electric field and ion current distribution under HVDC transmission lines depends mainly on the conductor size and the minimum conductor height above ground of conductors. Pole spacing has a minor influence on the ground level electric field and ion current distributions [44]. Hence the proposed compact design maintains the same minimum conductor to ground clearance as the conventional line. The study results of the field effect performance of the Manitoba Hydro Bipole III transmission project is presented in [99].

A review of the scientific literature indicates that exposure to the levels of dc electric field, E, and ion current density, J, existing under operating HVDC transmission lines poses no risk to public health, but may cause some induced current and annoyance effects in humans [100]. In minimizing conductor spacing and height, compacting HVDC lines requires a much more careful assessment of acceptable field and corona and ground field effects than for conventional construction. As more compact and lower profile means of HVDC transmission are sought, the prospect that ground field effects will impose a limit to dc voltage

increases, as does the incentive for both a better understanding of those limits and of possible means for their amelioration.

In an effort to establish design criteria for levels unlikely to produce human complaints, based essentially on the results of the controlled scientific study of Blondin et al [101] on human subjects, experts have recommended that, at ground level, electric fields as cited above, not exceed E=25 kV/m and that ion current density not exceed J=100 na/m^2 [38]. But levels of both E and J vary over an extremely wide range since ion generation varies with both dc operating voltage and weather while the flow of ions is affected by even slight wind currents. Thus software packages attempting to predict E and J values estimate levels that will not be exceeded a certain percentage of the time, either 5% or 10%, depending on the software used [102].

Before judging a proposed compact dc configuration too strictly by the above guidelines one should observe that calculated levels for a number of existing HVDC lines show E and J levels exceeding those guidelines while having operated for many years without a history of complaints [102]. Furthermore, field experience has shown that the negative pole results in substantially higher ground level electric fields, ion current density and lower audible noise than the positive pole, opening the prospect of asymmetrical positive and negative voltages. When the Cahora-Bassa +/- 450 kV bipole line in South Africa, is operated at 533 kV, serious complaint problems occur under the negative pole but not the positive pole, the two poles, in this case, being separated by about 1 km [102]. A similar dominance of negative pole effects has been noted under 500 kV lines operated by the Bonneville Power Administration in the US and another by Furnas in Brazil [102].

Therefore, recently a replication study of Blondin et al is ongoing in Germany which includes more statistical considerations that may be helpful in arriving at more definitive guidelines. However, since no results of that study have been published yet, the old criteria are still used in the literature.

3.10   Conclusions

1. A number of design options may serve to reduce both the height profile and ROW width requirements of HVDC transmission lines. From the discussion in this chapter, their relative effectiveness is shown in Table 3-4.

Table 3-4 General impact of measures to compact HVDC Lines

Resource	Benefit			
	Tower height	ROW Width	Aesthetic Acceptance	Field
Shorter Span	High	High	Mixed	0
Tower Design	Medium	Medium	High	0
Conductor Selection	High	High	0	High
Insulator Configuration	Slight	Medium	0	0
DC overvoltage Reduction	Slight	Medium	0	0

2. The increase in significance of ground level field effects when going to compact construction of HVDC lines, taken together with the high economic impact of criteria adopted, suggest that attention be given to reassessment of criteria assigned to field effect limits.

3. No reliable information is yet available on comparative total costs of an HVDC lattice tower with an equivalent aesthetic designed compact HVDC pylon. However, due to its more pleasing visual profile as determined from public surveys, it is expected environmental, permitting and labor costs will be less for the compact pylon but material costs may be higher. Compact designs can also improve the prospect of HVDC siting on existing road, and rail ROW.

The proposed dc transmission line design, the main focus of this thesis in subsequent chapters, is based on a low profile compact tower structure as shown in Figure 3-12. The span length is reduced to about half of that the length required for conventional designs as shown in Figure 3-9, based on the arguments presented in Section 3.5. The insulators and conductor specifications are the same as Manitoba Bipole III HVDC line as listed in Table 3-1.

Chapter 4

Modelling the Control and Operation of MMC HVDC Transmission System

This chapter describes the development of a detailed electromagnetic transient model for a point to point MMC-VSC transmission with the proposed overhead line and cables. The model is used to assess the overvoltages on the HVDC transmission line for considering the dc line insulation coordination. It is shown that control methods and their parameters as proposed in the model can be designed to minimize the overvoltages. PSCAD/EMTDC, a powerful electromagnetic transient simulation tool, is the recommended tool for performing a comprehensive overvoltage assessment of the MMC HVDC transmission line.

As a prerequisite step, essential details associated with the system modeling, including both components and control systems, for the operation of the MMC HVDC transmission system, are provided in this chapter.

4.1   System Specifications under Consideration

Different converter technologies (MMC with half-bridge and full-bridge sub-modules) and transmission configurations (symmetrical monopolar and bipolar configurations) of MMC-HVDC systems that will be considered in this chapter are shown in Figure 4-1. The dc transmission line for each configuration are pure long distance compact overhead lines (1000 km) and also underground cables (200 km) in series with a short distance of compact overhead lines (50km).

Converter SM	System Configuration	HVDC Transmission Line
	Bipole	1000 km
	Symmetrical monopole	200 km 50 km
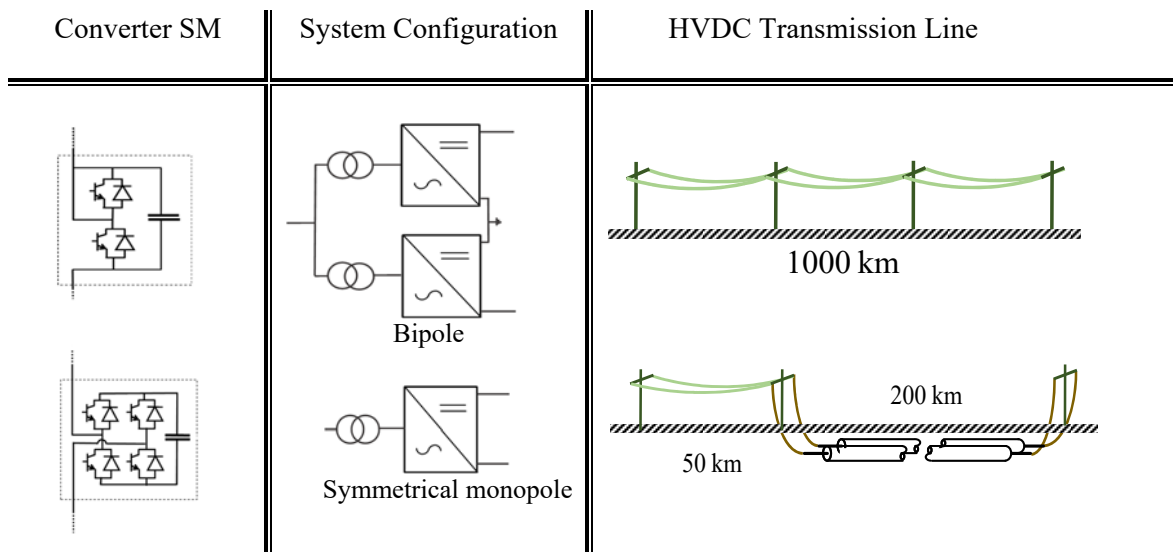
Figure 4-1 Overview of the system specifications under consideration

The specifications of these systems have the following characteristics:

- Each converter is rated at 1000 MW.

- The transmission line voltage for all the cases is ±500 kV.

- The line smoothing reactor is 10 mH.

- The ac system parameters at each end are listed in Table 4-1.

Table 4-1 AC system parameters

AC system 1		AC system 2	
Ac voltage	500 [kV]	Ac voltage	138 [kV]
SCR	$4 \angle 85^0$	SCR	$3 \angle 85^0$
Transformer(monopole)	500 :650 [kV]	Transformer(monopole)	138 :650 [kV]
Transformer(bipole)	500 :325 [kV]	Transformer(bipole)	138 :325 [kV]
	1200 [MW]		1200 [MW]
	0.1 [pu]		0.1 [pu]

4.2   Modular Multilevel Converters

4.2.1   Topology

The modular multi-level converter (MMC), which is shown in Figure 4-2, consists of three phase units, each with upper and lower arms. Each arm has a modular structure with a number of n series connected sub-modules which enables the MMC to generate a high number of voltage levels in each arm [10]. The MMC converters are classified into two groups based on the sub-module structure, which can be half-bridge or full-bridge structure, as explained in the next section.
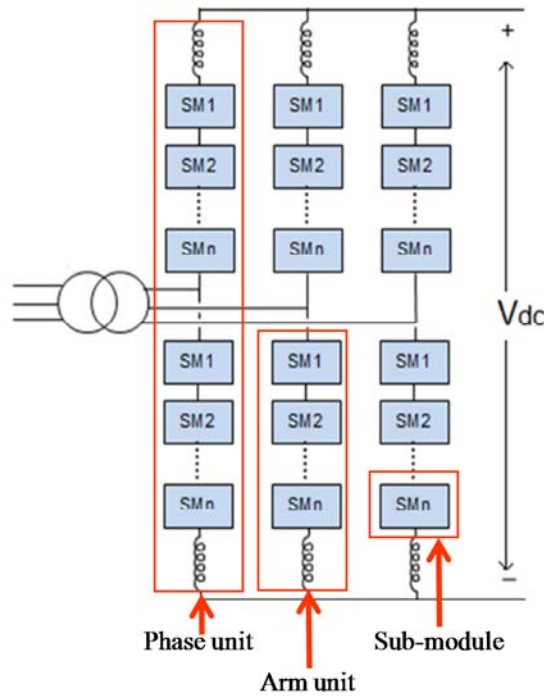
Figure 4-2 Schematic diagram of a Multi-Modular Converter (MMC)

4.2.2   Sub-Module Structure

The sub-module(SM) structures and their switching details are shown in Figure 4-3. A half-bridge SM as in Figure 4-3(a) contains two standard IGBTs and their respective free-wheeling diodes whereas a full-bridge sub-module has four of them. Assuming the capacitor voltage (V_c) is constant, the output voltage of each sub-module depends on the switching states. It can be V_c or zero, corresponding to the 'ON' or 'OFF' state for the SM. For the full-bridge sub-module shown in Figure 4-3(b) it also can be - V_c [103].

	S_1	S_2
V_c	on	Off
0	off	on
block	off	off

(a) Half Bridge Sub-Modules

	S_1	S_2	S_3	S_4
V_c	on	off	off	on
$-V_c$	off	on	on	off
0	on	on	off	off
0	off	off	on	on
block	off	off	off	off

(b) Full Bridge Sub-Modules
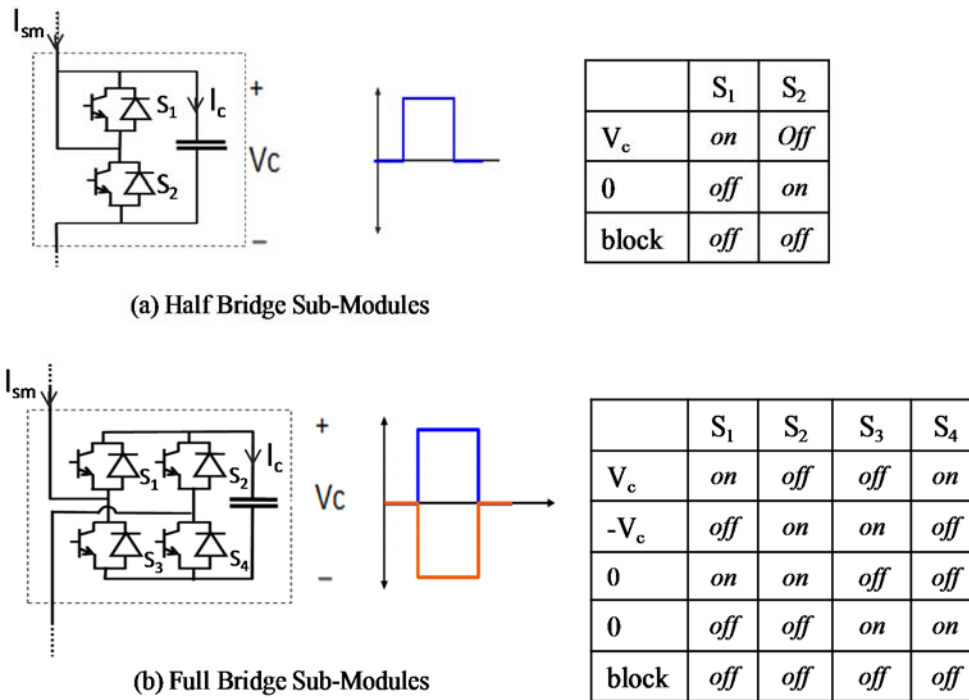
Figure 4-3 Schematic diagram of the MMC sub-modules along with the switching functions

The half-bridge converter structure has fewer switching elements in the current path and consequently less power loss and converter costs comparing to full-bridge converters. However, this structure cannot block the over-currents resulting from a dc side fault [48]. Since the full-bridge sub-modules can have a reverse voltage polarity, it is possible to reduce the dc voltage immediately to limit the fault current while maintaining the required ac voltage at the converter ac side [48]. Moreover, full-bridge converters are also capable of reduced dc voltage operation without tap changer action of the converter transformer in case of extensive polluted conditions such as brush fires. This feature of full-bridge converters will be demonstrated in Chapter 6.

From the dc side, all three phase units are a parallel connection of three voltage sources. Because practically there will be a small difference in instantaneous voltage values of the phase units that are connected in parallel, a valve reactor is located in each arm. The valve reactors reduce the circulating currents between individual phase units, and also are capable of reducing the rate of the rise of the current during the dc side faults [104].

4.3   MMC HVDC Control Systems

Figure 4-4 shows a single-line diagram of one side of a generic point to point MMC HVDC system which the converter is connected to a dc circuit on one side and to an ac circuit on the other. VSC based converters can exchange real (P) and reactive (Q) power with the ac system [46] and thus operate in all four quadrants of the PQ plane.
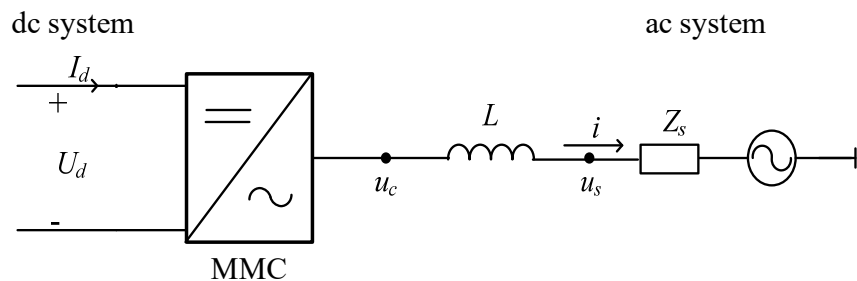
Figure 4-4 Single-line diagram of a generic MMC system configuration

The control system required for the MMC HVDC transmission systems includes three levels as shown in Figure 4-5, namely the dispatch controller, the upper level controller and the lower level controller systems, which will be described in the following sections [29].

Dispatch control	Upper level control	Lower level control
Set points for P_{dc}, V_{dc}, Q, V_{ac}, etc	V_{ac} reference signal	SM switching pulses
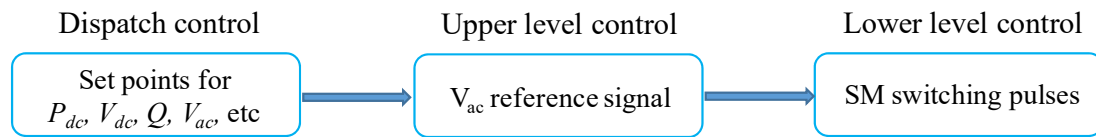
Figure 4-5 Control hierarchy in MMC HVDC systems

4.3.1   Dispatch Controller System

The dispatch controller originates from an offsite system operator or coordinator which is similar to or as part of the ac grid operator system. As dictated by market conditions or considerations by the Independent System Operators (ISO), it outputs the operating set points, such as real and reactive power and ac and dc voltages, or the operating control modes for the converter to meet both ac and dc system requirements [29]. The system controller mode depends on the system application or the specific condition, such as fault. The use of the most common control modes, such as choosing one ac operating variable (either ac voltage or reactive power) and one dc operating variable (either dc voltage or dc power), is explained as follows [29].

- Ac voltage vs. reactive power control

The ac voltage control is generally used to maintain the ac voltage at the connected bus especially when the ac system is weak. If the VSC is feeding into an isolated ac system with no other form of active power source of any significance, the ac voltage controller will automatically control power to the load. In this case, the dc voltage should be constant. Therefore, this assumes another converter, such as the sending end of a VSC transmission link, independently controls the dc side voltage [46].

When other ac controllers are operating to maintain ac voltage or the ac connection is strong, a reactive power controller can be used. Each converter can control its reactive

power flow independent of the other station at any set point between the limits of the con-
verter [46].

- Dc voltage vs. real power control

In order to regulate the required voltage level across the dc link, the active power flow into
the dc link needs to be controlled. Therefore, the converters at the two ends of the scheme
must be controlled to work together in a VSC transmission scheme. To do this one of the
two converters connected to the dc voltage bus is required to control the dc voltage. Both
the voltage and power controllers operate by controlling the power flow. For the voltage
controller, the desired dc bus voltage is used as a reference, and the power is controlled to
charge the dc line capacitance to this value [46].

To control the active power flow, the phase angle δ of the fundamental frequency compo-
nent of the ac voltage at the converter side of the interface reactance should be regulated.
Power is absorbed from or provided to the ac system depending on whether δ lags or leads
the phase angle of ac bus voltages. In most implementations, delta is not controlled directly,
but real and reactive components of the current are controlled using a decoupled control
strategy described below [46].

4.3.2   Upper Level Controller System

The control mode and the reference signals of the upper level control, such as active power,
reactive power, ac and dc voltages, comes from the dispatch controller system. A voltage
sourced converter has two degrees of freedom, namely the magnitude and phase angle of
the ac voltage generated by the converter. The exchange of active and reactive power be-
tween the MMC and the ac system is controlled by the phase angle and amplitude of the

MMC output ac voltage respectively in relation to the voltage of the ac grid system. Control

of these quantities is generally achieved by means of Decoupled Vector Control strategy

[59]. The upper level control eventually prepares the reference ac voltage waveforms for

the lower level control.

- Decoupled Vector Control

Decoupled vector control is a current control strategy that results in independent control of

real and reactive power by removing the coupling between the real and the imaginary com-

ponents of the output current [59]. One of the advantages of this method is that the current

control inherent in the strategy can limit overloading of the valves [105], [106].

The relationship between ac grid voltage, u_s, converter voltage, u_c, and the current, i, on

the ac side is:

$$u_c - u_s = L\frac{di}{dt} \qquad\qquad 4.1$$

By applying the Park transformation in a synchronous reference frame to equation (4.1),

the d-axis and q-axis components of the converter voltage are:

$$u_{cq} = L\frac{di_q}{dt} + \omega L i_d \qquad\qquad 4.2$$

$$u_{cd} = L\frac{di_d}{dt} - \omega L i_q + |u_s| \qquad\qquad 4.3$$

Note that in the synchronous reference frame, $u_{sq} = 0$ and $u_{sd} = |u_s|$. A phase-locked

loop module (PLL) generates the reference frame angle θ by locking onto the ac voltage,

u_s, at the point of connection with the ac grid.

In this system, the instantaneous active power can be expressed as:

$$P = u_{sa}i_a + u_{sb}i_b + u_{sc}i_c \qquad\qquad 4.4$$

Therefore, the active and reactive powers as a function of the d-axis and q-axis components

in the synchronous reference frame are expressed as follows.

$$P = \frac{3}{2}|u_s|i_d \quad\text{and}\quad Q = \frac{3}{2}|u_s|i_q \qquad\qquad 4.5$$

Equation 4.5 shows that independent control of active and reactive power is possible if i_d

and i_q can be controlled independently. However, equations 4.2 and 4.3 show that i_d

and i_q are coupled due to the terms $\omega L i_d$ and $-\omega L i_q + |u|$ in the corresponding equations,

requiring special measures to achieve their independent control. To solve this problem, a

decoupled controller, which consists of the feedback loops and proportional-plus-integral

(PI) compensation, as expressed in equations 4.6 and 4.7, can be used [59].

$$u_{cq} = (K_{pq} + \frac{K_{iq}}{s})(i_q^* - i_q) + \omega L i_d \qquad\qquad 4.6$$

$$u_{cd} = (K_{pd} + \frac{K_{id}}{s})(i_d^* - i_d) - \omega L i_q + |u_s| \qquad\qquad 4.7$$

This method consists of a two level cascaded control system as illustrated in Figure 4-6;

the system controllers that provide the d-axis and q-axis current reference values and the

internal current controller that generates the reference voltages for the converter [107].

As shown in equation 4.5, the reference value of the active current i_d can be derived from

the active power or the dc voltage controller, and the reference value of the reactive current

i_q can be obtained from the reactive power or the ac voltage.
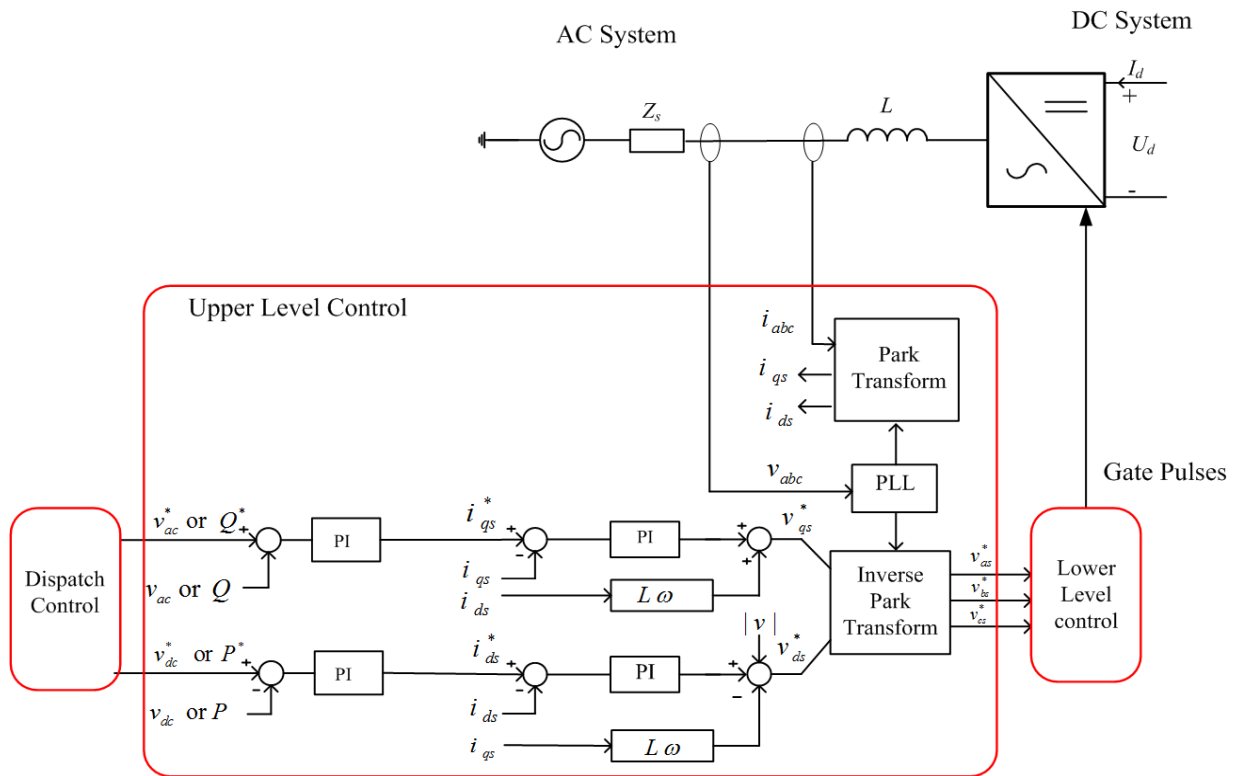
Figure 4-6 Detailed structure of the upper level control

4.3.3   Lower Level Controls

The main role of lower level controller is to generate the switching pulses for the converter

to produce the ac voltage waveforms that the upper level controller demands. Here a typical

ac voltage waveform generation method along with the sub-module capacitor voltage bal-

ancing in MMC HVDC systems will be explained.

- Output Voltage Waveform Generation

In MMC converters, the sum of the sub-module output voltages of each phase unit should

be equal to the reference dc voltage at any moment. Each of the half-bridge/full-bridge sub-

modules can be controlled independently and selectively so that the voltage of each sub-

module adds up to form a near-sinusoidal stepwise voltage waveform at the converter ac

terminals [104]. There are several output voltage synthesis methods proposed for the MMC

switching operation such as nearest level estimation [104] and multilevel PWM-based [108]. Since the details of a specific method do not have a significant impact on the dc link system performance, the nearest level estimation is used in this thesis for simulation models.

Figure 4-7a shows the reference waveform, V_{ref}, for ac voltage (m ($0 < m \leq 1$): modulation index, which is defined as the ratio between the peak value of the fundamental phase to ground ac output voltage of the converter to the pole to ground dc voltage). In order to generate this waveform by MMC, the instantaneous reference voltage of the upper arm and lower, V_{i-up} and V_{i-bt} respectively, should be,

$$V_{i-up} = V_{dc}/2 \times (1 - V_{ref}) \qquad V_{i-bt} = V_{dc}/2 \times (1 + V_{ref}) \qquad 4.8$$

If the output voltage of each sub-module is V_c, the output voltage of each arm can be a stepwise waveform as the multiples of V_c, at every instant. Therefore, to determine the required number sub-modules with "On" state at a certain moment, the arm reference voltage amplitude is compared with total n discrete quantization thresholds.
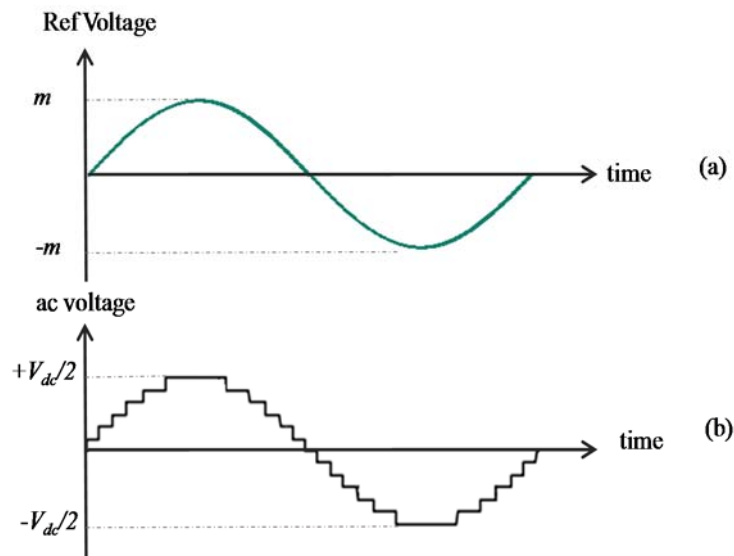
Figure 4-7 AC voltage output waveform generated by MMC converter

In half-bridge converters, the peak value of the ac voltage cannot exceed the dc pole voltage as shown in Figure 4-7b. During the steady state operation, the total number of sub-modules with the ON state on the lower and upper arms combined is constant at any instant, and is equal to n, where $n = V_{dc} / V_c$. In other words, if the number of sub-modules with ON state on upper arm is n_{up}, then the number of sub-modules with ON stare on lower arm should be $n - n_{up}$ [109]. However, due to bipolar output voltages of the sub-modules in full-bridge converters, the ac voltage can be controlled independently of the dc voltage, which can result in a modulation index greater than one [48], which will be explained more in the next chapter.

- Capacitor Voltage Balancing

Once a sub-module capacitor is inserted in the arm, it will be charged if the direction of the arm current is positive or discharged if it is negative. The capacitor voltage remains unchanged when the sub-module is "OFF". Therefore, a capacitor voltage balancing control mechanism is required to maintain the charge and voltage of the sub-module capacitors balanced during the steady state operation. One of the commonly used capacitor voltage balancing algorithms, proposed for the MMC operation is based on sorting the sub-module capacitor voltage values [109].

Figure 4-8 illustrates the block diagram of the "nearest level estimation" control technique. As explained before, the total number of 'ON' state sub-modules is changing between 0 to *n* during one cycle generation of the converter output voltage waveform. However, there are different switching combinations that can produce any desired voltage level at any instant [109].
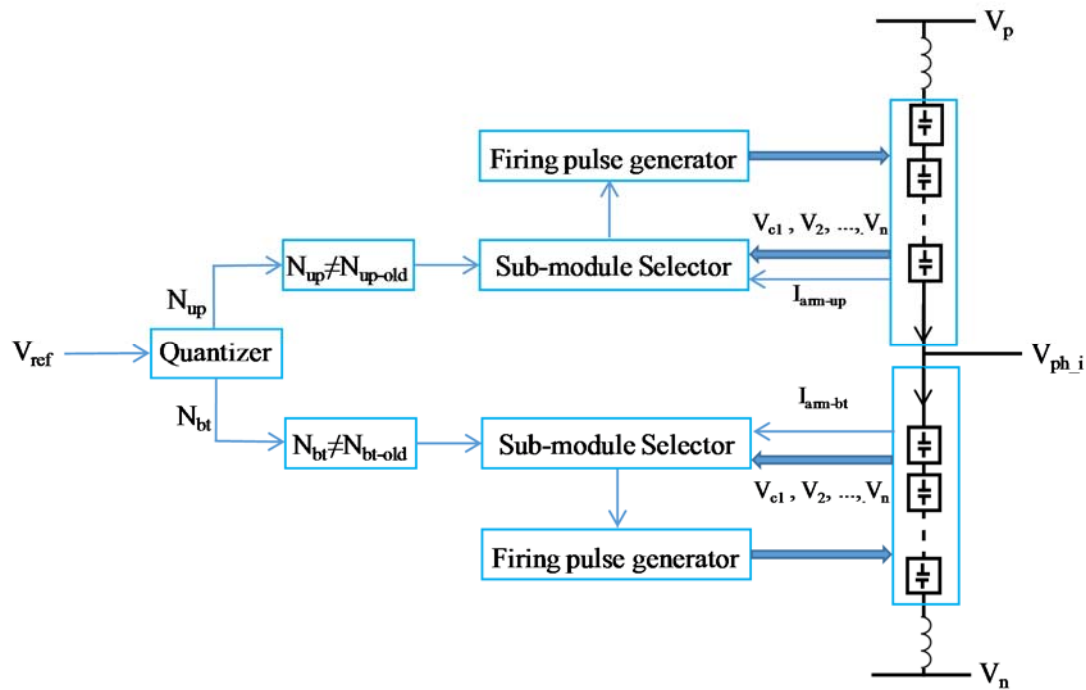
Figure 4-8 Block diagram of the "nearest level estimation" control technique

As shown in Figure 4-8, the 'Quantizer' calculates the required number of 'ON' state sub-modules based on the reference voltage. When a step change happens at the output signal of the "Quantizer", the 'Sub-Module Selector' should select the appropriate sub-modules in the arm unit to turn on [108]. This component receives the measured arm current along with the capacitor voltages of each sub-module in the associated arm unit. First, it creates a list of sub-modules by sorting them from the lowest to highest capacitor voltage. Then, it detects the direction of the arm current. If the direction of the current is positive, the sub-modules at the bottom of the sorted list (i.e. with lowest voltages) are selected so that their capacitor voltage can be increased. On the other hand, when the current direction is nega-tive, the sub-modules at top of the list are selected hence their voltages can be decreased. This process is applied for all the MMC arm units [108].

4.4   DC Transmission Line and Cable Models

Overhead lines consist of a number of cylindrical conductors in a bundle. Since the voltage of each sub-conductor is the same and the pole current is evenly divided among them, the conductor bundle can be reduced to a single equivalent conductor [38]. As explained in Chapter 2, single core underground/undersea cables also have multiple conducting layers in most practical systems. They consist of the core conductor in the center and usually up to three concentric, grounded conducting layers which are separated by the insulating layers. Hence, each single core cable is equivalent to a multi-conductor system, e.g. consisting of three conductors as the core conductor, metallic sheath and armor [10].

Therefore, for HVDC lines with positive and negative poles, there are mainly two conductors for overhead lines and six conductors for underground/undersea cables that need to be considered in the modeling methods. For simplicity in the following discussion, the term 'transmission line' refers to both the overhead line and the underground/undersea cable systems, as the model development for both are the same. Each conductor in the line modeling is also referred to as a "phase". Note that it is not the ac side phases.

In transmission lines, a voltage signal will travel from one end along a conductor at its propagation velocity (near the speed of light), until it is reflected at the other end. Therefore, the analysis of voltage and current along a transmission line can be described by the wave equations or also known as 'telegrapher's equations' [110]. Assume a short segment of the transmission line, as shown in Figure 4-9, whose length is small comparing to the wavelength. The line voltages and currents are related by equations 4.9 and 4.10, where Z and Y are series-impedance and shunt-admittance of the line per unit length [110].

$$\frac{dV}{dx} = -Z \cdot I \qquad\qquad 4.9$$

$$\frac{dI}{dx} = -Y \cdot V \qquad\qquad 4.10$$
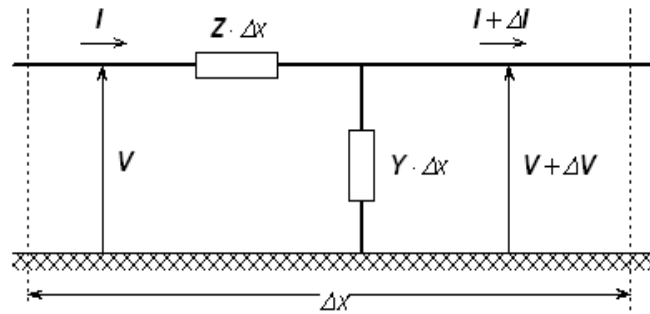
Figure 4-9 An equivalent circuit of a short transmission line segment [111]

In multi-phase systems, Z and Y are square matrices, and V and I are vectors, both with dimension equal to the total equivalent number of conductors. Z and Y are generally calculated by the method of coaxial loops [110].

4.4.1   Modeling Techniques in Electromagnetic Transient Simulations

In electromagnetic transient simulations, there are generally two techniques to represent the transmission lines; the π-section approach, where the multi–phase systems can be modeled by lumped passive circuit elements and the distributed parameter models which are based on the traveling waves [111]. The transmission lines are nonlinear in nature due to frequency dependency in conductors and the ground or earth return path. Therefore, distributed modeling approach can be further sub-divided into single-frequency, also known as Bergeron model [110], and the frequency-dependent models. Frequency dependent models include the frequency dependency of all distributed parameters of the line [112].

There are two popular frequency dependent models available, the frequency dependent mode model (FDMM) [112] and the frequency dependent phase model (FDPM) [113]. An overview of each modeling method is presented in Appendix C.

The studies have shown that the choice of transmission line model can have a significant impact on the overall result for typical HVDC transient studies. Simulation models for such systems are required to be accurate over a very wide frequency range from zero or near zero Hz, which is the nominal frequency on the HVDC lines, to several tens of kHz for converter switchings and other transients. Therefore, the frequency dependent phase model is the most suitable and reliable model to use for overvoltage assessment of the MMC-HVDC system. However, it still requires diligence in some cases to ensure accurate curve fitting [114].

Table 4.2 and Table 4.3 show the detailed data of the geometry and some material properties of the compact overhead lines and underground cables that should be provided for frequency dependent models in PSCAD/EMTDC simulation cases used for studies in Chapter 5. The per unit length parameters of each line are given in Table 4.4.

Table 4-2 Compact overhead line parameters for FDPM

Conductor Type	806-A4-61 AAAC (=1,590 MCM ACSR)
Total bundled sub-conductor	3
Diameter	38.01 [mm]
Sub-conductor spacing	45.7 [cm]
Pole to pole spacing	13 [m]
Conductor sag	5.8 [m]
Conductor height at the tower	18.4 [m]
Shield wire height at the tower	24.4 [m]
Spacing between shield wires	13 [m]
Conductor dc resistance	0.03206 [Ω /km]
Shield wire dc resistance	2.8645 [Ω /km]

Table 4-3 Underground cable parameters for FDPM

Cable Layer	Radial Thickness [mm]	Resistivity [Ωm]	Relative Permittivity	Relative Permeability
Core conductor	26.5	2.82e-8	-	1
Insulator 1	26	-	2.5	1
Sheath	4.25	2.06e-7	-	1
Insulator 2	5.5	-	4	1
Armour	7.5	1.8e-7	-	400
Insulator 3	6.8	-	4	1

Table 4-4 Per unit length parameters of the overhead line and underground cable

	R(Ω/km)	L[mH/km]	C[μF/km]
Compact DC OHL ($\pm$ 500 kV)	0.011	0.85	0.013
Underground cable ($\pm$ 500 kV)	0.07	0.21	0.34

Chapter 5

Slow Front Overvoltage Analysis of MMC HVDC Systems under Fault Condition

Chapter 4 described fundamental background regarding the control, operation and modeling of MMC HVDC systems for electromagnetic transient (EMT) studies such as insulation coordination. This chapter describes several major contributions of this thesis. These contributions are key to maximizing the degree of compaction that it is practical to achieve with HVDC lines, recognizing that the need to accommodate overvoltages is critical to insulator length requirements as well as clearances required within the tower structure and, according to many electrical codes [115], the minimum clearance to ground. Thus overvoltage limitation is important to both tower height and right-of-way width requirements. The chapter first presents the results of a comprehensive transient overvoltage assessment of MMC HVDC systems due to faults on the transmission lines. The fault contingencies that result in the most significant overvoltage stresses on the symmetrical monopole and bipole transmission configurations are considered. The studies include overhead HVDC lines as well as overhead lines and underground cables in the same circuit. A sensitivity

analysis on the most important parameters, such as line length, fault time and location, etc., that may impact the magnitude and duration of overvoltages in the dc line is also performed. The worst case scenarios are determined for the design of overvoltage limiting devices, such as surge arresters and for finding minimum air clearances.

In this chapter, new control approaches are also proposed that significantly reduce the dc side overvoltage and consequently minimize insulator length and air clearances for maximum compaction of the HVDC overhead lines. Moreover, due to these control actions for overvoltage reduction, the required surge arrester size for line insulation is also reduced.

5.1   Slow Front Overvoltage Assessment in MMC-HVDC

Slow-front overvoltages on HVDC transmission lines may result from ac or dc side faults, transformer saturation, line energization, line switching and other system events [47]. The most significant slow-front overvoltages occur on the un-faulted conductor due to single pole to ground faults [116]. The magnitude and duration of these slow-front overvoltages depends on system configuration, fault location, line length, line smoothing reactor (L_l as shown in Figure 5-1) and etc. The duration of these overvoltages is typically in the order of milliseconds.

Dc pole to pole faults reduce the dc pole-to-ground voltages to zero, which is verified by the simulation results shown in subsequent paragraphs. But they result in overcurrents that may be large enough to damage converter stations [30]. These overcurrents need to be

considered in the design of the protection systems for such stations. However overcurrents due to pole to pole faults need not be considered for dc line insulation coordination.

In this section overvoltages are first evaluated without any control action from the converter station or limitation by surge arresters. Therefore the resulting overvoltages are the same whether converters are full-bridge or half-bridge in design.

The location of a fault has a significant impact on the overvoltage magnitudes that appear on a long dc overhead line during a pole to ground fault. Therefore in order to assess the maximum overvoltage magnitudes at any location, it is convenient to divide the line into small segments, each of 50km in length as shown in Figure 5-1. Thus the faults are considered at different positions along the line, i.e., at F_{NG1}, F_{NG2}, ..., F_{NGn}. The fault is consecutively applied at each of these locations on one pole (e.g., the negative pole) and the overvoltages, V_{P1}, V_{P2}, ..., V_{Pn} along the line on the complementary pole (e.g. positive pole) are measured and recorded for each of those faults. Eventually, the maximum overvoltage magnitude at each location is determined by recording the largest voltage found at that location. Note that the maximum overvoltage always occurs on the complementary pole due to fact that the first pole is faulted and that, due to symmetry, it is not necessary to repeat this test with the faulted poles switched.
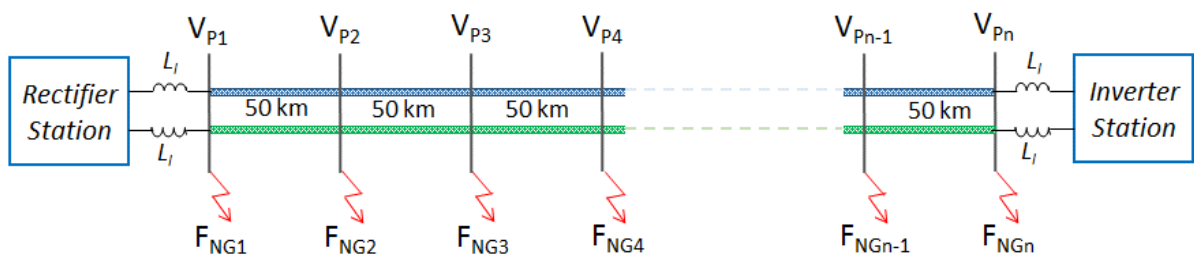
Figure 5-1 Overhead line arrangement for dc overvoltage assessment

Figure 5-2 shows that in case of an underground cable in series with a short section of overhead line dc transmission, the fault is applied at the rectifier station, at the cable and overhead line junction, and at the middle of the cable and at the inverter station. The resultant overvoltages are measured and recorded at each of these intersections.
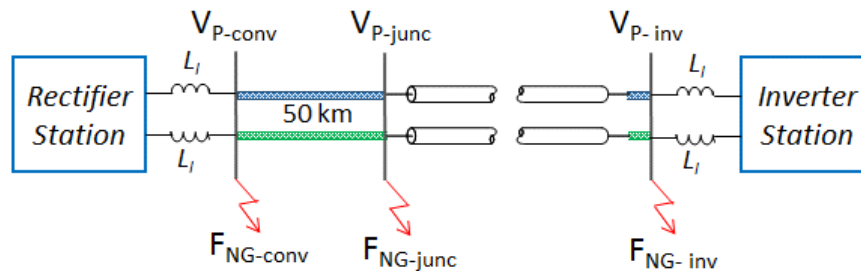
Figure 5-2 Overhead line and cable arrangement for dc overvoltage assessment

To consider the impact of the line geometry, the study was performed for both the conventional and compact overhead lines. Moreover, in order to consider the impact of the line length and line smoothing reactors on the slow front overvoltages, the study was also repeated for:

1. lines with 500 km and 750km length, and

2. lines with smoothing reactors of 100 mH at each end.

The modeling of the study cases are explained in Chapter 4. The following subsections present the simulation results of each case. Then the simulation results reported here will be explained by analytical considerations in Section 5.2.

5.1.1   Overvoltages in the Symmetrical Monopole MMC-VSC Case, using OHL Transmission

Figure 5-3 shows the peak value of the slow front overvoltage that can occur at any point throughout conventional and compact HVDC overhead transmission lines with symmetrical monopole configuration. This graph shows that the compact line has lower overvoltage magnitude.

Figure 5-3 Maximum peak value of slow front overvoltages on compact and conventional dc overhead lines of symmetrical monopole configuration

The simulation results of these contingencies demonstrate that for the symmetrical monopolar systems, the maximum peak value of the overvoltage along the line is about 3 pu and is larger close to the converter stations than in the middle of the line. The maximum overvoltage at each converter station occurs when the fault location is closer to the converter station at the opposite end of the line. For instance, when the fault is closer to the rectifier station, the maximum overvoltage occurs at the complementary pole of the inverter station and vice versa. Moreover, in this configuration, the minimum peak value of the overvoltage on the unfaulted pole appears in the proximity of the fault location. The dc line voltage

waveforms at the terminals of the rectifier and inverter stations during a pole to ground dc

faults resulting in maximum and minimum overvoltages at each converter station are

shown in Figure 5-4.

(a)

(b)

(c)

(d)
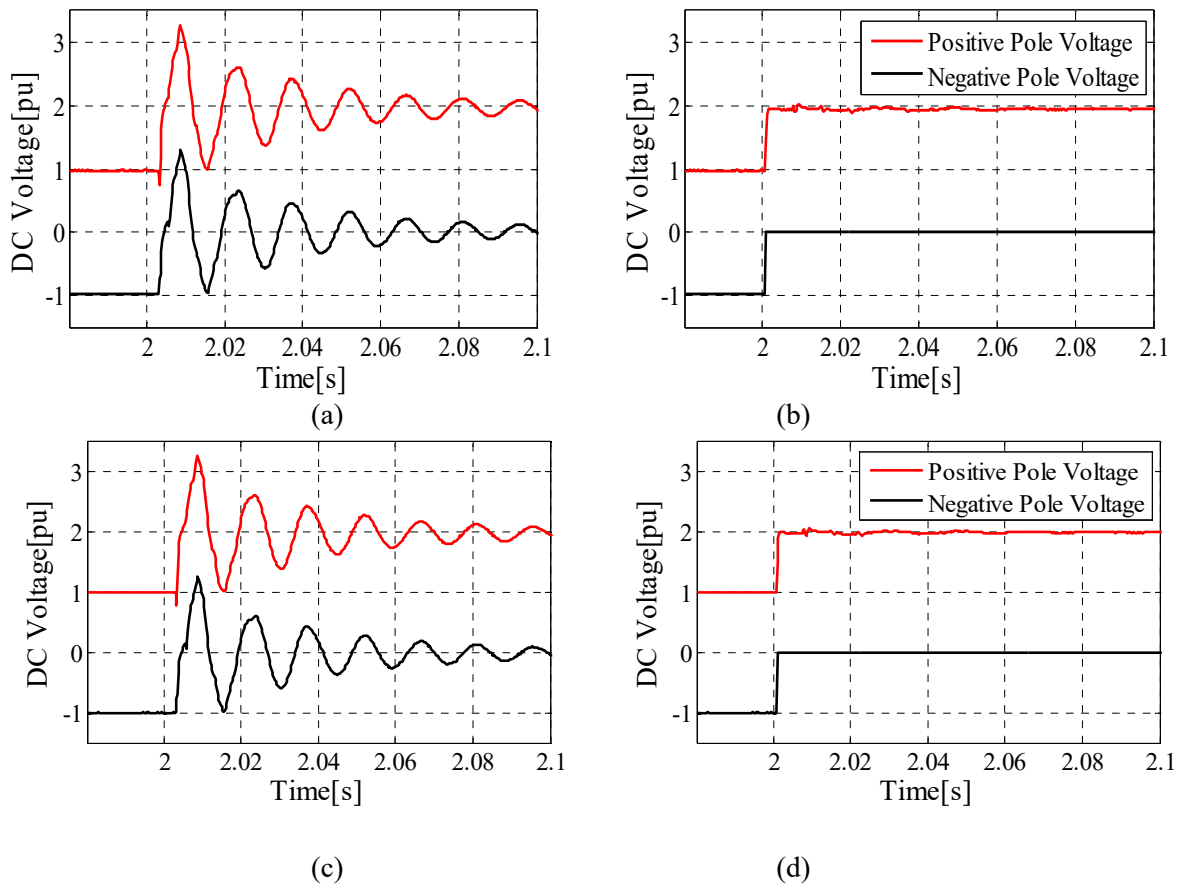
Figure 5-4 Dc line voltage waveforms at: (a) the rectifier terminals due to the fault that results in maximum overvoltage, (b) the rectifier terminals due to the fault that results in minimum overvoltage(c) the inverter terminals due to the fault that results in maximum overvoltage, (d) the inverter terminals due to the fault that results in minimum overvoltage

Figure 5-5 shows the impact of ac network side faults on the dc overvoltages. Both three

phase to ground and single phase to ground faults are considered on the ac side of the

rectifier station, and the (rectifier side) dc overvoltage is measured. It can be observed that

resulting overvoltage at dc side of the rectifier is negligible.
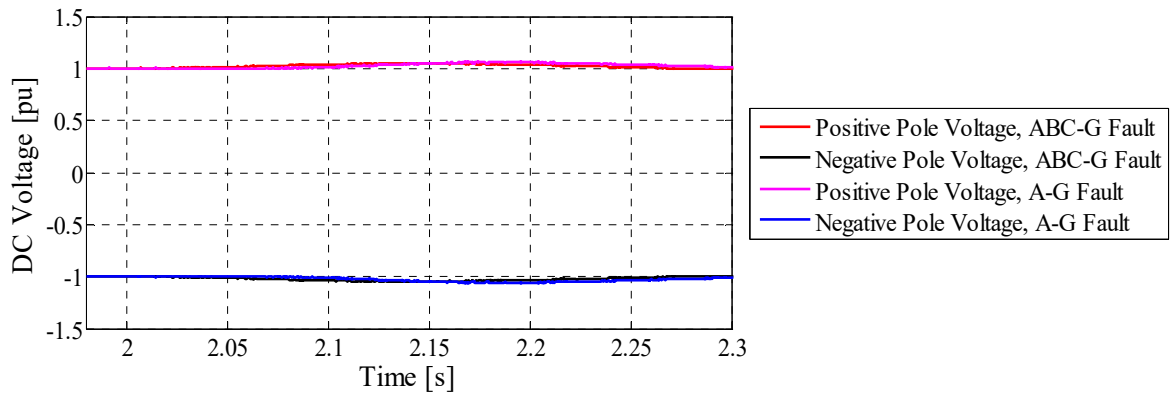
Figure 5-5 Dc line voltage waveform at the rectifier side due to three phase-to- ground and single phase- to-ground faults on the ac side of the rectifier station

Figure 5-6 shows the dc line voltage waveforms at the rectifier and inverter stations for a pole to pole line fault on the dc side close to the inverter station. It can be observed that pole to pole faults result in no overvoltage at the remote converter (rectifier) and a small overvoltage (no more than 20%) of very short duration (~1ms); and hence from the insulation point of view, need not be a concern compared to other scenarios.
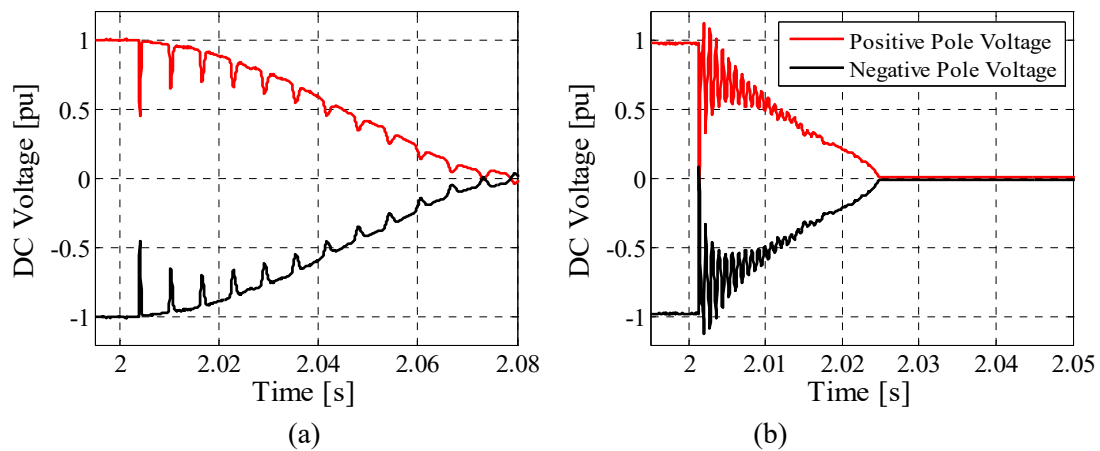
Figure 5-6 Dc line voltage waveforms at (a) rectifier, (b) inverter side due to pole to pole fault dc side close to the inverter station

To investigate the impact of the line length, the maximum peak value of the slow front overvoltages of a 750 km and 500 km dc overhead lines, along with the base case (1000

km), are presented in Figure 5-7. Simulation results show that these values are smaller for

the shorter lines. However, it is also obvious that in symmetrical monopole configurations,

regardless of the line length, the overvoltages at line sections close to the converter stations

are larger than other locations. Moreover, from the voltage waveforms shown in Figure

5-8, it is evident that the voltage of a longer overhead line oscillates with a lower frequency.

This is due to its larger equivalent line inductance and capacitance and eventually lower

resonance frequency; an issue which will be explained in more detail in Section 5.2.
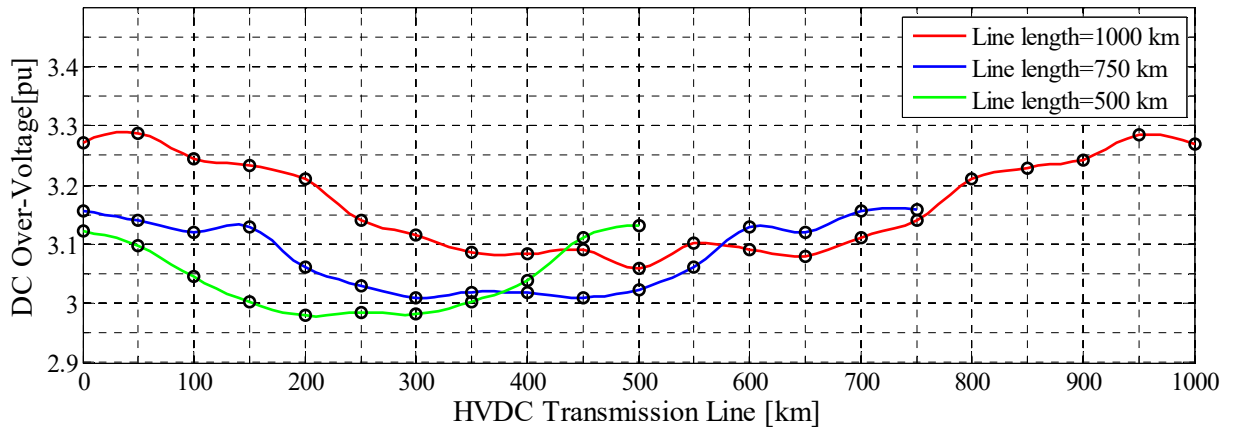
Figure 5-7 Maximum peak value of the slow front overvoltages on the symmetrical monopolar dc overhead lines with different line length
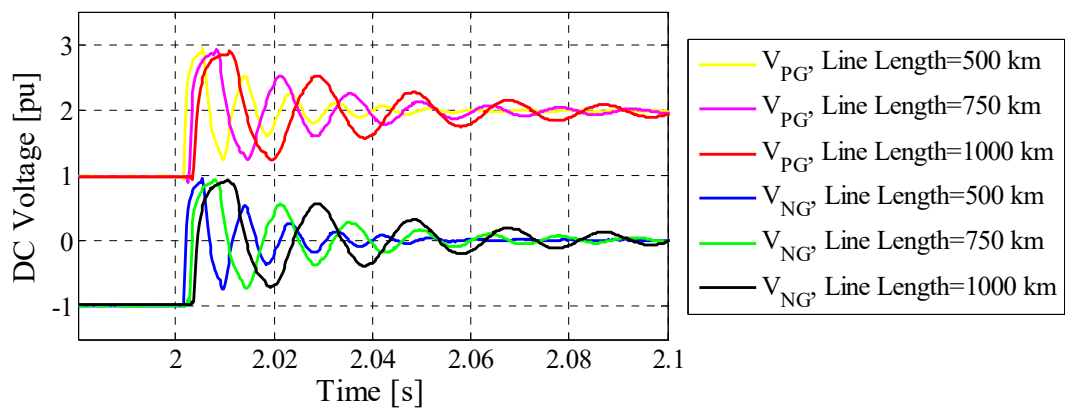
Figure 5-8 Dc line voltage waveforms at the rectifier terminals for different dc line length during pole to ground fault at the inverter side

Since the smoothing line reactor also affects the line equivalent impedance and conse-quently transient performance of the dc line, the fault study is also repeated for the system with a smoothing line reactor of 100 mH as shown in Figure 5-9. The dc line voltage wave-forms at the rectifier side shown in Figure 5-10, demonstrate that a larger value of the line reactance results in a delay in voltage rise at the remote station.
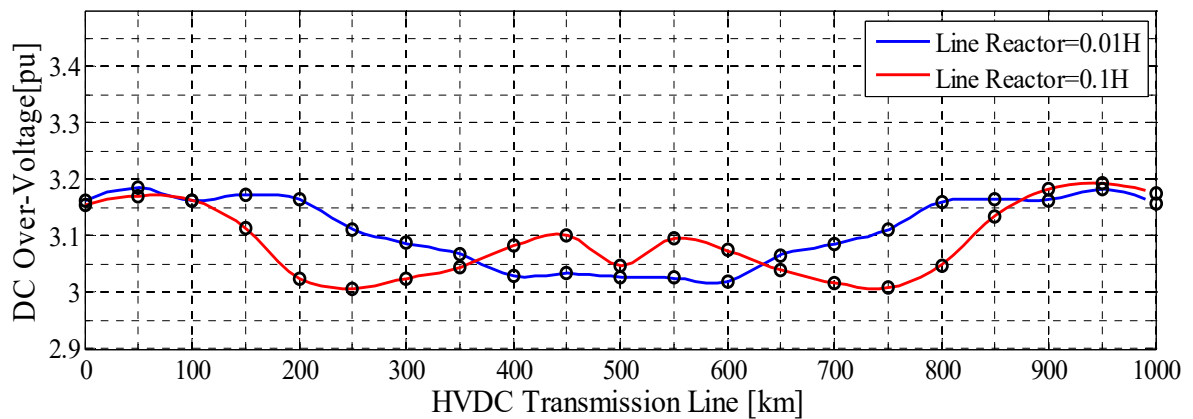
Figure 5-9 Maximum peak value of a slow front overvoltages on the symmetrical monopolar dc overhead lines with different line smoothing reactors
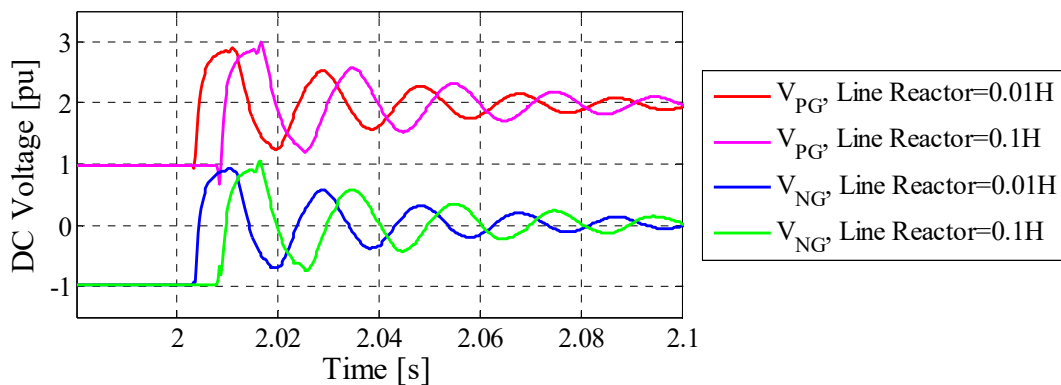
Figure 5-10 Dc line voltage waveforms at the rectifier side for different line reactors during pole to ground fault

5.1.2   Overvoltages on the Bipole MMC-VSC Case, using OHL Transmission

The maximum peak value of slow front overvoltages throughout the conventional and compact HVDC overhead transmission lines with bipole configuration are presented in Figure 5-11. Note that a metallic return conductor is assumed in this system. The results show that in bipolar configurations, the line design, whether conventional or compact, has minor impact on the slow front overvoltages. Comparing Figure 5-11 with Figure 5-3 shows that the maximum slow front overvoltage magnitudes are considerably lower for the bipolar configuration than the symmetrical monopolar configuration.
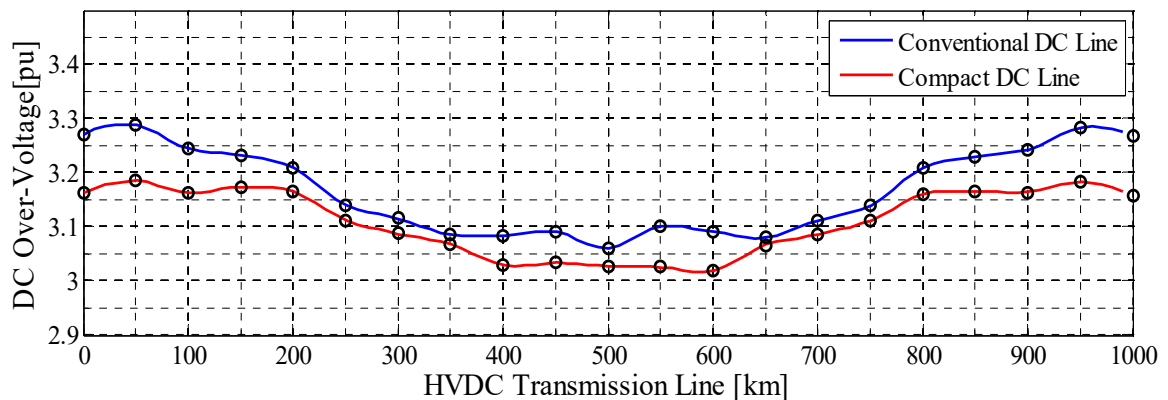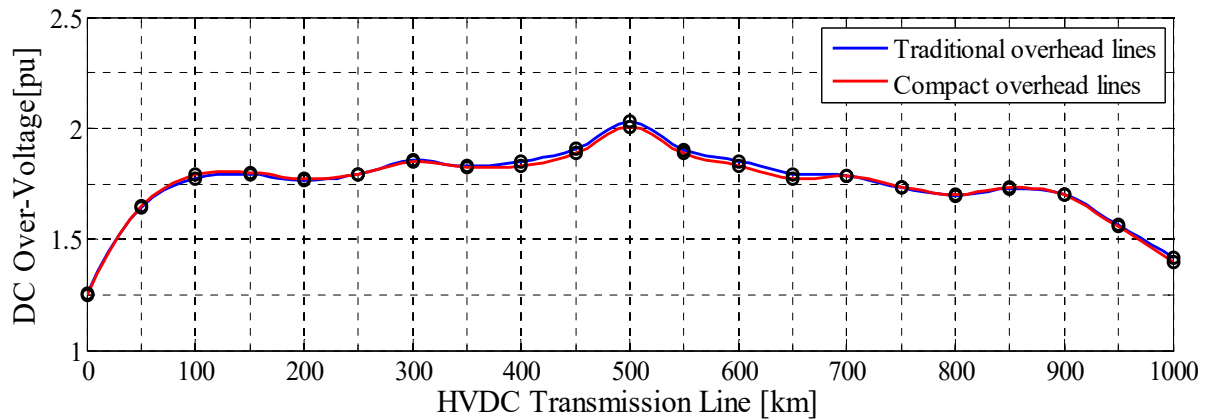

Figure 5-11 Maximum peak value of slow front overvoltages on compact and conventional dc overhead lines of bipole configuration

This study also shows that in a bipolar system, the peak value of the overvoltage occurs in the middle of the line on the unfaulted pole for a pole to ground fault at the same location on the other pole. The voltage waveforms at the terminals of the converter stations as well as at the fault location during the pole to ground fault at the middle of the line are shown in Figure 5-12.
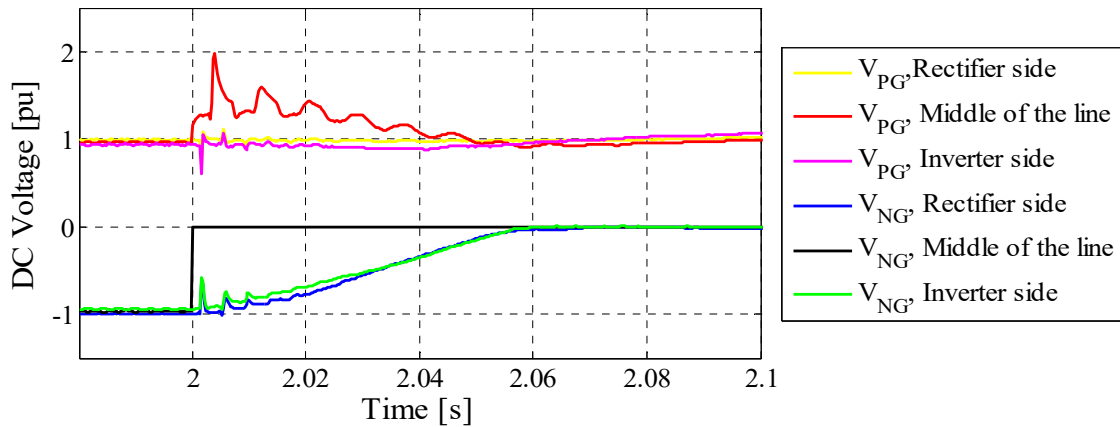
Figure 5-12 Dc line voltage waveforms at the rectifier side, middle of the line and inverter side during the pole to ground fault at the middle of the line

As with symmetrical monopole configurations, the pole to pole line fault on the dc side result in a negligible (or no) overvoltage as shown in Figure 5-13.

(a)   (b)
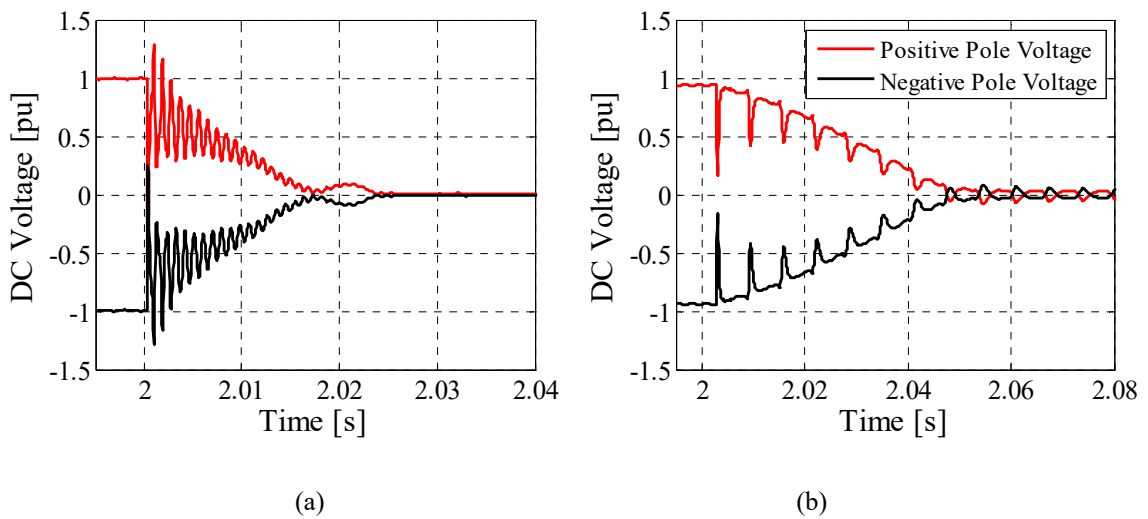
Figure 5-13 Dc line voltage waveforms at: (a) rectifier, (b) inverter station due to pole to pole fault

To investigate the impact of line length with bipole configurations, the study results for a 500 km, 750 km and 1000 km (the base case), are shown in Figure 5-14 and Figure 5-15.

While the peak value of the slow front overvoltage always occurs at the middle of the line

for bipolar configurations, it is lower for the shorter lines.
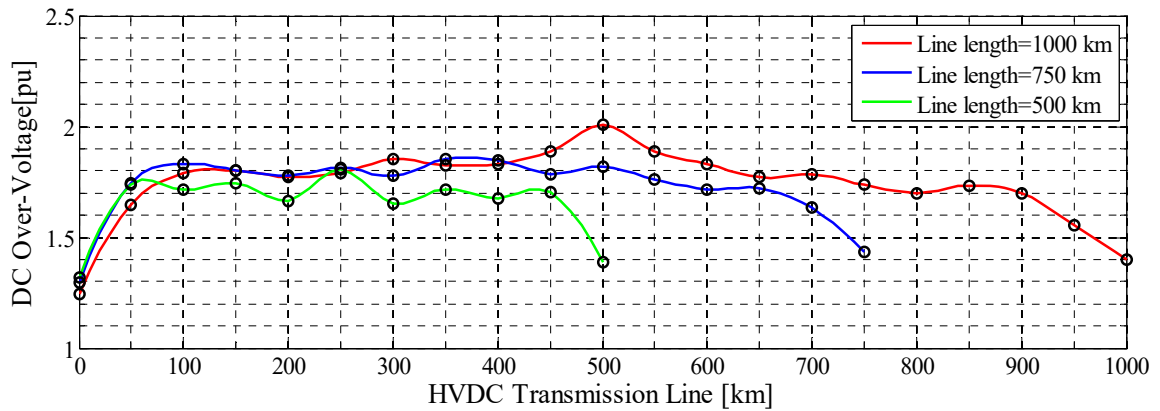
Figure 5-14 Maximum peak value of slow front overvoltages on bipolar dc overhead lines of varying length
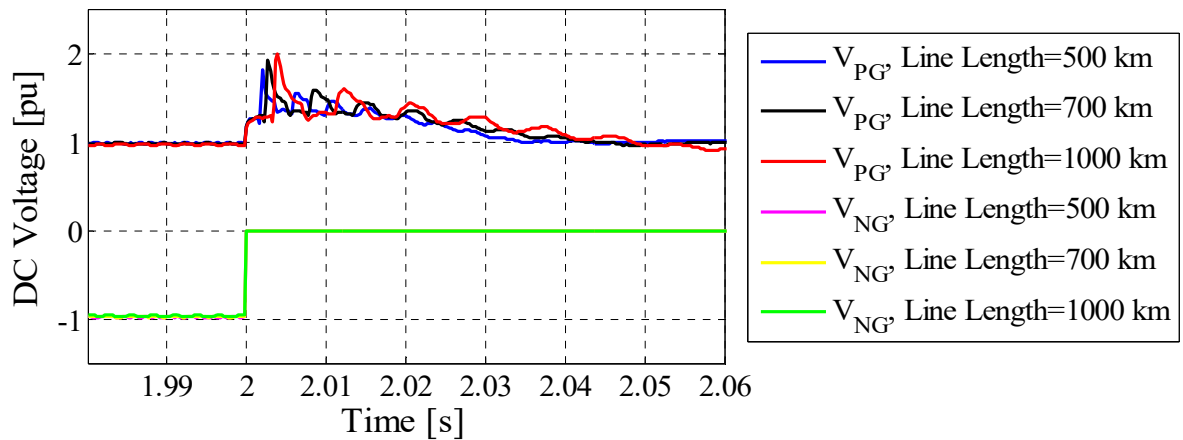
Figure 5-15 Dc line voltage waveforms at the middle of the line for different dc line length during pole to ground fault at the middle of the line

As with fault studies for symmetrical monopole configuration, the impact of the smoothing

line reactor is also considered here for the bipolar configuration.

Figure 5-16 shows that the peak value of slow front overvoltages is larger for smaller line reactors, however, Figure 5-17 shows that dc line voltage waveform at the middle of the line during the fault is similar for two reactance values.
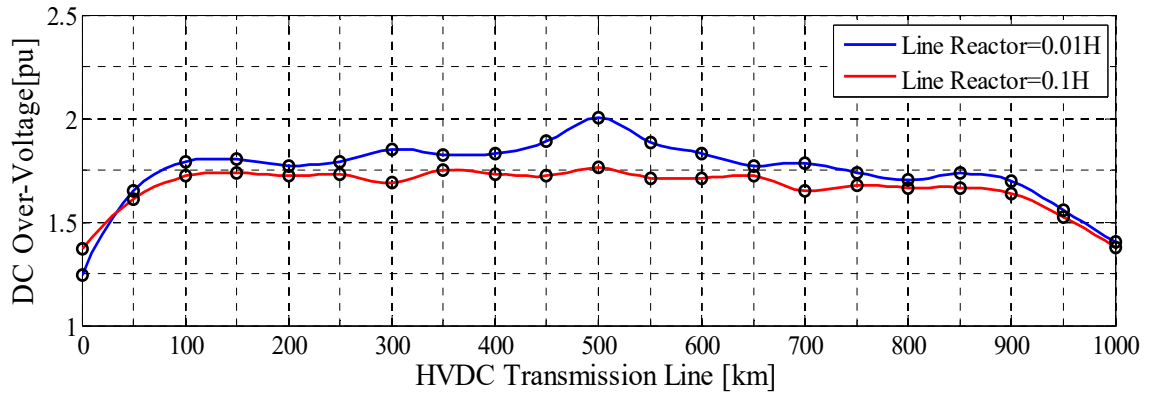
Figure 5-16 Maximum peak value of the slow front overvoltages on the bipolar dc overhead lines with different line reactors
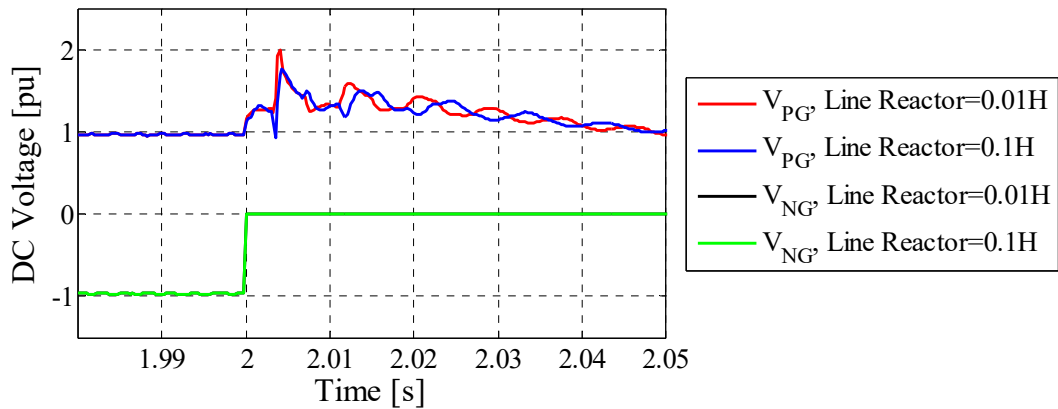
Figure 5-17 Dc line voltage waveforms at the middle of the line for different smoothing line reactors during pole to ground fault at the middle of the line

5.1.3 Overvoltages in the Symmetrical Monopole MMC-VSC Case, using OHL and Cable Transmission

Several HVDC transmission systems (e.g. the South-West Scheme in Sweden [117]) use an underground cable in series with a short section of overhead line dc transmission. The fault is applied at the rectifier station, cable and overhead line junction, middle of the cable and the inverter station. Table 5-1 shows the maximum peak value of the slow front overvoltage at each of these intersections. The dc line voltage waveforms on the overhead line, e.g. at rectifier terminals, cable and OHL junction and inverter terminals, for each of the system scenarios listed in Table 5-1, are presented in Figure 5-18, Figure 5-19 and Figure 5-20 respectively. It can be observed that the line geometry, compact or conventional, has almost no impact on the voltage waveforms since the length of the overhead line is short in this case. Moreover, the study results show larger values of smoothing reactance increases the peak value of the slow front overvoltage on the line. However, on the other hand it also delays the time of the voltage overshoot.

Table 5-1 Maximum peak value of overvoltages due to pole to ground faults at converter side, cable and OHL junction, middle of the cable and inverter side for symmetrical monopole configuration

	Converter side	Cable and OHL junction	Cable middle	Inverter side
Conventional OHL 0.01[H] smoothing reactor	2.49[pu]	2.67 [pu]	2.66 [pu]	2.58 [pu]
Compact OHL 0.01[H] smoothing reactor	2.49 [pu]	2.67 [pu]	2.66 [pu]	2.58 [pu]
Compact OHL 0. 1[H] smoothing reactor	2.67 [pu]	2.87 [pu]	2.88 [pu]	2.82[pu]

(a)   (b)
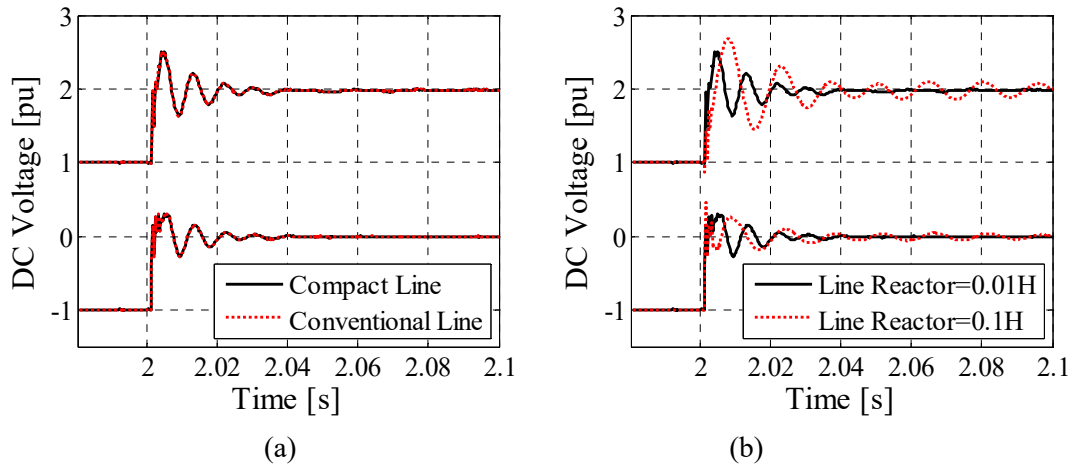
Figure 5-18 Dc line voltage waveform at the rectifier terminals: (a) compact vs. conventional line, (b) with different line reactor values

(a)   (b)
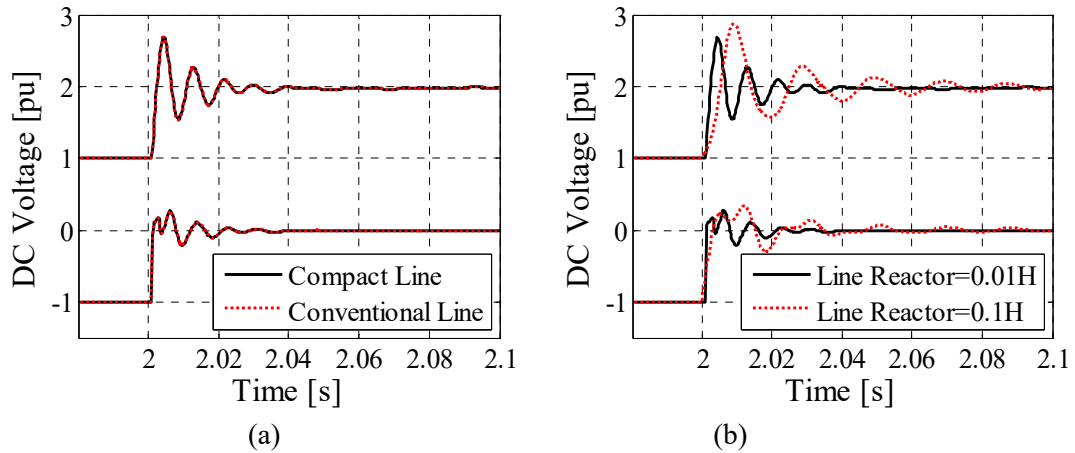
Figure 5-19 Dc line voltage waveform at the OHL and cable junction: (a) compact vs. conventional line, (b) with different line reactor values

(a)   (b)
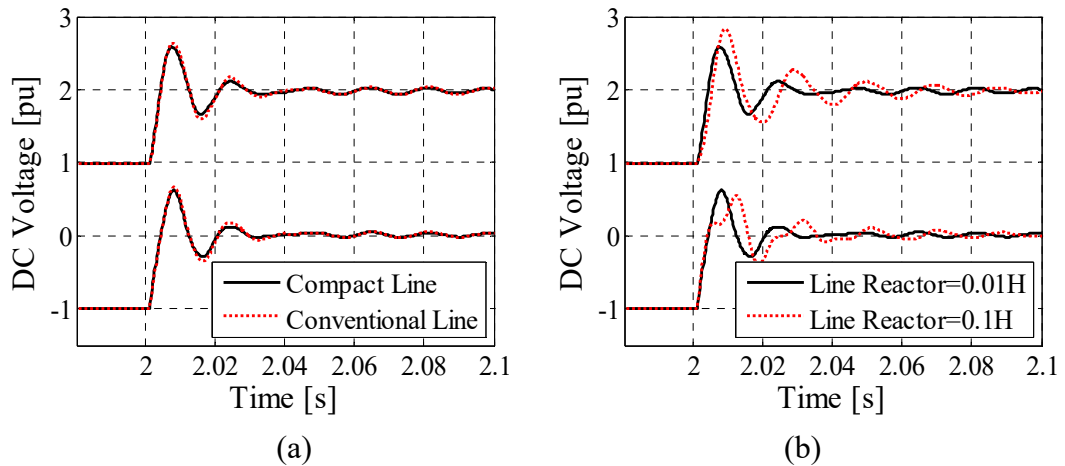
Figure 5-20 Dc line voltage waveform at the inverter side: (a) compact vs. conventional line, (b) with different line reactor values

5.1.4   Overvoltages in the Bipole MMC-VSC Case, using OHL and Cable Transmission

A fault study similar to that discussed in Section 5.1.3 was repeated for the bipolar config-uration. As explained in the previous section, since the line section is short and has no impact on the results, only the compact line is considered in this case. Table 5-1 presents the maximum peak value of slow front overvoltages at each of the intersections shown in Figure 5-2. It can be observed that the overvoltages are larger at the converter side than at other locations, yet are still much lower than with the symmetrical monopole configuration. Figure 5-21 shows the dc line voltage waveform at each end of the compact dc overhead line.

Table 5-2 Maximum peak value of overvoltages due to pole to ground faults at the converter terminals, ca-ble and OHL junction and inverter side for bipole configuration

	Converter side	Cable and OHL junction	Middle of the cable	Inverter side
Compact OHL 0.01[H] smoothing reactor	1.32 [pu]	1.25 [pu]	1.18 [pu]	1.12 [pu]
Compact OHL 0. 1[H] smoothing reactor	1.45 [pu]	1.16 [pu]	1.12 [pu]	1.13 [pu]
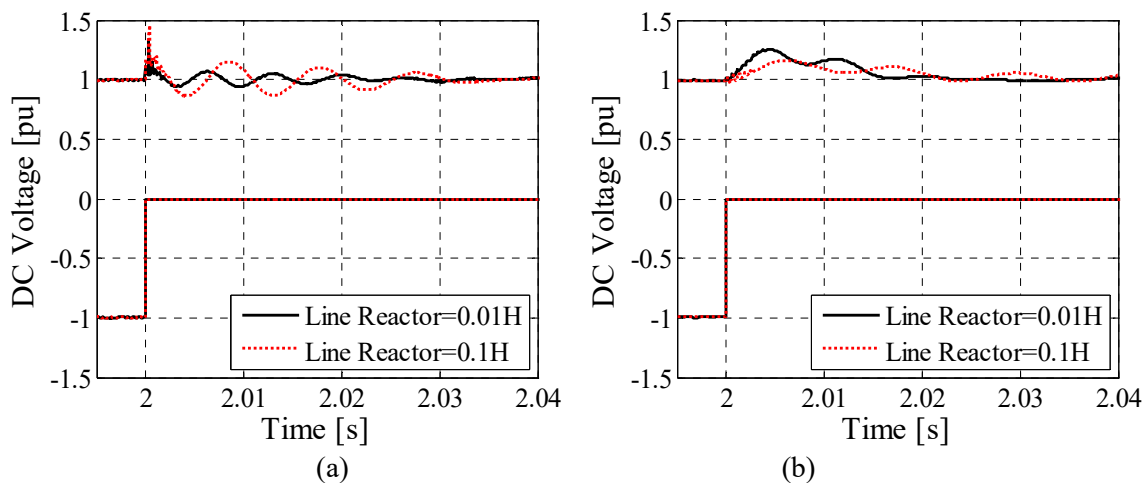
Figure 5-21 Dc line voltage waveform at: (a) the rectifier terminals (b) the OHL and cable junction

5.2   Rationalization of the Overvoltage Simulation Results

The above section presented the waveforms of dc transient overvoltage of MMC HVDC systems, which were simulated using detailed frequency dependent overhead line models. It was shown that the maximum peak values of slow front overvoltages in grounded bipole systems without any control actions or surge arresters are generally at most around 2.0 pu depending on other system parameters; similar to the case for LCC HVDC systems [47]. However these values in MMC-HVDC systems with symmetrical monopolar configuration are significantly larger. This section uses an analytical solution to show that the behaviors shown earlier are as expected.

In MMC-HVDC with symmetrical monopole configuration, since the pole-to-pole voltage, controlled by the converter, remains essentially constant during the pole to ground fault, one would expect that in a high-resistance grounded dc system the voltage of the un-faulted pole would rise to twice the rated value. However, simulation results demonstrate that the transient during a fault has an overshoot that results in an overvoltage of about 3.0 pu. In order to rationalize the simulation results, a simple transmission line model is considered here and is shown in Figure 5-22. This simple model demonstrates the essential behavior of the dc side waveforms.
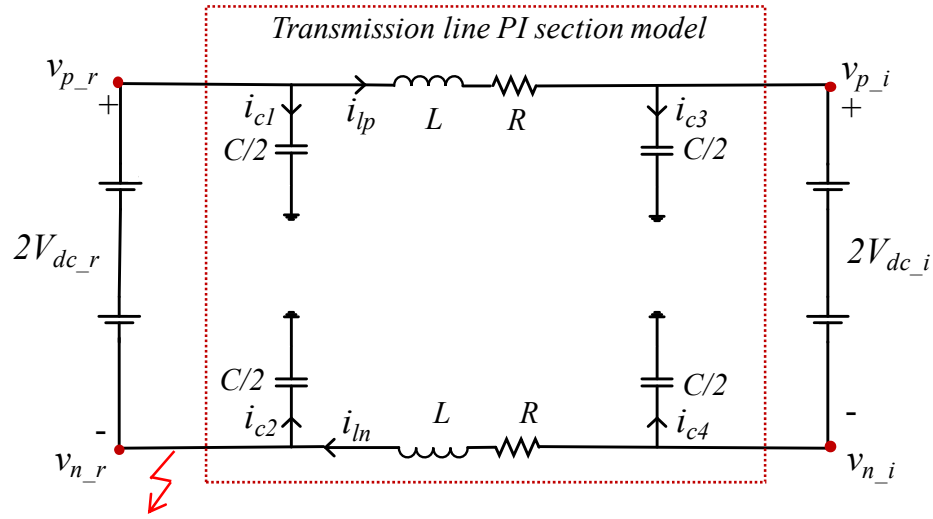
Figure 5-22 Simplified symmetrical monopole configuration with π-section transmission line model

In this model, the transmission line is represented as a π-section model, where C and L represent the inductance and capacitances of the line. The dc terminals of the MMC converters are modeled as ideal dc voltage sources. In this circuit, when a pole to ground fault is applied at the negative pole of the rectifier, first the positive pole voltage at the rectifier terminal obviously jumps to two per unit, as also seen in the detailed simulated waveforms in Figure 5-4. Then the transient responses of the negative and positive pole voltages at the inverter station can be derived from a circuit solution of Figure 5-22 as given by equations 5.1 and 5.2 below:

$$v_{p-i} = 2V_{dc\_i} + v_{n\_i} \qquad\qquad 5.1$$

$$v_{n-i} = L \cdot \frac{di_{ln}}{dt} + R \cdot i_{ln} \qquad\qquad 5.2$$

The inductor current at the negative pole is

$$i_{ln} = -i_{c4} = -\frac{C}{2} \cdot \frac{dv_{n\_i}}{dt} \qquad\qquad 5.3$$

Therefore the first derivative of the inductor current as a function of the capacitor voltage

is:

$$\frac{di_{In}}{dt} = -\frac{C}{2} \cdot \frac{d^2 v_{n\_i}}{dt^2} \qquad\qquad 5.4$$

The differential equation of the voltage v_{n-i} can be derived by combining equations 5.2,

5.3 and 5.4 as expressed in equation 5.5.

$$\frac{d^2 v_{n\_i}}{dt^2} + \frac{R}{L} \cdot \frac{dv_{n\_i}}{dt} + \frac{2}{LC} \cdot v_{n-i} = 0 \qquad\qquad 5.5$$

The general form of the solution of equation 5.5 is $v_{n-i} = A_1 \cdot e^{s_1 t} + A_2 \cdot e^{s_2 t}$, where A_1 and A_2

depends on the initial values of the capacitor voltages and inductor currents in the circuit,

and S_1 and S_2 are the roots of the characteristic equation of the above differential equation

as expressed in equation 5.6.

$$s^2 + \frac{R}{L} s + \frac{2}{LC} = 0 \qquad\qquad 5.6$$

By solving equation 5.6, the roots of this characteristic equation are

$$s_1, s_2 = -\alpha \pm \sqrt{\alpha^2 - \omega_0^2}$$

$$\alpha = \frac{R}{2L}; \omega_0 = \sqrt{\frac{2}{LC}} \qquad\qquad 5.7$$

where α and ω_0 are called the system resonant frequency and damping coefficient respec-

tively. Since in the long transmission lines normally $\left(\frac{R}{2L}\right)^2 < \frac{2}{LC}$, the roots are complex

numbers. Therefore the solution can be expressed as

$$v_{n-i} = A_1 \cdot e^{(-\alpha + j\omega_d)t} + A_2 \cdot e^{(-\alpha - j\omega_d)t}$$
$$= e^{-\alpha t} \cdot K \cdot \sin(\omega_d \cdot t + \theta) \qquad\qquad 5.8$$

$$\alpha = R/2L \;\; ; \;\; \omega_d = \sqrt{\omega_0^2 - \alpha^2}$$

where K and θ can be calculated directly from initial and steady state condition of the cir-

cuit. In this system, the voltage exhibits an oscillatory response around the steady state and

this oscillation decays with time since the real parts of roots are negative.

Before the fault occurrence, v_{n_i} is equal to $-V_{dc\_i}$ and its steady state value is *zero* (assum-

ing the line current goes to zero, otherwise it is RI, where R is the line resistance and I is

the line current which is still negligible). Therefore, after the fault the negative pole voltage

response is:

$$v_{n\_i}(t) = -V_{dc\_i} \cdot e^{-\alpha t} \cdot \cos(\omega_d t) \qquad\qquad 5.9$$

and the positive pole voltage is:

$$v_{p\_i}(t) = V_{dc\_i} \cdot (2 - e^{-\alpha t} \cdot \cos(\omega_d t)) \qquad\qquad 5.10$$

The per unit length parameters of the HVDC transmission lines are listed in Table 4-4. For

long transmission lines, (e.g. line length (l)> 250km) the lumped parameters can be derived

as:

$$L_{line} = Ll \frac{\sinh \gamma l}{\gamma l}$$
$$\qquad\qquad 5.11$$
$$C_{line} = Cl \frac{\tanh(\gamma l/2)}{\gamma l/2}$$

where $\gamma = \omega\sqrt{LC}$ is the propagation constant. Using these lumped parameters in equation

5.9 and 5.10, the voltages of the positive and negative pole at the inverter station during a

pole to ground fault at the rectifier station can be derived in a π-section model. Figure 5-23 demonstrates the detailed simulated voltage waveforms using frequency dependent model and the simplified π-section model to verify the voltage overshoot seen in the simulation results of the previous section.
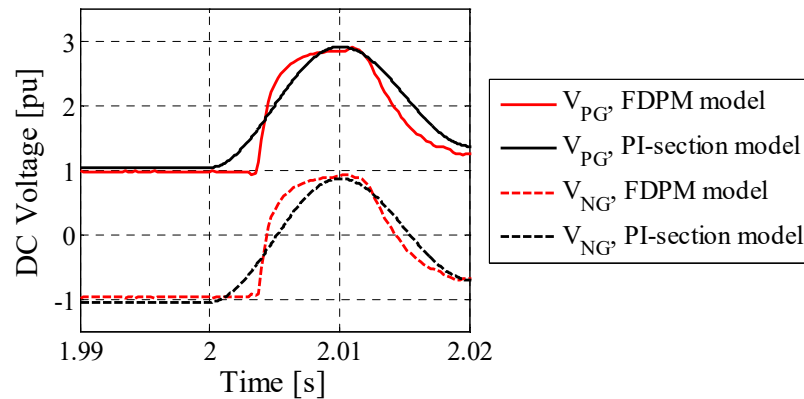
Figure 5-23 Inverter terminal voltage waveforms using detailed frequency dependent model and the simplified π-section model

Equation 5.10 shows that the peak value of the positive pole voltage, which occurs at $t = \pi / \omega_d$, is $3 \cdot V_{dc\_i} \cdot e^{-\alpha\pi/\omega_d}$. The relative value of the system resonant frequency and damping coefficient, which is called damping ratio $\zeta = \alpha / \omega_0 \propto \sqrt{C/L}$, impacts the peak value of the overvoltage. As the damping ratio increases the voltage overshoot decreases. The damping ratio and the frequency of oscillations depend on the system parameters such as line inductance and capacitance.

In dc transmission lines with positive and negative poles, the line inductance and capacitance per unit length are a function of the distance between the conductor and a neutral, D, and the conductor equivalent radius, R, as follows [118]:

$$L = 2 \times 10^{-7} \ln\left(\frac{D}{\sqrt[n]{0.7788R}}\right) \quad [\text{H/m}]$$

$$C = \frac{2\pi(8.85 \times 10^{-12})}{\ln\left(\frac{D}{R}\right)} \quad [\text{F/m}]$$

5.12

where n is the number of sub-conductors in a conductor bundle. Equation 5.12 shows that decreasing pole to neutral distance of overhead lines reduces the inductance of the line. Moreover, due to the low distance from the core to screen in underground cables, series inductance of cables is much smaller than the inductance of overhead lines. On the other hand, decreasing the pole to neutral distance makes the capacitance of the line larger. Therefore, shunt capacitance of cables is much larger than the capacitance of overhead lines. Due to these reasons, the capacitance to inductance ratio in the cable models is much larger than the transmission lines. Therefore in systems with cable transmission, the voltage overshoot is generally less than in transmission systems with overhead lines. Moreover, as transmission line length increases the inductance and capacitance in the line model increases. Therefore the system resonance frequency decreases.

5.3   Overvoltage Reduction in HVDC Transmission Lines

Dc line overvoltage transients are important in determining air clearances, line insulation level and converter station clearances. Overvoltage transients must also be investigated at the junction between an overhead line and cable to consider the insulation level of the cable. For example, XLPE DC cables are type tested (UT) to sustain only about 1.85 pu

over voltages as per CIGRÉ Technical Brochure 496 recommendations [119]. Therefore

means must be found to limit the voltage of the un-faulted pole as quickly as possible.

In MMC-HVDC, the dc pole-to-pole voltage of each converter is controlled by the con-

verter itself. Moreover the converter dc terminal is equivalent to a dc voltage source from

the dc line's point of view. Thus after the pole to ground fault in high-resistance grounded

symmetrical monopole configurations, if no control adjustments are made to reduce the dc

terminal voltage after the fault, the pole-to-pole voltage remains essentially constant. This

will cause the voltage of the unfaulted pole to stay at 2 pu after the initial oscillatory re-

sponse. Therefore, this section looks at methods to reduce the overvoltages and also iden-

tifies a method to detect the faults.

Surge arresters are generally used to limit the transient overvoltage before the converter

effectively reduces the line dc overvoltages. They have nonlinear voltage current charac-

teristics, as shown in Figure 5-24 [120] that, when connected in parallel to the terminals of

electrical equipment, limit the voltage across the equipment to levels below its insulation

withstand voltage.
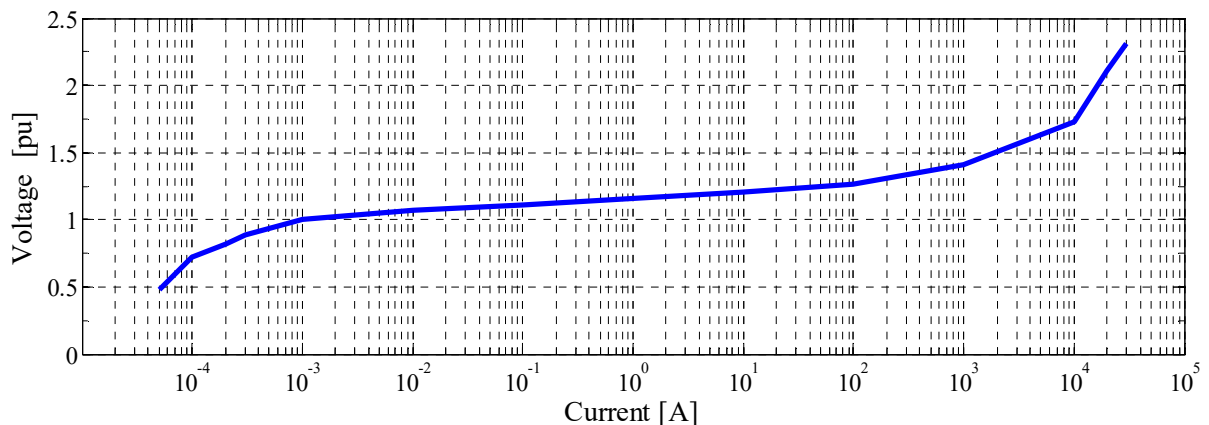
Figure 5-24 V-I characteristic of surge arrester

To effectively protect electrical equipment in power systems, surge arresters have to fulfill two basic requirements: The arrester must be rated to provide sufficient electric protection of the equipment installed in the system and it must remain thermally stable even under the most severe operating conditions. The arrester must be rated so that a specific internal temperature is not exceeded after absorption of energy and loading with voltage under normal and fault circumstances [120]. A surge arrester's overvoltage capability, i.e. the steady state operating voltage capability and also its insulation level, can be increased by more elements in series. But an arrester's energy capability is increased by adding parallel columns.

The size of the arrester required to properly handle high energy depends on the magnitude and duration of the expected overvoltages which would otherwise cause damage due to thermal instability of the arresters. Selecting a surge arrester with higher energy capability increases its transient overvoltage withstand capability and thus its ability to survive the system voltage stresses, albeit at increased cost [85].

Therefore, a combination of an appropriate fault detection method and a modified control technique in MMC-HVDC converter station, not only helps reduce the required size of the surge arresters, but also can even make it possible to maintain partial power flow during temporary faults. Note that the alternative strategy of blocking the converter and using ac breakers to protect the system will also result in power interruption for non-permanent faults.

5.3.1   Pole to Ground Fault Detection in High Resistance Symmetrical Monopole Configuration

Following a dc side pole-to-earth fault, first the line capacitors are discharged to the fault path with a large current. Even though it is a dc fault the current has a number of zero crossings. Figure 5-25 shows a typical fault current waveform in a symmetrical monopole HVDC system.
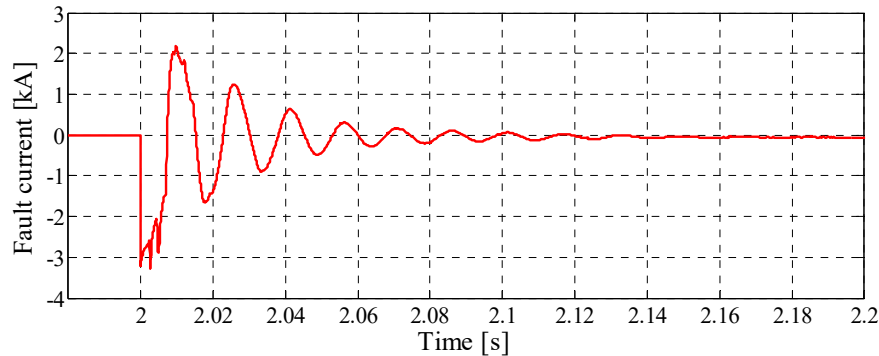
Figure 5-25 Fault current waveform during pole to ground fault in HVDC overhead transmission line with symmetrical monopole configuration

Since there is almost no steady state path for the dc fault current in no- or high-resistance grounded symmetrical monopoles, the fault current reduces rapidly to almost zero after a short period of time and may result in the arc fault self-extinction. Thus a significant benefit of this configuration is its ability to lose little or no power transfer during the temporary faults, since load current still flows while the pole-to-pole voltage stays the same and no surge of fault current flows through the VSC converters [65]. However, as previously ex-plained, one result of a pole to ground fault in these systems is the significant overvoltage. Pole voltage can be used to detect pole to ground faults. The measurement system is placed at the converter side in order to read voltage magnitude as soon as possible. When that magnitude exceeds a pre-set threshold value, it triggers the controller system to reduce the pole to pole voltage.

Since both rectifier and inverter stations should detect the fault and take action, the minimum overvoltage that can occur at each converter terminal, which is 2.0 pu as shown in Figure 5-4, needs to be considered in determining the threshold voltage magnitude. Therefore, the maximum threshold value $V_{pole-thr}$ is considered here as 1.7 pu. In the following section, the reason for selecting this value and the effectiveness of this detection method is demonstrated.

5.4 Control Method to Reduce the Overvoltage of MMC-HVDC with Full-Bridge Converter Topology

In Chapter 4, the topology of a Multi-Modular Converter was illustrated in Figure 4-2. In order to explain the relationship between ac and dc voltages at the terminals of the converter, an equivalent model is used as shown in Figure 5-26. In this model, the sub-modules (SM) in each arm are represented by an equivalent voltage source. The output voltage of all the SMs in each arm is determined based on the dc voltage of the pole that the arm is connected to from one side and the required ac voltage at the other side. Therefore upper and lower arm voltages are expressed in equations 5.13 and 5.14. On the other hand, the output voltage of each phase unit should be equal to the required dc voltage as expressed in 5.15.

$$v_{a-up} = V_{dc} - v_a \qquad\qquad 5.13$$

$$v_{a-bt} = V_{dc} + v_a \qquad\qquad 5.14$$

$$2V_{dc} = v_{a-up} + v_{a-bt} \qquad\qquad 5.15$$
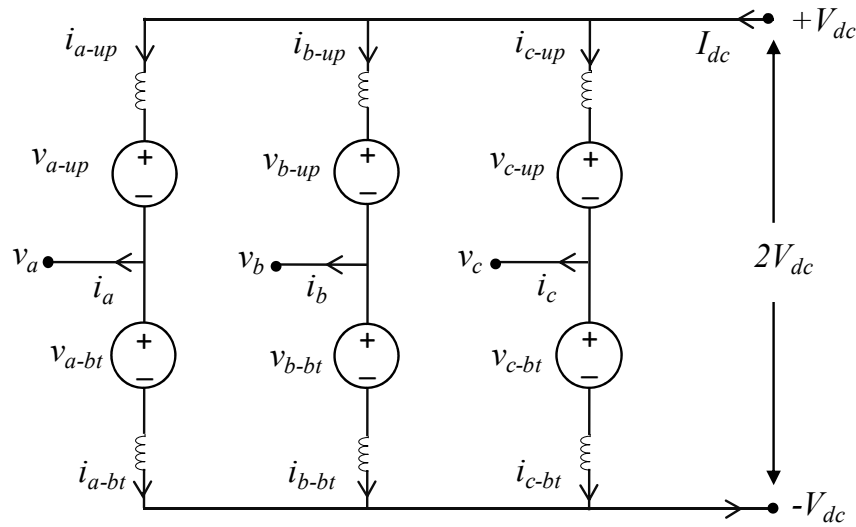
Figure 5-26 MMC equivalent model

As explained in Chapter 4, in MMC-HVDC with half-bridge SMs, the peak ac voltage cannot exceed the dc pole voltage, since the output voltage of each half-bridge SM is either zero or positive. Therefore the arm voltage, which is the sum of all the SM voltages, is always positive. However, it will be shown here how the peak ac voltage and the dc voltage magnitude can be independent in a MMC with full-bridge SMs.

SMs in full-bridge converters are able to either bypass the SM capacitor, insert it directly, or insert it with reverse polarity. Therefore if there are N submodules in each arm and the rated voltage of each SM is V_{sm}, the output voltage of each arm can vary stepwise between $-N \cdot V_{sm}$ and $N \cdot V_{sm}$. This feature allows the ac peak voltage to exceed the dc pole voltage. However, it should be still verified that the average energy stored in the capacitors of the SMs remains constant during the steady state operation.

Assuming the voltage across the inductor is negligible, the lower and upper arm voltages are:

$$v_{a-up} = V_{dc} - V_a \sin(\omega t) \qquad\qquad 5.16$$

$$v_{a-bt} = V_{dc} + V_a \sin(\omega t) \qquad\qquad 5.17$$

Therefore the required number of submodule at every instance is

$$n_{a-up} = \frac{1}{V_{SM}}(V_{dc} - V_a \sin(\omega t)) \qquad\qquad 5.18$$

$$n_{a-bt} = \frac{1}{V_{SM}}(V_{dc} + V_a \sin(\omega t)) \qquad\qquad 5.19$$

where V_{SM} is the rated voltage of each SM and C is the SM capacitor. In order to show that

the energy storage in MMC is balanced, the capacitor voltage variations in one cycle should

be zero as is expressed 5.20 and 5.21.

$$\int \frac{1}{C_{eq-up}} \cdot i_{a\_up} \cdot dt = 0 \qquad\qquad 5.20$$

$$\int \frac{1}{C_{eq-bt}} \cdot i_{a\_bt} \cdot dt = 0 \qquad\qquad 5.21$$

The equivalent capacitance is each arm at every moment is determined based on the num-

ber of capacitors that are in series in the arm current path

$$C_{a-up} = \frac{C}{n_{a-up}} \qquad\qquad 5.22$$

$$C_{a-bt} = \frac{C}{n_{a-bt}} \qquad\qquad 5.23$$

Current in each arm is a combination of ac and dc currents. Assume I_{dc} is the dc current and

i_a, i_b are i_c the ac currents of each ac phase. Assume further that circulating current is sup-

pressed by the control system [121]. The dc current distribution in each arm is $I_{dc}/3$ and the

ac current distribution in each arm is *i(t)/2*. Therefore, as an example, the arm currents for phase *a* are:

$$i_{a-up} = \frac{I_{dc}}{3} + \frac{I_{a-peak}}{2}\sin(\omega t + \theta) \qquad\qquad 5.24$$

$$i_{a\_bt} = \frac{I_{dc}}{3} - \frac{I_{a-peak}}{2}\sin(\omega t + \theta) \qquad\qquad 5.25$$

Note that the other phases are the same in magnitude with 120^0 phase shift. Now using equation 2.22 and 5.24 in equation 5.20 and also equation 5.23 and 5.25 in equation 5.21, the voltage variations of the capacitors in one cycle in upper arm and lower arm of phase *a* can be calculated as

$$\int \frac{1}{V_{SM}}(V_{dc} - V_a\sin(\omega t)) \cdot (\frac{I_{dc}}{3} + \frac{I_a}{2}\sin(\omega t + \phi)) \cdot dt = 0$$

$$\int \left(\begin{array}{c} \dfrac{V_{dc}I_{dc}}{3} - \dfrac{V_a I_{dc}}{3}\sin(\omega t) + \dfrac{V_{dc}I_a}{2}\sin(\omega t + \phi) + .. \\[2mm] .. \dfrac{V_a I_a}{4}\cos(2\omega t + \phi) - \dfrac{V_a I_a}{4}\cos(\phi) \end{array} \right) \cdot dt = 0 \qquad 5.26$$

$$\int \frac{1}{V_{SM}}(V_{dc} + V_a\sin(\omega t)) \cdot (\frac{I_{dc}}{3} - \frac{I_a}{2}\sin(\omega t + \phi)) \cdot dt = 0$$

$$\int \left(\begin{array}{c} \dfrac{V_{dc}I_{dc}}{3} + \dfrac{V_a I_{dc}}{3}\sin(\omega t) - \dfrac{V_{dc}I_a}{2}\sin(\omega t + \phi) + .. \\[2mm] .. \dfrac{V_a I_a}{4}\cos(2\omega t + \phi) - \dfrac{V_a I_a}{4}\cos(\phi) \end{array} \right) \cdot dt = 0 \qquad 5.27$$

In both equation 5.26 and 5.27, there are constant terms and oscillating terms. The integral of the oscillating terms in one cycle is zero. However, the constant term in both equations is $\dfrac{V_{dc}I_{dc}}{3} - \dfrac{V_a I_a}{4}\cos\phi$.

In power electronic converters the input and output power should be the same, therefore,

$$P_{ac} = P_{dc}$$

$$\frac{3}{2}\cdot V_a \cdot I_a \cdot \cos\phi = 2\cdot V_{dc}\cdot I_{dc} \qquad\qquad 5.28$$

Equation 5.28 shows that the constant terms in equation 5.26 and 5.27 are zero. This is also true for other phases. Therefore the energy into and out of the MMC can remain balanced, and so the average capacitor energy can remain constant even with varying the dc voltage magnitude.

The advantage of this feature is that it can be used to reduce the significantly large over-voltages that happen in symmetrical monopole configuration due to pole to ground faults without impacting the ac side voltage. Therefore the reactive power exchange can remain controlled. If the fault is temporary the power flow can remain uninterrupted. However, as action is taken to lower the dc pole to pole voltage from insulation considerations, some power derating will have to be done so that the dc current does not exceed the rated value. In order to reduce the dc voltage, the dc bias on the reference voltage of each arm needs to be reduced to the desired value. The modified control diagram of full-bridge MMC HVDC that can detect the pole to ground fault and reduce the dc overvoltage immediately is presented in Figure 5-27.
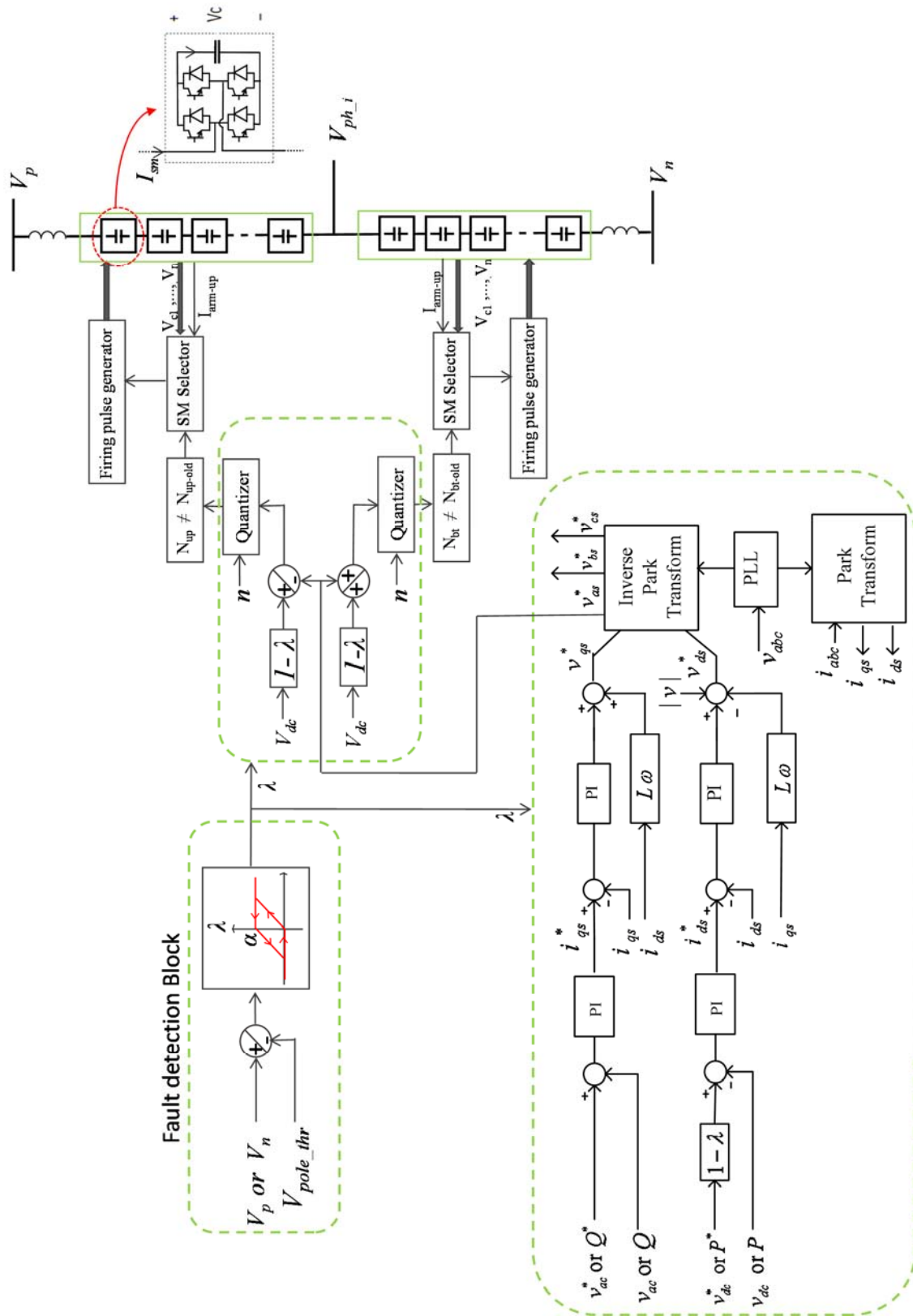
Figure 5-27 Modified control diagram of full-bridge MMC HVDC with pole to ground fault detection

5.4.1   Symmetrical   Monopole   MMC-VSC   Case,   using   OHL

Transmission

In the modified control diagram of the full-bridge MMC HVDC control system shown in

Figure 5-27, there are two parameters that need to be specified: $V_{pole-thr}$ which is the thresh-

old dc voltage value for the fault detection, and α which is the dc voltage reduction factor.

In order to consider the impact of the $V_{pole-thr}$ value on the dc pole voltage after the fault,

two different values, 1.2 pu and 1.5 pu are considered. In each case, the fault is applied

close to the rectifier station; therefore the maximum overvoltage occurs at the inverter sta-

tion (as discussed in Section 5.1) after which the control system reduces the pole to pole

dc voltage. Two situations are considered; first an ideal one, where the dc voltage reduction

is instantaneously applied as soon as the fault happens, i.e., assuming zero fault detection

time; and secondly allowing for a 1 ms detection delay time. Figure 5-28 shows the simu-

lation results of the pole voltages at the rectifier and inverter terminals. It can be observed

that the delay in the detection can lead to a much larger overvoltage than the ideal case.

Also shown in Figure 5.28 is that if $V_{pole-thr}$ is increased from 1.2 to 1.5, there is no appre-

ciable impact on the overvoltage, indicating that this overvoltage is more dependent on the

delay than on the threshold overvoltage voltage.
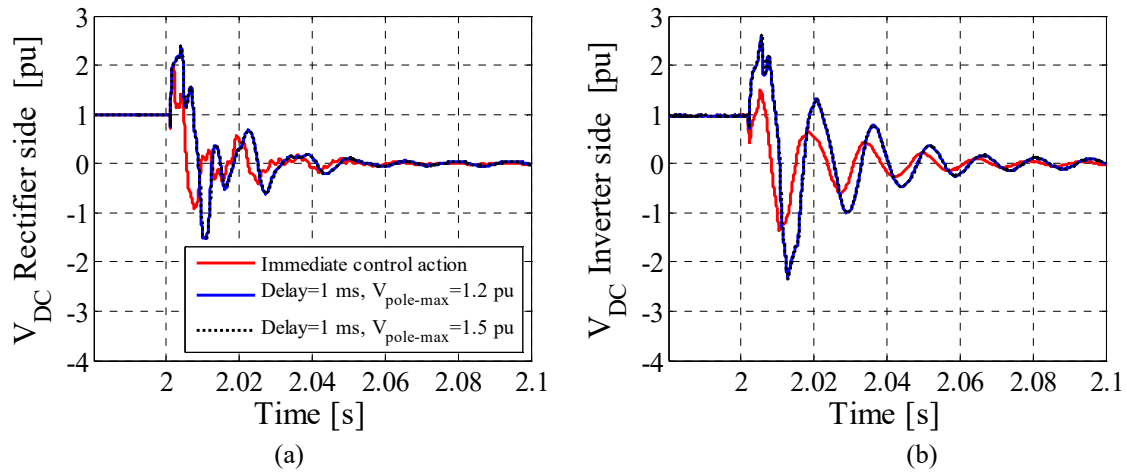
Figure 5-28 Dc line voltage waveforms at: (a) the rectifier and (b) the inverter terminal considering the impact of the delays in the fault detection

After the fault occurs, the pole to pole dc voltage can be reduced by a dc voltage reduction factor $(1-\alpha)$. For example, the dc voltage will be reduced to zero by setting $\alpha=1$. However, for temporary faults on overhead lines the dc transmission line can still transfer part of the power with the reduced dc voltage. By setting $\alpha=0.5$, the voltage of the unfaulted pole can be reduced to the rated value. Figure 5-29 shows the impact of different values of α (e.g. $\alpha=1$ and $\alpha=0.5$) on the unfaulted pole transient overvoltage and compares the results with the original case. It can be observed that this approach not only reduces the overvoltage magnitude, but also reduces the duration of the overvoltage.

Figure 5-30 shows the maximum peak value of the overvoltage throughout the line with applying this control method. It can be observed that the value of α only makes a very slight difference in overvoltage reduction at the converter stations, and has no impact on the overvoltage occurring throughout the line. Therefore, $\alpha=0.5$ is chosen for the rest of the studies here, since it still allows fifty percent of power flow for non-permanent faults while reducing the overvoltage.
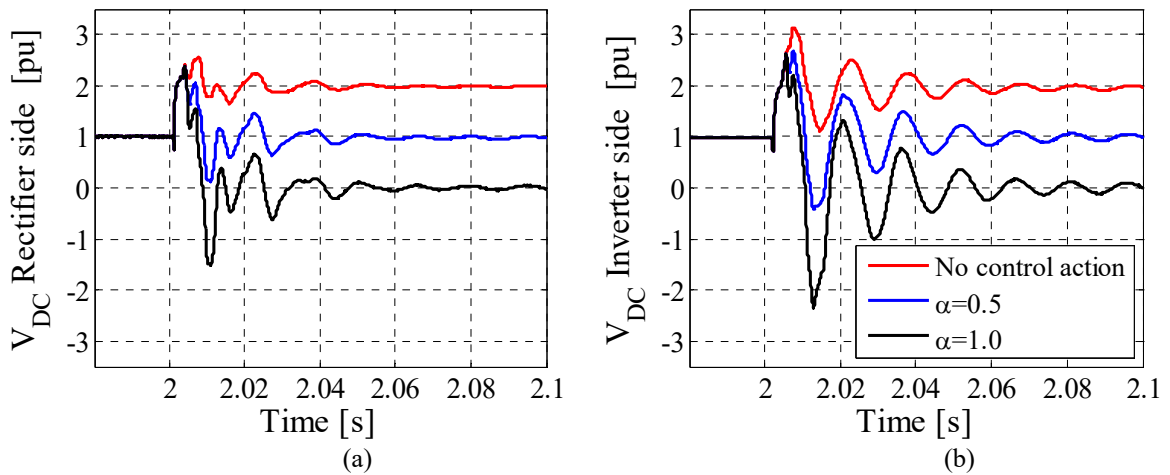
Figure 5-29 Dc line voltage waveforms at the (a) rectifier, (b) inverter terminal considering the impact of different voltage reduction factor on the transient overvoltage on the dc poles

Figure 5-30 also shows the overvoltage reduction at the converter stations is more signifi-cant than at the middle of the line, and this is due to delays in traveling waves in transmis-sion lines. This shows that surge arresters are also required in some locations in the line. However, since the duration of the overshoot is also reduced by this method, a smaller surge arrester size is required.
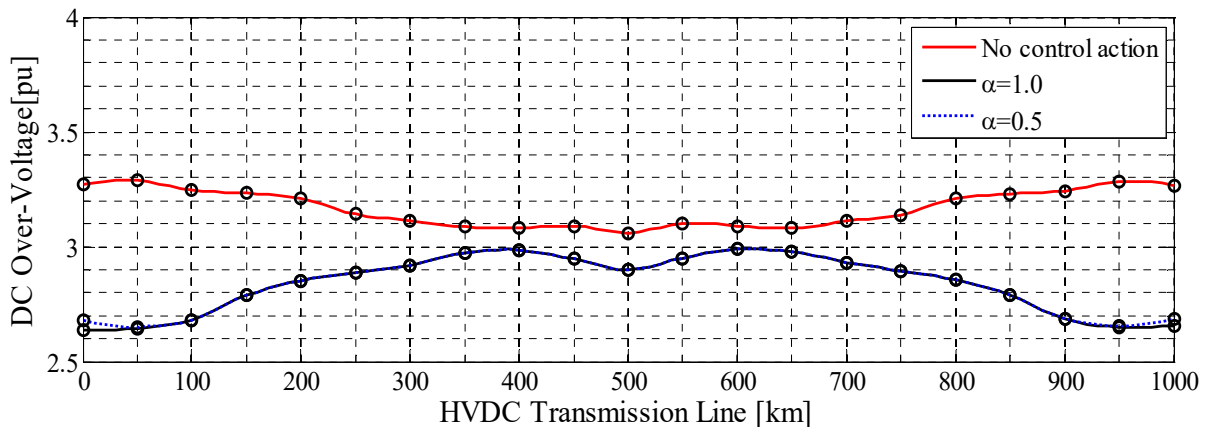
Figure 5-30 Maximum peak value of overvoltage for different settings for α along with the case without the control action

Earlier in this section, it was explained that the dc and ac voltage magnitudes are independent in a full-bridge MMC system. To verify this, the ac voltage waveforms of the ac network at the rectifier and inverter stations, when the dc voltage is reduced to zero during a pole to ground fault at the dc side, are presented in Figure 5-31.
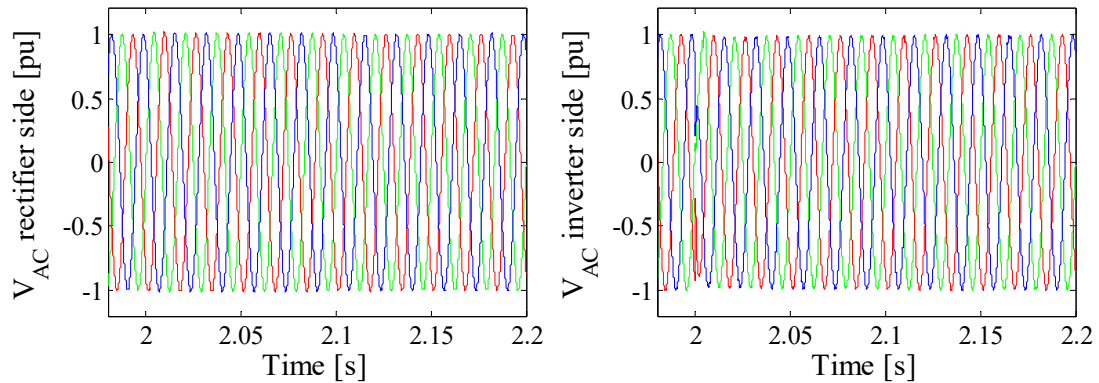
Figure 5-31 Ac voltage waveforms of the ac network at the rectifier and inverter stations when the dc voltage is reduced to zero during a pole to ground fault at the dc side

The simulation results in Figure 5-29 verify that the dc transient overvoltages, caused by pole to ground faults, can be reduced significantly by this control approach while system operation remains uninterrupted. However, due to the delay in the fault detection method and also the delays caused by propagation time in transmission lines, there is still a voltage overshoot on the unfaulted pole that occurs before the controller effectively reduces the dc voltage. This overvoltage can be limited by using surge arresters in the transmission line. As the initial step, the surge arresters are just used at the terminals of the converters to limit the overvoltage below a certain value, e.g. 2 pu. However, it will be shown that this arrangement is not capable of reducing the overvoltage all along the overhead line to the same degree. One solution is to place surge arresters at strategic locations along the line so

that the transient voltage overshoot is reduced for the entire overhead line. Here, along with

the initial case, two more options are considered as shown in Figure 5-32:

- Surge arrester set 1: surge arresters, SA_rec and SA_inv, at the rectifier and inverter

  stations respectively

- Surge arrester set 2: surge arresters, SA_rec, SA_500 and SA_inv, at the rectifier,

  middle of the line and inverter stations respectively

- Surge arrester set 3: surge arresters are placed every 250 km , SA-250, SA-500 and

  SA-750, along with surge arresters, SA_rec and SA_inv at the rectifier and inverter
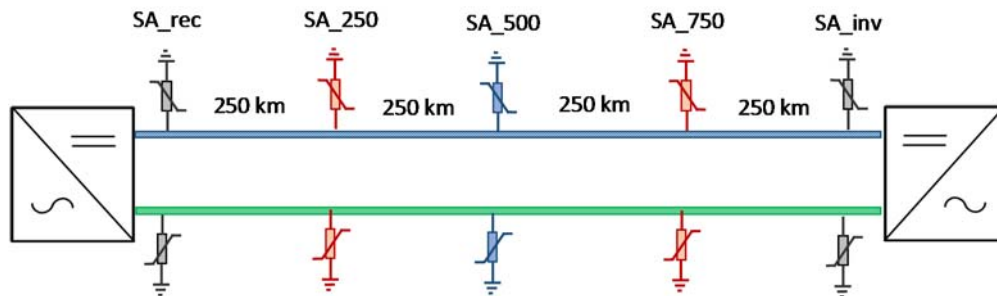
  stations

Figure 5-32 Possible surge arrester locations in dc line; (1) surge arrester set1: using SA_rec and SA_inv, (2) surge arrester set2: using SA_rec, SA_500 and SA_inv, (2) surge arrester set3: using SA_rec, SA_250, SA_500, SA_750 and SA_inv

Figure 5-33 shows the maximum peak value of the slow front overvoltage using these surge

arrester arrangements. This figure shows that using more surge arresters along the line does

not impact the maximum peak value of the overvoltage at the converter terminals, which

is also demonstrated in Figure 5-34. However, it will reduce the overvoltage throughout

the entire overhead line more effectively, which will reduce overvoltage clearances re-

quired within the tower.
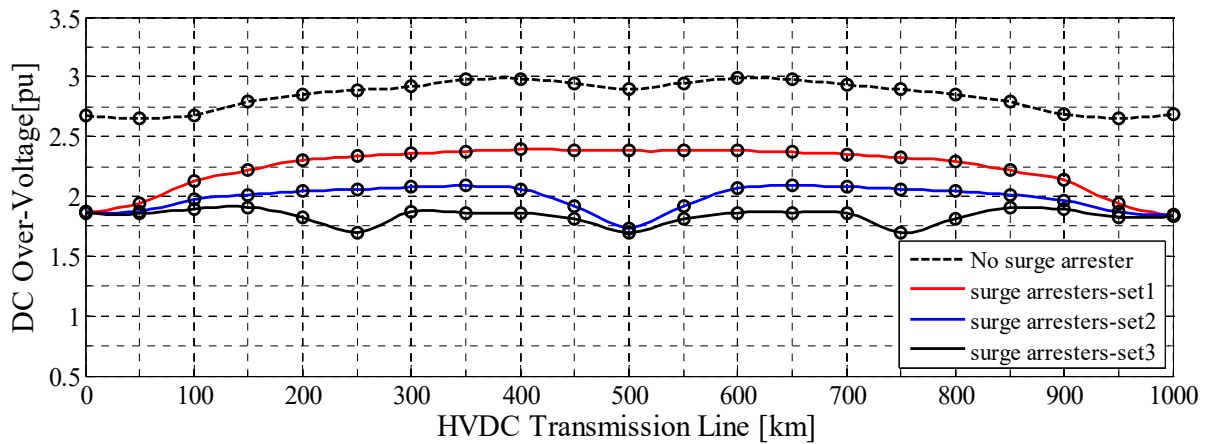
Figure 5-33 Maximum peak value of slow front overvoltages using different surge arrester arrangements
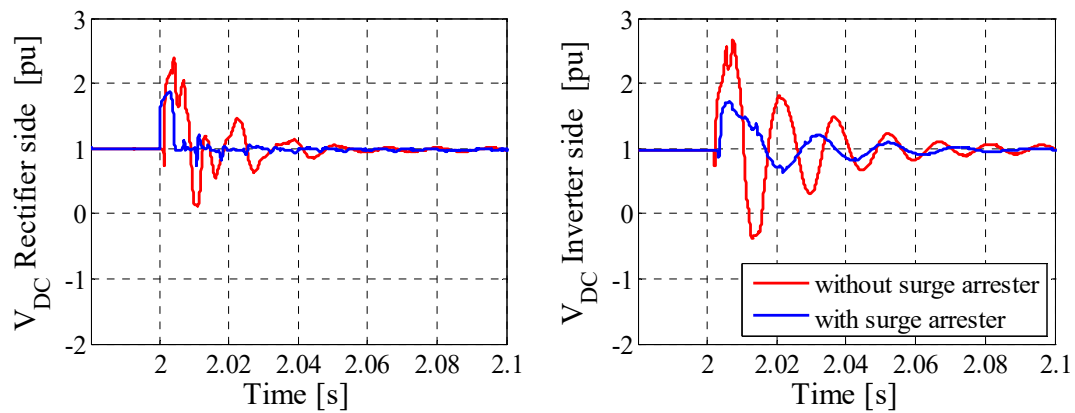
Figure 5-34 Dc line voltage waveforms at the (a) rectifier, (b) inverter terminal considering the impact of using surge arrester together with the control action

In order to determine the required surge arrester ratings, the energy discharge in them must be predicted. The energy discharge in each of the surge arresters as a function of the fault location, using surge arrester set 1 and surge arrester set 3, are shown in Figure 5-35 and Figure 5-36 respectively. It can be observed that the maximum amount of energy discharge in each of the arresters is when the fault occurs in their proximity. Moreover, Figure 5-36

shows that the required size of the surge arresters in the middle of the line is significantly

less than surge arresters located at the converter terminals.
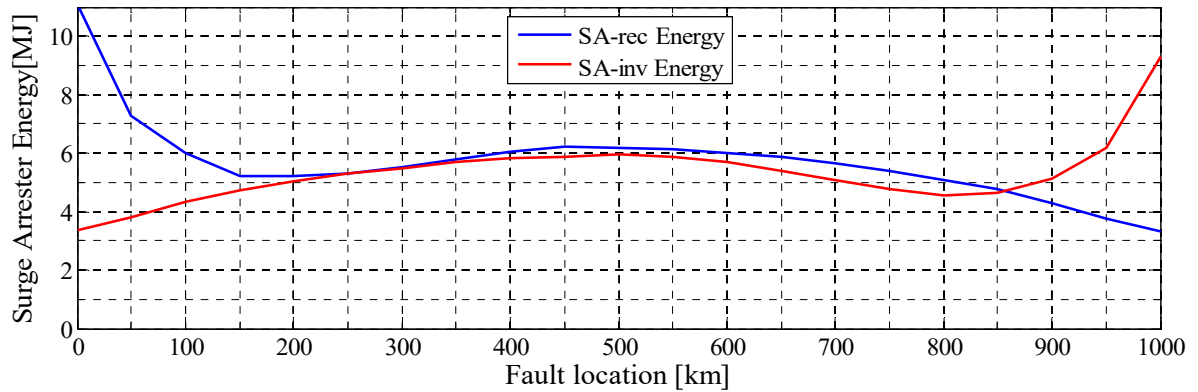
Figure 5-35 Energy discharge in the surge arresters as a function of the fault location, using surge arrester set 1
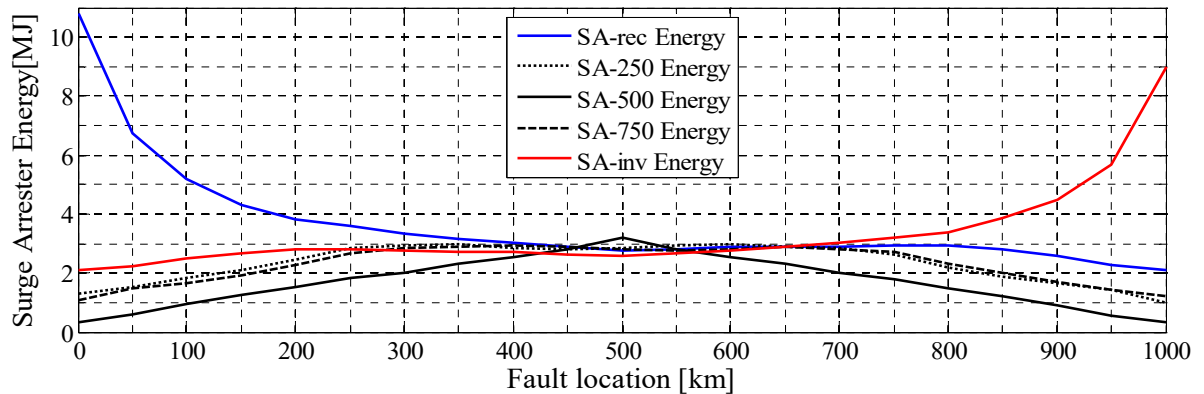
Figure 5-36 Energy discharge in the surge arresters as a function of the fault location, using surge arrester set 3

The maximum peak values of the overvoltages that can occur all along the overhead line

were presented in Figure 5-33. It was also shown that using this control approach along

with surge arrester set 3 can effectively reduce the overvoltages throughout the entire line.

In addition it will also be desirable to find out the fault locations in this system that result

in most significant overvoltages throughout the line. Figure 5-37 shows that fault locations

FG4, and *FG18* results in the maximum overvoltages of 1.91 pu on the line, at 850 km and 150 km respectively. A fault at FG9 or FG13 also result in high overvoltages (1.87 pu). In this figure, the overvoltages due to faults at each converter stations, as *FG1* and *FG21*, are also shown. These two fault locations result in the overvoltage magnitudes between 1.55 pu and 1.85 pu. Therefore faults at any other locations in the line results in an overvoltage between 1.55 pu to 1.91 pu.
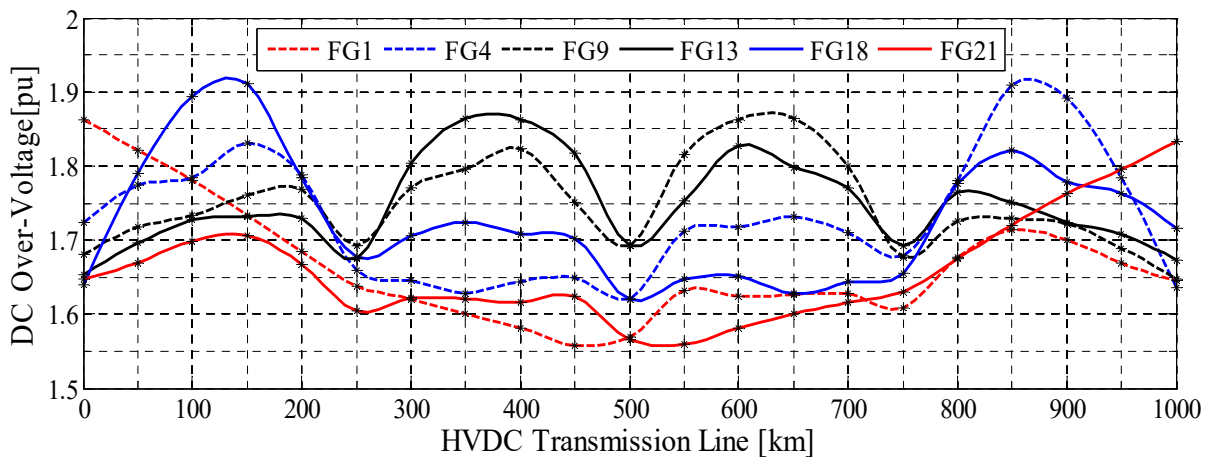
Figure 5-37 Peak value of the overvoltage along dc line for faults that results in maximum overvoltages

5.4.2   Symmetrical Monopole MMC-VSC Case, using OHL and Cable Transmission

As explained in Section 5.2, the capacitance of underground cables is much higher and their reactance is much lower than that of the overhead lines. Consequently their damping ratio ($\zeta \propto \sqrt{C/L}$) is higher. Therefore, the transient voltage overshoot in a cable transmission is generally less than in an overhead line transmission system.

Due to the fact that the cable reactance is normally low, the line smoothing reactor helps

to decrease the oscillation frequency of the transient overvoltage. Table 5-3 shows the max-

imum peak value of the overvoltage for systems with different line smoothing reactor val-

ues, for the proposed control strategy. It can be seen in Figure 5-38 that the control action

is more effective with higher values of line smoothing reactors since it reduces the resonant

frequency on the dc system and so slows down the overvoltage rate of rise, making it easier

for the controller to regulate the voltage.

Table 5-3 Maximum peak value of overvoltages at converter side, cable and OHL junction, middle of the
cable and inverter side for symmetrical monopole configuration after the controller action

	Converter side	Cable and OHL junction	Cable middle	Inverter side
Compact OHL 0.01 [H] smoothing reactor	2.50 [pu]	2.68 [pu]	2.57 [pu]	2.43 [pu]
Compact OHL 0. 1 [H] smoothing reactor	2.05 [pu]	2.18 [pu]	2.20 [pu]	2.14 [pu]
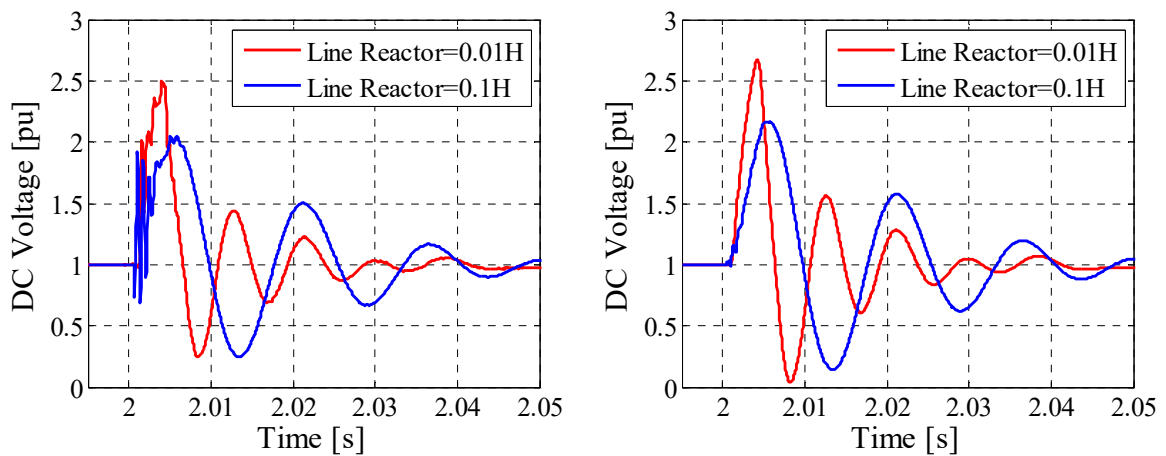
Figure 5-38 Dc line voltage waveform at: (a) the rectifier terminals (b) the OHL and cable junction with the
control action to reduce the overvoltage

As mentioned in Section 5.3, in order to comply with CIGRÉ Technical Brochure 496 recommendations [119], the line surge arresters, as shown in Figure 5-39, should limit the sustained overvoltage for XCLPE DC cables to 1.85 pu. The dc line voltage waveforms at each end of the overhead line for lines with different line reactors after using the surge arresters to reduce the overvoltage are shown in Figure 5-40.
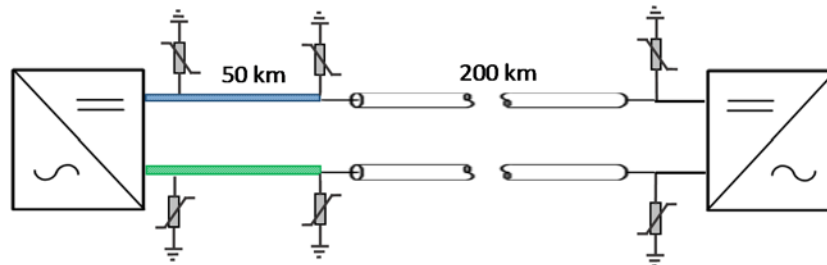
Figure 5-39 Line surge arrester locations in dc systems with OHL and underground cable
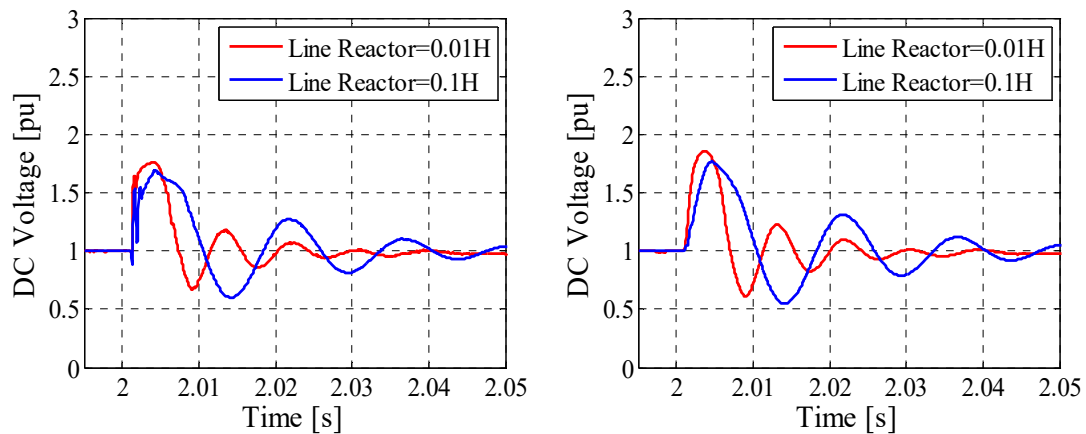
Figure 5-40 Dc line voltage waveforms at: (a) the rectifier terminals (b) the OHL and cable junction with control action and surge arrester

The maximum peak values of the overvoltage after using the same surge arresters for each case and the maximum energy discharge in each of these surge arresters are presented in Table 5-5 5-4 and
Table 5-5 5-5 respectively. These results confirm that the higher smoothing reactors not only reduce the overvoltage more effectively but can also reduce the required surge arrester size since the higher rise time gives more time to the control system to reduce the overvoltage.

Table 5-4 Maximum peak value of overvoltages at converter side, cable and OHL junction, middle of the cable and inverter side for symmetrical monopole configuration after the controller action

	Converter side	Cable and OHL junction	Cable middle	Inverter side
Compact OHL 0.01 [H] smoothing reactor	1.77 [pu]	1.87 [pu]	1.94 [pu]	1.95 [pu]
Compact OHL 0. 1 [H] smoothing reactor	1.69 [pu]	1.76 [pu]	1.81 [pu]	1.77 [pu]

Table 5-5 Maximum energy discharge in the surge arresters

	Converter side	Cable and OHL junction	Inverter side
Compact OHL 0.01 [H] smoothing reactor	5.602[MJ]	10.652[MJ]	11.135 [MJ]
Compact OHL 0. 1 [H] smoothing reactor	2.540 [MJ]	5.480 [MJ]	5.655 [MJ]

5.5 Control Method to Reduce the Overvoltage of Symmetrical Monopole MMC-HVDC with Half-Bridge Converter Topology

The dc voltage of half-bridge converters cannot be reduced as much as full-bridge converters. However, in order to reduce the overvoltage to below 2 pu after oscillatory response limited by surge arresters, the dc terminal voltage should be sufficiently below the rated voltage of the surge arrester. Otherwise, the surge arresters will keep conducting and provide a path to the ground for the dc fault current, thus not allowing temporary faults on the overhead lines to self-extinguish. It is therefore beneficial to reduce the dc voltage of the half-bridge converters marginally to the point where the power flow is uninterrupted during temporary faults, while the surge arresters reduce the overvoltage.

As demonstrated in Section 5.3.2, in MMCs with half-bridge sub-modules, the output voltage of each sub-module can take on one of two different voltage levels, zero or V_{sm} which is the voltage of the SM capacitor, namely 'OFF' or 'ON' state. Since at any moment, the sum of the sub-module output voltages of each phase unit is equal to the pole to pole dc voltage in a monopole configuration, the total number of sub-modules with the ON state on the lower and upper arms is constant and equal to N [109] where it is

$$N = \frac{2V_{dc}}{V_{sm}}$$ 5.27

In other words, if the number of sub-modules with ON state on upper arm is n_{up}, the number of sub-modules with ON state on lower arm is [109]:

$$n_{bt} = N - n_{up}$$ 5.28

To reduce the dc voltage after the fault occurs, simply reducing the reference value of the controller is not helpful since it will result in reducing the voltage of each sub-module capacitor which is not desirable and based on their time constant will not be adequately fast. However, reducing the total number of sub-modules of each phase unit with the ON state will immediately drop the dc voltage. To do so, the same quantity of the sub-modules (about 10% of the total number) from the upper and lower arms should be bypassed at the same time. The reference value of the voltage controller has to be reduced simultaneously in order to prevent the voltage increase of the other sub module capacitors. The reference power is also reduced accordingly, in order to prevent over current on the dc line. The modified control diagram of half-bridge MMC HVDC that also includes the fault detection unit is presented in Figure 5-41.
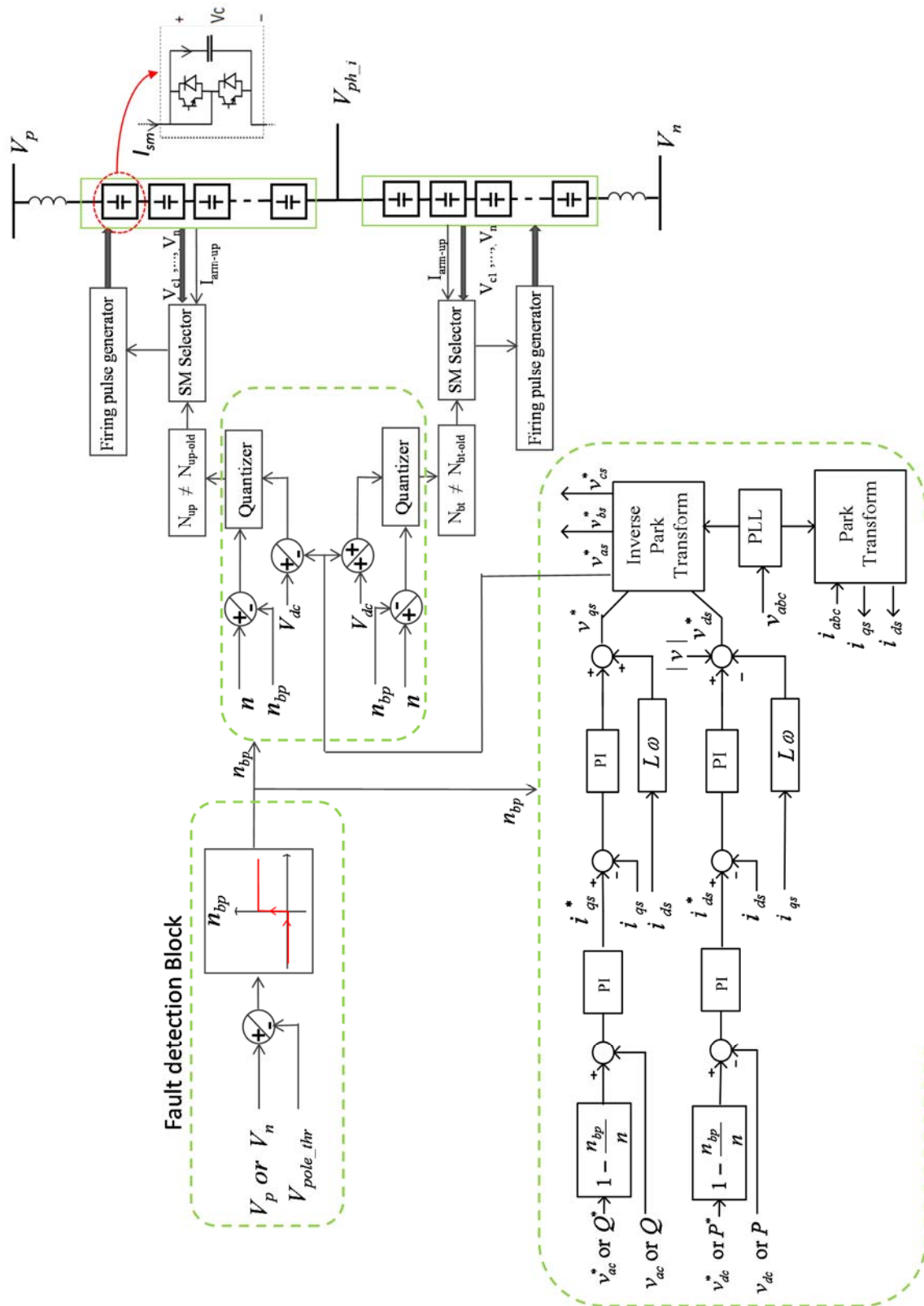
Figure 5-41 Modified control diagram of half-bridge MMC HVDC with pole to ground fault detection

Figure 5-42 shows the voltage waveforms at each end of the overhead line using this control method. The ac voltage waveforms of the ac network at the rectifier and inverter stations are also presented here in Figure 5-43.
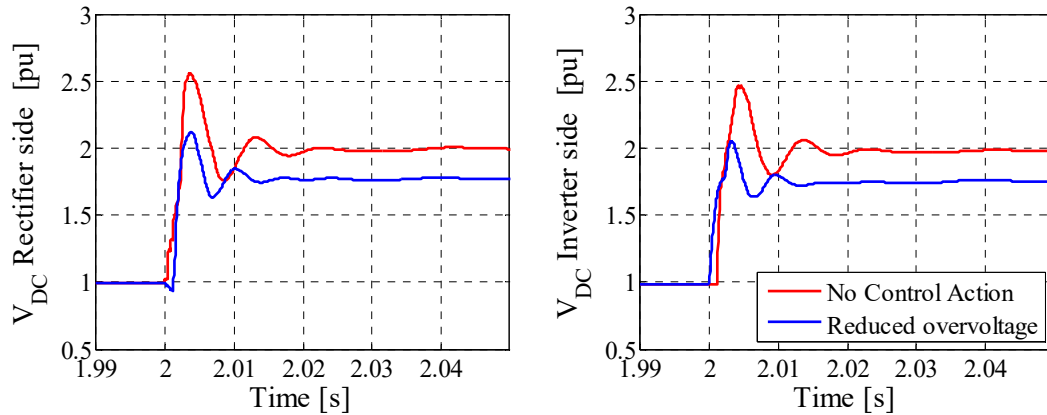
Figure 5-42 Dc voltage line waveforms at the (a) rectifier, (b) inverter terminal
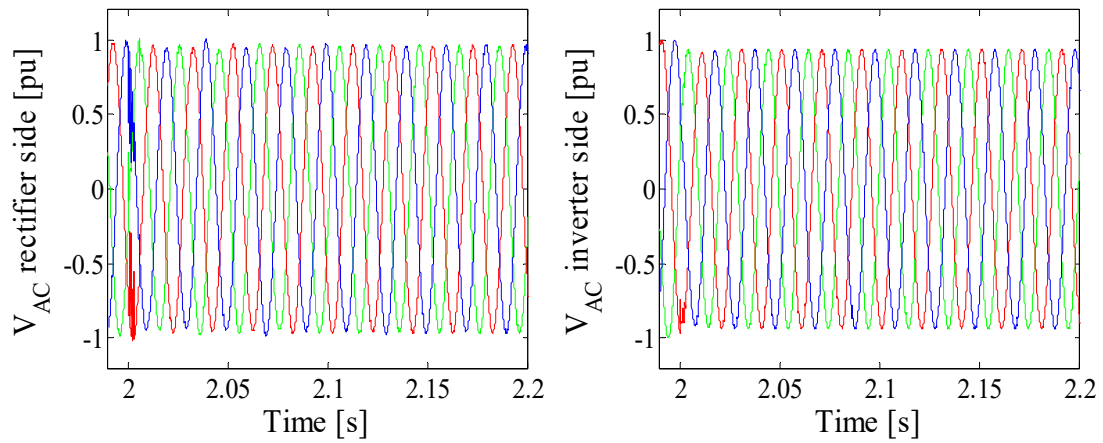
Figure 5-43 Ac voltage waveforms of the ac network at the rectifier and inverter stations

5.6   Conclusion

A comprehensive analysis on slow front overvoltages on transmission lines of MMC HVDC systems was performed in this chapter. Several major conclusions of this study can be summarized as follows:

- Reducing the pole to neutral and pole to pole spacing of the overhead lines, which increases capacitance and decreases reactance, results in a larger damping factor for transient overvoltages. Doing so can therefore reduce slow front overvoltages, especially for symmetrical monopole configurations.

- The proposed control approaches in both full- and half-bridge MMCs reduce the pole to pole voltage on fault application. This also has the beneficial effect of reducing the required surge arrester size for line insulation. It also can minimize air clearances, insulator length and in some cases minimum ground clearances – thus achieving maximum compaction of HVDC overhead lines.

- With the proposed control approach, by reducing slow front overvoltages in the symmetrical monopole systems, partial power can still be transmitted during non-permanent single pole to ground faults.

- Line surge arrester arrangements that reduce the slow front overvoltages, and consequently the required air clearances, along the entire HVDC overhead lines are identified.

Chapter 6

Lightning Performance and Fast Front Overvoltage Analysis of the Proposed Compact HVDC transmission Line

Lightning strikes are the main source of the fast front overvoltages on overhead transmission lines. The goal of this chapter is to evaluate the response of the proposed compact structure to lightning. The focus is mainly on evaluation of the critical lightning currents that results in fast front overvoltage stresses and may cause insulation failure.

Lightning performance analysis of overhead transmission lines involves looking at both the characteristics of lightning and the response of transmission lines to it. The knowledge of the latter is more complete because it has been studied in the laboratories [122], [123], [124] and the knowledge of the former relies primarily on incidental observations and conclusions both from records and from field measurements [50], [69], [125].

Lightning strike in the proximity of transmission lines may hit the conductor, the tower or the shield wires which are placed above the conductors to protect them against direct

strikes. Lightning hitting the conductor causes overvoltage on the line which, if the lightning current exceeds a certain value, will result in an overvoltage large enough to cause insulator flashover. Lightning strikes hitting the tower and shield wires lead to an overvoltage on top of the tower that is also a function of the lightning current as well as the tower grounding. This voltage is coupled to the conductor; it stresses the tower insulation and may cause back flashover.

There are many different methods proposed to analyze lightning performance of transmission lines, including electro-geometric models (EGM) [50], [125], generic models and statistical approaches [126], [127]. The electro-geometrical model is used in this thesis, since in general it results in the highest shielding failure current and thereby assumes a worst case scenario, according to [127] and is also the recommended as a standard by IEEE [86]. In order to investigate back flashover, an accurate transmission line model is required [128] which is available in simulation packages such as PSCAD/EMTDC and which is used in this thesis.

In order to evaluate the impact of the line compaction on lightning performance, the results are compared with the conventional overhead dc line described in Section 3.1. The conductor locations on each tower are shown in Figure 6-1 and the detailed parameters of each line structure are listed in Table 6-1. The conductors are assumed to be the same for both designs and their properties are listed in Table 3-1.
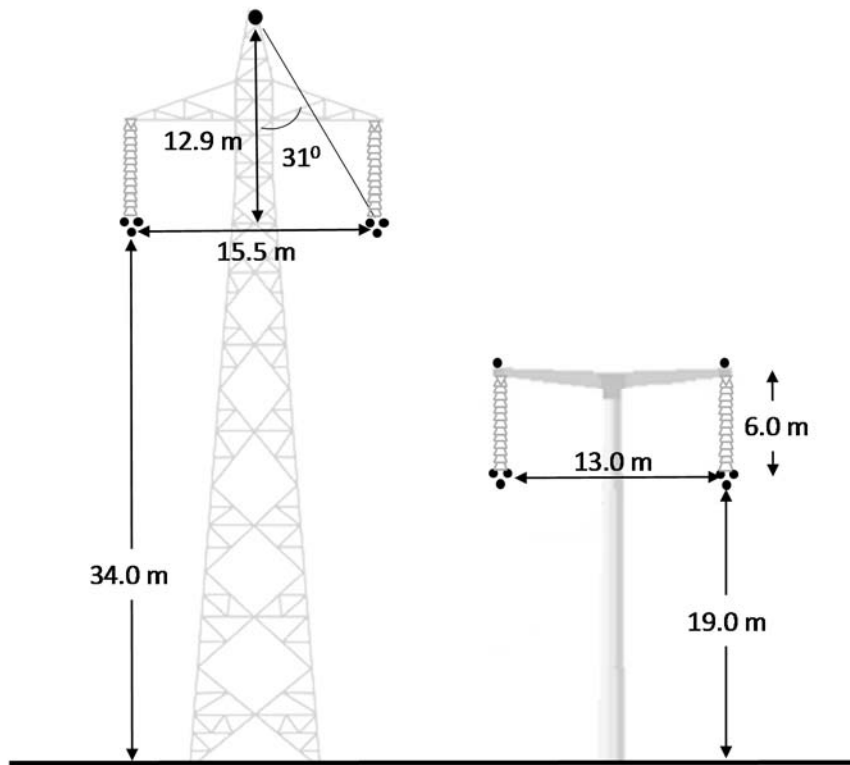
Figure 6-1 Tower Geometry

Table 6-1 Detailed parameters of the line geometry

Tower parameters		
	Conventional [m]	Compact [m]
Cross arm length	7.75	6.5
Tower height	46.9	25
width at conductor height	2.1	1
width at ground	7.85	1.5
Insulator length	5	5
Span length	488	244
Wire locations		
Shield wire height at the tower	46.9	25
Conductor height at the tower	34	19
Shielding angle	30	0
Conductor sag	20.8	5.8
Shield wire sag	8	2.5

6.1   Impact of the Structure Height on Frequency of the Lightning Flash Collection

The first step to analyze lightning performance of the high voltage transmission lines is to estimate the frequency of the lightning strike occurrence in the region that the transmission line is located. Nowadays, ground flash density in any area can be estimated from records of lightning locating equipment and flash counter networks. It is quantified as the number of flashes occurring per unit area per year [69]. The ground flash density maps for Canada and the United States are available in [129], [130]. Obviously, when two routes with similar soil characteristics are being compared, the route through a region with lower density of severe flashes will definitely have fewer outages.

In order to estimate the number of flashes to earth that are intercepted by the transmission line, a simplified method [69] assumes that the line throws an electrical shadow on the land beneath. If a lightning flash terminates within this area, it is attracted to the line, whereas flashes outside this shadow will entirely miss the line. Figure 6-2 shows a comparative demonstration of the shadow width, W_1 and W_2, for a conventional and a low-profile line. Generally, more flashes are collected by the taller towers especially if they are higher than the surrounding terrain or tree profile.
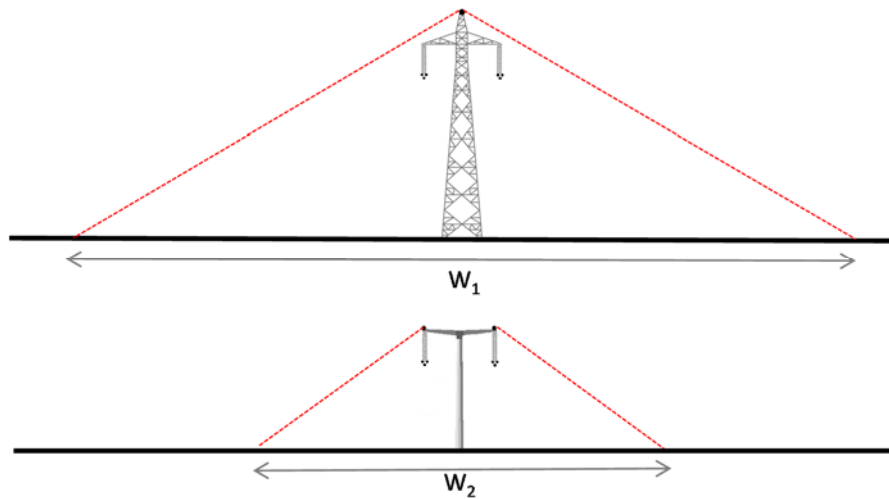
Figure 6-2 Lightning shadow area

From the shadow area, W, and the ground flash density, N_g, the expected number of light-

ning strikes on the line can be estimated. Initially, based on inadequate available data, the

shadow area was estimated as four times the tower height plus the distance between the

shield wires [69]. Later on, some researchers modified this approximation [131]. The most

widely used empirical equations are the Whitehead equation [132] and the Erikson equa-

tion [133]. Whitehead first offered the modified empirical equation, as expressed in equa-

tion 6.1, which obtained a better correlation with the observed data. Erikson later addressed

another equation based on more comprehensive empirical and analytical studies as given

in equation 6.2.

$$\text{Whitehead} \; : \; N_l = 0.1 N_g \cdot (4h^{1.09} + D) \quad [\frac{flashes}{100km.year}] \qquad 6.1$$

$$\text{Erikson} \quad : \; N_l = 0.1 N_g \cdot (28 \cdot h_t^{0.6} + D) \quad [\frac{flashes}{100km.year}] \qquad 6.2$$

In Equation 6.1 and 6.2, N_l is the number of flashes/100km/yr, N_g is the ground flash density (flashes/km^2/yr), h is the average conductor height (m), h_t is the tower height (m) and D is the overhead shield wire seperation distance (m).

Eriksson's model depends only on tower height, while the Whitehead's model is derived for average conductor height, which is a function of both tower height and the conductor sag. In order to compare these models, the average conductor height should be generally offset to 10- 20% greater than the conductor height [131]. The shadow area as a function of the conductor height for each model is presented in Figure 6-3. This graph shows that the Whitehead model (also known as the IEEE model) may lead to underestimations of up to 50% of the number of incidents in the height range of 10 - 30 m. However, it can also overestimate the expected strike incidence to taller structures above 65m.
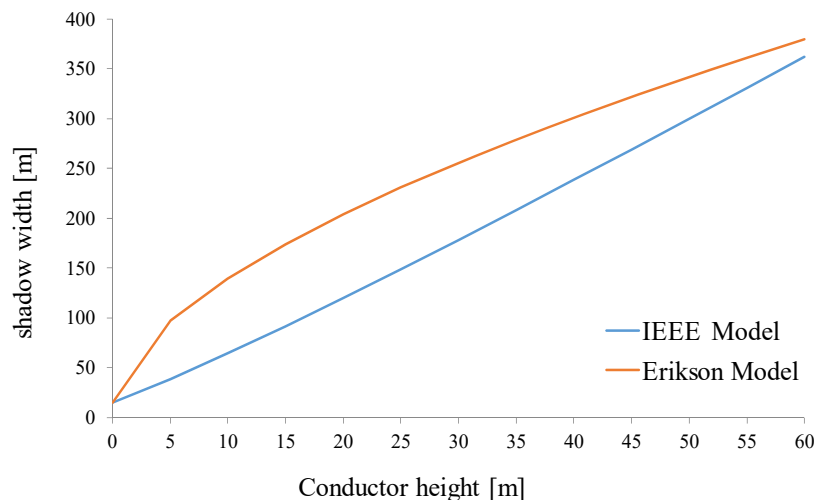
Figure 6-3 Shadow area for lightning models

The worst case of ground flash density in Southern Manitoba, from 1999 to 2008, was 1.0 flashes/km^2/year [129]. Table 6-2 shows the number of flashes per 100km of the line length per year for both compact and conventional HVDC lines in Southern Manitoba using the above models.

Table 6-2 Number of flashes per100km per year for both compact and conventional lines

	Conventional DC Line	Compact DC Line
Whitehead model	11	9
Erikson model	28	20

6.2   Lightning Flash on Transmission Lines

Lightning is an electric discharge in the form of a spark or flash originating from a charged region in a thundercloud. This channel of ionized air is also called a "leader", and over 90% of which have negative polarity [134]. As the downward leader approaches earth, its space charge sheath induces significant charges on the objects in the vicinity and results in enhancement in their electric field and stresses the ambient air. When the electric field reaches critical levels the ambient air is ionized, the stem from the objects starts to grow to form a leader discharge. For a strike to occur, a downward leader has to grow and connect to an available upward leader from the objects in the vicinity that will eventually form a low-resistance path. The distance between the descending leader tip and the object at the instant of inception of the upward leader is called the maximum radial attractive distance of a structure (or the maximum lateral attractive distance of a conductor) [134]. Several different models for the zone-of-attraction have been developed [124], [134]. The models treat the zone-of-attraction as a 'strike distance' and are called electro-geometric models [124]. With this concept, a zone-of-attraction can be defined for any object in the vicinity such that any lightning strike entering an object's zone-of-attraction will strike that object. In the case of several tall objects close together, lightning will strike the object with the largest and outermost zone-of-attraction. In other words, this object will effectively shield the

other objects from lightning. Based on this lightning characteristic, ground wires, also

known as shield wires, are placed on top of the towers to attract the lightning strikes and

protect the overhead lines against lightning [69].

When a downward leader approaches the OHL from a charged cloud, upwards leaders are

launched from the ground, the ground wires and the energized conductors. Figure 6-4

shows the striking distances from each of them. Therefore there are three possible dis-

charge paths for the lightning strike. For example, if an upwards leader from a ground wire

reaches the downwards leader the lightning will terminated on the ground wire. However,

the ground wires do not always protect the conductors from a direct strike, resulting in

"shielding failure" [69].
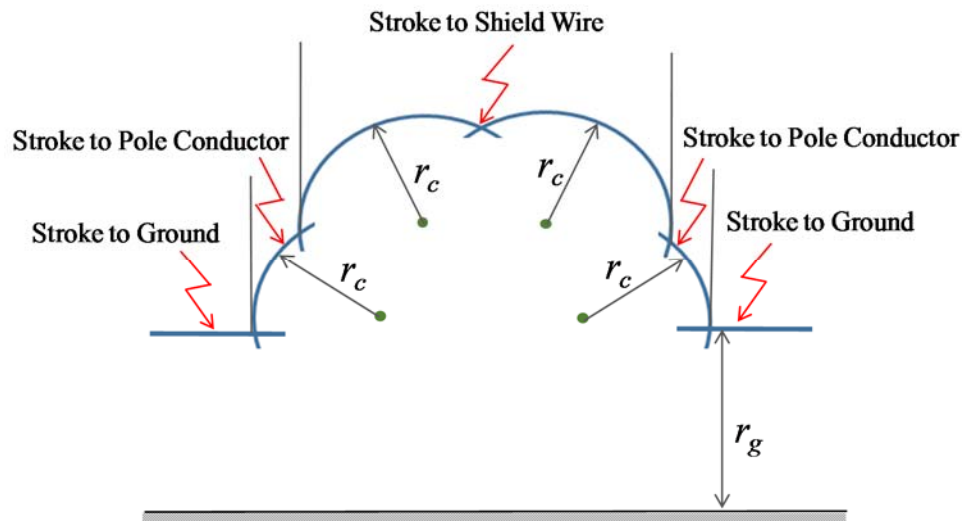
Figure 6-4 Striking distances for final jump in Electro-geometric models

If a lightning stroke hits the dc pole conductor, it injects the main discharge current into

the conductor, thus developing a voltage across the insulator string proportional to the

surge impedance of the conductor. Even for relatively low lightning current, the resulting

voltage will normally exceed the critical value of the insulator voltage withstand strength

and a *flashover* may occur [69]. If lightning strike hits the shield wire, the current waves

will travel down each direction of the shield wire with the larger residual amount and also

down the tower and, through its effective impedance, raise the potential of the tower top to

a point where the difference in voltage across the insulation is sufficient to cause flashover

from the tower back to the conductor which is called *back flashover* mode [69]. This chap-

ter is mostly focused on investigating the critical currents and voltages that have a serious

impact, e.g. shielding failure or insulator flashover on a compact transmission line.

6.2.1   Striking Distance and Shielding Effect

As described previously, shielding analysis according to electro-geometric models is based

on striking distance [131]. The striking distance to an object, r_c, is a function of the pro-

spective lightning peak current, I. It can be associated with striking distance to earth sur-

face, r_g, by using a factor γ. In general, striking distance based on the normal electro-geo-

metrical model is given in described in equation 6.3 [86].

$$r_c = A \cdot I^B = \gamma \cdot r_g \qquad\qquad 6.3$$

where I is the lightning peak current in kA, r_c and r_g are the striking distances of the con-

ductor/shield wires and the ground respectively in m and *A, B* and γ are constants. Note

that the strike's current amplitudes within a lightning flash are described in terms of prob-

abilities [50]. Commonly used cumulative statistical distributions, which are largely based

on direct lightning current measurements, are presented in [50].
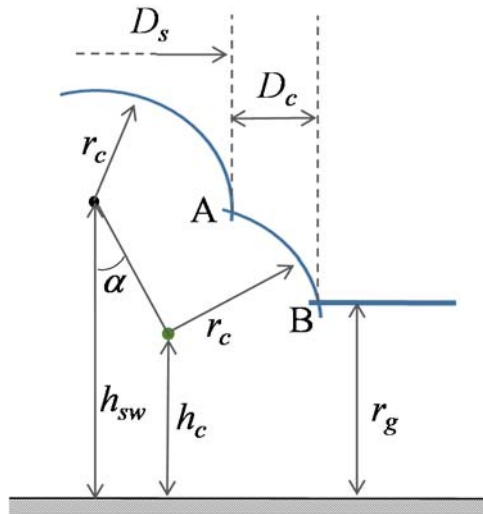
Figure 6-5 Striking distances in electromagnetic models

Figure 6-5 illustrates the resultant striking distance for a specific value of strike current. It is represented as a sector of a circle surrounding a conductor, with radius r_c as formulated in equation 6.3. A striking distance to the ground, generated in the same manner, is also shown in Figure 6-5 as a horizontal line above the ground with radius r_g. Striking distance from the conductor is usually considered to be greater than that from the ground since local electric field gradients around conductors are somewhat higher than at ground level [86]. If the downwards leader reaches the striking distance in between points A and B, (D_c, as shown in Figure 6-5), the lightning will terminate on the pole conductor. However, if the leader reaches the area D_s, the lightning will terminate on the shield wire. Lightning striking outside these areas will terminate on the ground.
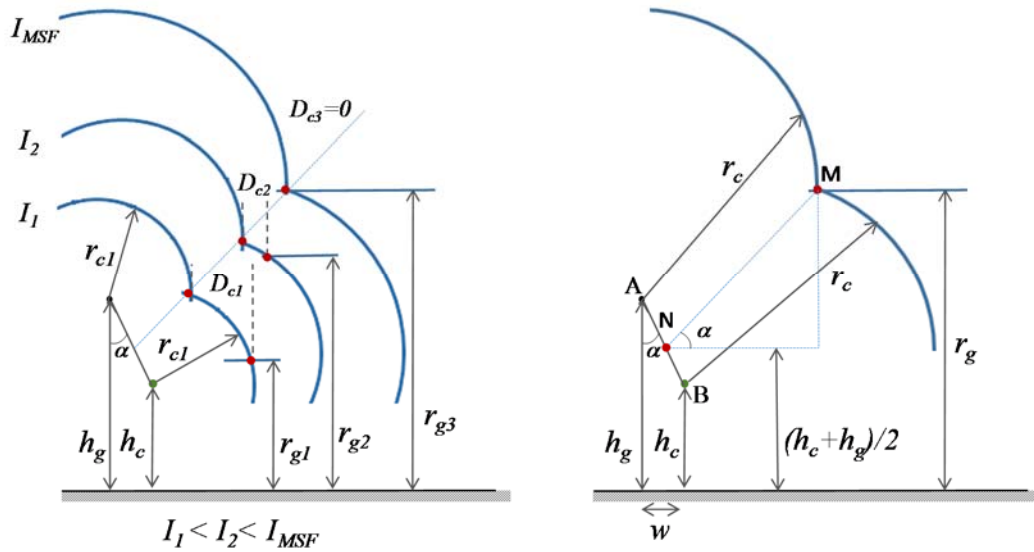
Figure 6-6 (a) D_c decreases as the lightning current increases, (b) maximum shielding failure current

As shown in Figure 6-6 (a), the distance Dc, in where the lightning strike can hit the pole conductor, decreases as the lightning current increases. The largest current that can terminate on the pole conductor is defined as the maximum shielding failure current (I_{MSF}). In other words, no shielding failure can occur for lighting strike currents above the maximum shielding failure current. As shown in Figure 6-6 (b), general expressions of I_{MSF} can be derived as follows:

$$\sin \alpha = \frac{r_g - (h_g + h_c)/2}{NM} \qquad 6.4$$

Since $r_C >> AN$, $MN \approx r_c$; therefore

$$\frac{r_c}{r_g}\sin \alpha = 1 - \frac{(h_g + h_c)}{2 \cdot r_g} \qquad 6.5$$

From equation 6.3, $r_c / r_g = \gamma$. Hence equation 6.5 can be expressed as:

$$r_g = \frac{(h_g + h_c)/2}{1 - \gamma \sin \alpha} \qquad 6.6$$

Also from equation 6.3, when the lightning current is I_{MSF}, $r_g = (A/\gamma)I_{MSF}^B$ which when

substituted in equation 6.6, I_{MSF} can be calculated as given in 6.7.

$$I_{MSF} = \left(\frac{\gamma(h_g + h_c)/2}{A(1 - \gamma\sin\alpha)}\right)^{1/B}$$ 6.7

Several researchers, particularly Wagner et al., [135], [136], Young et al., [137], Armstrong

and Whitehead [138], Brown and Whitehead [139], Love [140], and Mousa [141], have

contributed to formulate the striking distances of the lightning strike in the electro-geomet-

ric model. Eriksson [142], using leader progression model concepts, modified the electro-

geometric model by introducing the attractive radius at which the upward and downward

leaders will grow and eventually meet when sufficient field strength is present. Eriksson

has noted that the striking distance is not only a function of the lightning peak current but

is also significantly sensitive to height of the conductor. Therefore, the attractive radius, r_c,

of a conductor is expressed as follows [142]:

$$r_c = 0.67\, h^{0.6} I^{0.74}$$ 6.8

where I is the lightning peak current in kA and h is conductor height in meters. Note that

here the striking distances of the shield wire and pole conductor are different and depend

on their height. Further, the strike terminating to earth is assumed as a default condition

and therefore a striking distance equation to earth is not required [142].

In Eriksson's model, similar shielding analysis to that of electro-geometric models is per-

formed by using the appropriate attractive radius to draw arcs from the shield wire and pole

conductor. Thus, for shielding failure width $D_c = 0$ the maximum shielding failure current

I_{MSF} (kA) can be derived similarly as follows [142]:

$$I_{MSF} = \left[\frac{w + \sqrt{w^2 + y^2(x^2 - 1)}}{0.67 \cdot h_c^{0.6}(x^2 - 1)} \right]^{1/0.74} \qquad 6.9$$

where $x = (h_g/h_c)^{0.6}$, $y^2 = (h_g - h_c)^2 + w^2$ and h_g, h_c and w are shown in Figure 6-6 (b).

As described earlier, different values for the constants in equation 6.7 and equation 6.9 are given from various sources. Table 6-3 shows the maximum shielding failure current and the striking distances of compact and conventional lines using different models. The results from the different models show considerable variation. Nevertheless, regardless of the model used, it can be observed that the maximum shielding failure current of the compact design is significantly lower than in the conventional design. This is due to two factors; the shorter tower height and the location of the shield wires, also known as shielding angle, shown in Figure 6-1. However, a review of literature indicated that for studies conducted on Bipoles I and II of the Nelson River HVDC Transmission system, Eriksson's model yielded failure rates most consistent with the recorded data in [143].

Table 6-3 Calculation of striking distances and I_{MSF} for compact and conventional design

	Constants			Conventional design			Proposed compact design		
	A	B	γ	I_{msf}	r_c	r_g	I_{msf}	r_c	r_g
Young	27 γ	0.32	1.07	41.72	95.27	89.04	0.53	23.54	22.0
Armstrong-Whitehead	6.72	0.8	1.11	30.50	103.48	93.22	5.02	24.42	22.0
Brown-Whitehead	7.1	0.75	1.11	35.60	103.48	93.22	5.19	24.42	22.0
Love	10	0.65	1	25.72	82.55	82.55	3.36	22.00	22.0
IEEE Working Group	8	0.65	1	36.26	82.55	82.55	4.74	22.00	22.0
Erikson	6.74	0.74	NA	16.31	43.86/53.2	NA	3.36	13.62/16.52	NA

The conventional design, as shown in Figure 6-1, has one shield wire with the shielding angle of 30^0. The vertical distance between the shield wire and the pole conductor is 12.9 meters in this tower design. Assuming the tower top geometry remains the same, the impact

of conductor height on maximum shielding failure current in a conventional dc line using different constants in the electro-geometric model is shown in Figure 6-7. In addition, Figure 6-8 shows the impact of shielding angle on maximum shielding failure current, assuming the conductor and shield wire heights are constant. It can be observed that although there is a great variability in I_{MSF} among lightning attachment models, all models agree in predicting that I_{MSF} increases with shielding angle and conductor height.
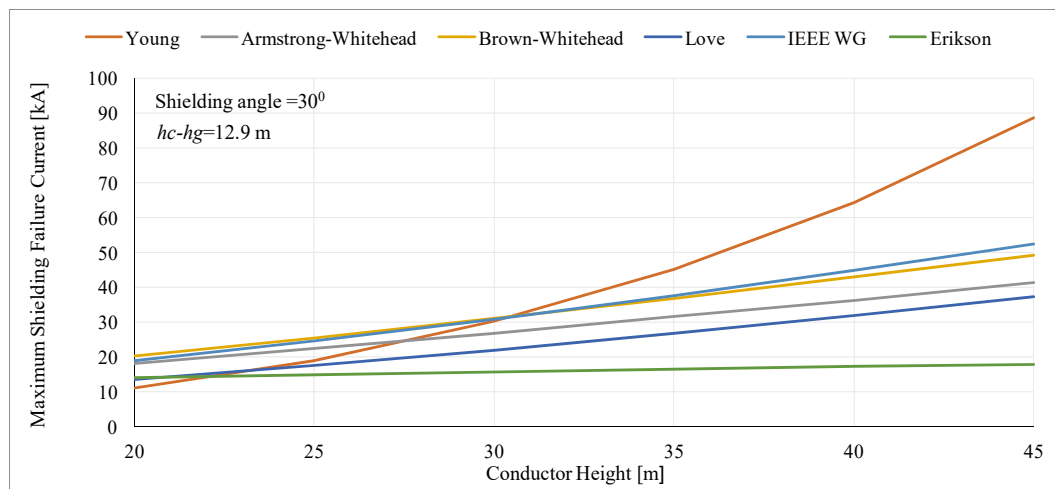
Figure 6-7 Impact of conductor height on maximum shielding failure current in conventional dc line
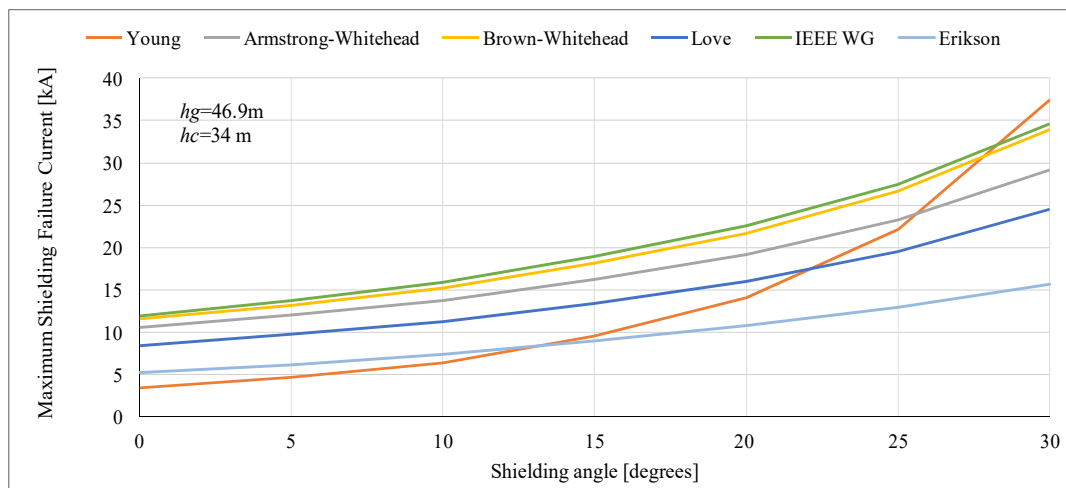
Figure 6-8 Impact of shielding angle on maximum shielding failure current in conventional dc line

6.2.2   Critical Current

So far it has been shown that a lightning strike with current of less than or equal to I_{MSF}, within the lightning shadow of transmission lines can result in shielding failure and hit the pole conductor. It is also important to find the minimum lightning current, also known as critical current (I_C), that is required for a flashover of the tower insulators. The critical current can be calculated from the characteristic impedance of the line and the critical flashover voltage (CFO) of the tower insulators [69]. Assuming the effect of conductor voltage is neglected, the critical current has been determined using equation 6.10 and 6.11.

$$I_c \frac{Z_0}{2} = CFO \qquad\qquad 6.10$$

$$Z_0 = 60\sqrt{\ln\frac{2h}{r}\ln\frac{2h}{R_c}} \qquad\qquad 6.11$$

Here, Z_o is the conductor surge impedance under corona, h is the average conductor height, r is the conductor equivalent radius m, R_c is the corona radius of the conductor at a gradient of 1500kV/m [69] and CFO is the insulator string critical flashover voltage. For lightning performance analysis with standard lightning impulse waveforms, the CFO is 490 kV/m when the time to flashover is greater than 16 us [49].

For a dc line with a pole to ground voltage magnitude Vp and Vn for positive and negative poles a similar approximate relationship for the positive pole would be [134]:

$$I_c \frac{Z_0}{2} - V_p = CFO \qquad\qquad 6.12$$

$$I_c \frac{Z_0}{2} + V_n = CFO \qquad\qquad 6.13$$

Therefore the critical current for the positive and negative poles can be expressed as:

$$I_c = \frac{2 \cdot (CFO + V_p)}{Z_0}$$
6.14

$$I_c = \frac{2 \cdot (CFO - V_n)}{Z_0}$$
6.15

It is obvious from equations 6.14 and 6.15 that considering the effect of dc pole voltage, the critical current of the positive pole will be higher than the negative pole. Table 6-4 shows the critical currents for positive and negative pole for both compact and conventional lines.

Table 6-4 Critical current of the compact and convention design for CFO=2450 kV (5[m] × 490[kV/m])

		Conventional Lattice	Proposed compact
Surge impedance (Ω)		357	340
Critical current (kA)	Positive pole	16.52	17.35
	Negative pole	10.92	11.47

6.3   Shielding Angle and Height

As described earlier, the geometry and the placing of the ground wires have significant influence on their capability to protect the conductors (shielding effects) and eventually in the overall lightning performance of the OHL [49]. Perfect shielding can be obtained when the maximum shielding failure current is equal to or less than the critical current ($I_{MSF} \leq I_c$) [49]. In order to achieve an effective shielding of the overhead lines, the shielding angle α, as shown in Figure 6-6, should be decreased as the height of the transmission line structures increases. A demonstration of the relationship between the shielding angle and conductor height with the maximum shielding failure current using different models is presented in

Figure 6-9. It can be observed that the Young model is the most sensitive model to con-
ductor height, while the Erikson model is the least sensitive. After calculating the critical
current of a transmission line, the data shown can help to find the perfect shielding angle
for different tower heights.
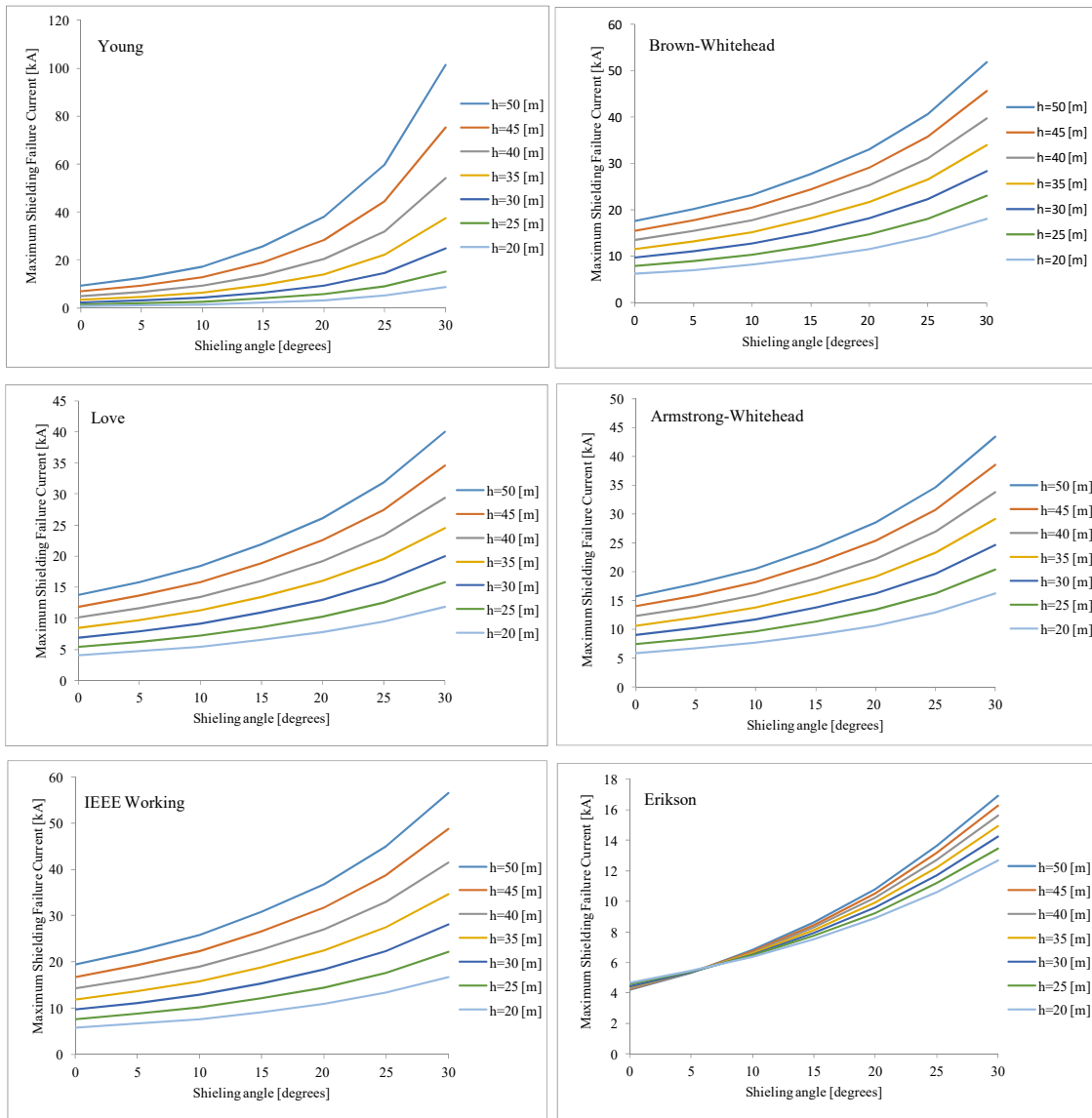
Figure 6-9 Relationship between the shielding angle and conductor height with the maximum shielding
failure current using different models

However, this perfect shielding solution has a limitation. Even if the first stroke-current magnitude is less than the critical current I_c, subsequent strokes that follow the same leader may possess current magnitudes that exceed I_c and result in flashover. The amplitude of the first and second stroke is independent in the recorded data [69]. However the first stroke-current waveform in a flash tends to rise more gradually to its crest than the waveform in the subsequent stokes. Experiments have shown [69] that for typical transmission lines, the subsequent stoke is not likely to be dominant more than 20% of the time primarily because its voltage generating effects are of fractional microsecond duration at a time when the volt-time strength of an insulator string is extremely high. Therefore $I_{MSF}=I_c$ can result in a very low but non-zero shielding failure flashover rate.

6.4   Back Flashover

When a lightning strike contacts the ground wire or the tower, a portion of lightning current enters the ground through the tower and the remainder travels along ground wires in each direction. The initial fractions along these two paths depend on the relative surge imped-ances of the ground wires and the tower. This current produces a voltage surge on the top of the tower structure. Considering capacitance and inductance coupling between guard wires, tower structure and pole conductors, another surge voltage with the same waveform and lower amplitude is induced and superimposed on the existing pole conductors. Figure 6-10(a) illustrates the tower top voltage V_2 and the pole voltage, V_1. The voltage difference between the tower top and the pole conductor will appear across the insulator string, V_{string}. If the potential of a tower rises to a value where the insulator string can no longer withstand the voltage between the tower and the phase conductor, i.e., $|V_1-V_2| > V_w$, an electrical arc

starts from tower structure toward the pole conductor and a back flash will occur, as shown

in Figure 6-10 (c). As a result, the major part of electrical charges transmits to pole con-

ductor through the arc path, and increases the pole voltage from V_1 to V_2. Note that the

withstand voltage V_w is also time dependent, i.e., a significantly large voltage can be with-

stood for a short time, but this withstand capacity decreases with time [69].
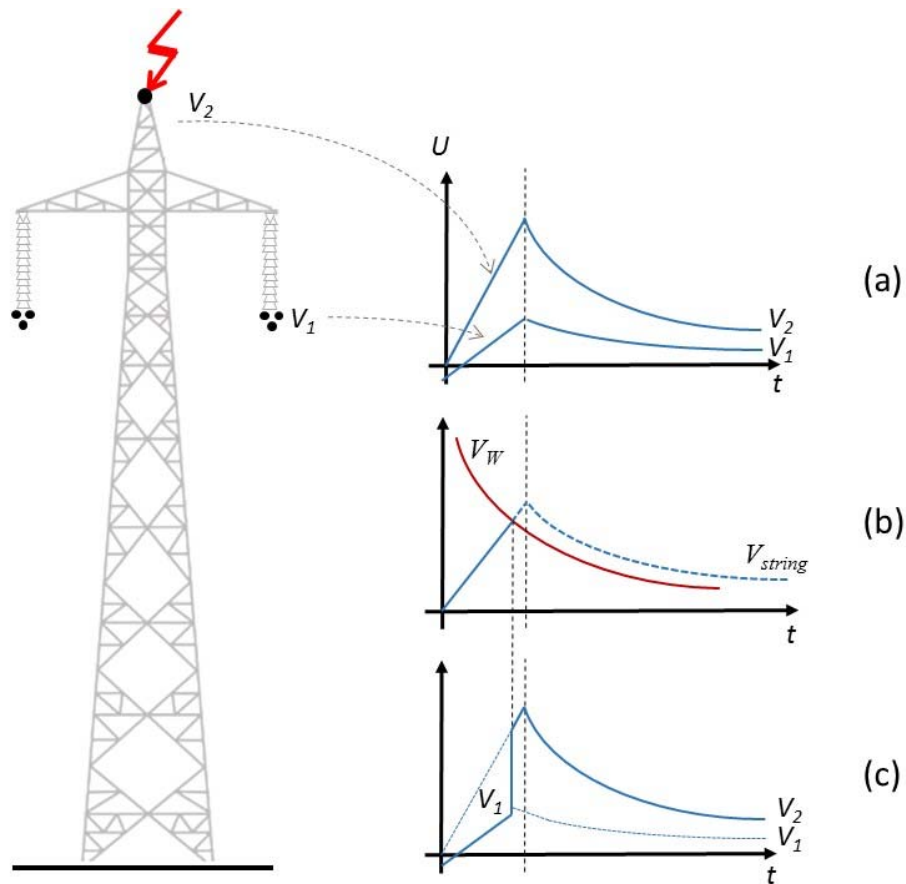
Figure 6-10 Back flashover mechanism

The most important factor affecting back flashover is the surge impedance of current path

to ground through the tower structure - including the footing resistance as well as the tower

structure impedance. Surge impedance of the tower is a function of the tower height and

cross section. The discharge speed of electrical charges to ground increases as this imped-

ance decrease and consequently causes the amplitude of surge voltage created on the tower

structure to decrease [69].

6.4.1   Back Flashover Modeling

In order to find the minimum lightning current that results in back flashover in the low

profile compact design compared to the conventional HVDC transmission lines, the light-

ning incidence needs to be simulated by an electromagnetic transient simulation software,

such as PSCAD/EMTDC [128]. The following sections describe the modeling of the tower

structure, footing resistance, transmission line, insulator, lighting strike currents and related

components in detail, and then the simulation results are presented.

Selection of the calculation time step is an important consideration in fast front overvoltage

studies. Waves on the transmission lines travel at speeds close to the speed of light, at 0.3

meters per nanosecond. Considering the shortest line length in the model (i.e. the cross arm

length that will be explained in the next section) a space resolution of 0.3 m appears ade-

quate, corresponding to a travel time of 1 nanoseconds. Therefore lightning simulation

studies can be conducted with calculation time steps of 1 ns [128].

- Tower model

In order to model the fast front surges of the lightning current travelling through the tower,

each major tower section can be represented as a short transmission line Bergeron model

[128]. The equivalent models of each section of the proposed low-profile tower and the

conventional lattice tower are illustrated in Figure 6-11. For each section, the propagation

time and surge impedance are required for the equivalent transmission line model. The

travel time of a wave down the tower should be the tower height divided by the velocity of light. However, full measurements of the surge responses of the lattice towers, varying in height from 26m to 216 meters, showed that measured velocity of propagation of the surge was about $0.7 \times C$ to $0.9 \times C$ (where C = velocity of light in a vacuum) [69]. Table 6-5 shows the surge impedance of each section, using approximations given in [69] and the tower parameters listed in Table 6-1.
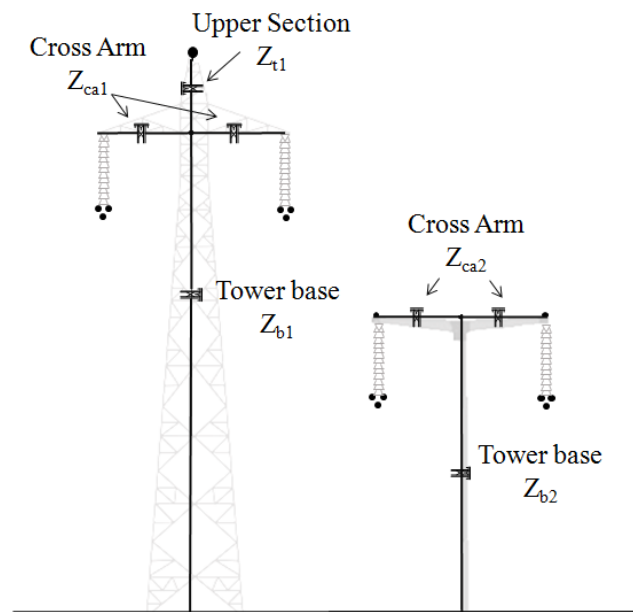
Figure 6-11 Equivalent model of the tower structure

Table 6-5 Surge impedance of the tower sections [69]

Surge Impedance	Lattice Tower	Low profile tower
Tower base	$Z_{b1} = 60 \ln \cot(0.5 \tan^{-1}(\frac{r_1 + r_2}{h}))$	$Z_{b2} = 132.8 \log(\frac{h}{r}) + \frac{90r}{h} - 60$
Tower cross arm	$Z_{ca1} = 60 \ln(\frac{2h}{r})$	$Z_{ca2} = 60 \ln(\frac{2h}{r})$
Tower Upper Section	$Z_{b1} = 60 \ln \cot(0.5 \tan^{-1}(\frac{r_1 + r_2}{h}))$	NA

- Tower Footing Resistance

Tower footing resistance is another important parameter in lightning back flashover analysis. High structure footing impedances cause increased voltages and more lightning outages for a given lightning strike current. Unfortunately, this resistance is a fluctuating statistical variable, that its magnitude is governed not only by geography but also by nonlinear conduction physics in the earth [69]. It is generally agreed that the resistance of an earth electrode decreases with the applied current due to ionization of the soil. A simplified method for calculating the reduction in ground resistance is given in [50] in which the current dependence footing resistance is expressed in equation 6.16:

$$R_T = \frac{R_0}{\sqrt{1 + I/I_g}}$$
                                                                                           6.16

where R_T (Ω) is tower footing resistance, R_0 (Ω) is the tower footing resistance at low current and low frequency, I_g (A) is the limiting current to initiate sufficient soil ionization and I (A) is the lightning current through the footing impedance. The limiting current is a function of soil ionization as follows [50]:

$$I_g = \frac{E_0 \cdot \rho}{2\pi \cdot R_0^2}$$
                                                                                           6.17

where ρ is the soil resistivity (Ω.m), E_0 is the soil ionization gradient (kV/m) which is about 300-400 kV/m [4]. The soil resistivity ρ varies greatly over the length of the line, a typical value of 100 Ω. m [50], [143] was used in this thesis. A typical tower grounding resistance of 5 ohms [49] is also used for both compact and conventional design.

- Insulator model

The flashover or back flashover along the insulator string can occur when the electric stress between the conductor and the tower cross-arm exceeds the withstand voltage of the insulator string. The insulator string model can be represented as a capacitor in parallel with a voltage-controlled switch connected between the pole conductor and the tower to represent a flashover [128]. For a simplified analysis, a detailed arcing model for flashover is not necessary. Thus a short circuit (ideal switch) representation is adequate. The capacitance value of suspension insulator and pin insulators are typically 80 pF/unit and 100 pF/unit respectively while the capacitance value of ceramic insulators are an order of magnitude more for equivalent non-ceramic insulators [69], [143].

There are many methods to model the breakdown performance of the insulators, including a volt–time curve and the leader propagation method [144]. The leader propagation method is more accurate for standard or non-standard lightning impulses, since it gives special consideration to breakdown parameters and to physical aspects associated with the discharge mechanism. However, the volt-time characteristics curve method is sufficient for standard lightning impulses, which are also of main concern for insulation coordination studies [50], [144]. In the volt-time curve method the voltage withstand capability of the insulator, which is a function of insulator length, is represented in equation 6.18 [49]:

$$U = K_1 + \frac{K_2}{t^{0.75}} \qquad\qquad 6.18$$

where U is the insulator breakdown voltage, $k_1{=}400{\times}L$, $K_2{=}710{\times}L$, L is the insulator length [m] and t is elapsed time after lighting strike [usec]. In the simulation, the insulator flashover voltage is calculated using equation 6.18, and compared to the actual insulator

voltage. If the insulator voltage exceeds the withstand voltage, a flashover occurs across the insulator and the switch status changes to the closed (low resistance) position [128]. Manitoba Hydro's Bipole III uses insulators with a string of porcelain or toughened glass discs. In southern Manitoba where the towers are self-supported, each tangent suspension insulator string's length is 5 m and comprises 25 discs with a diameter of 380 mm (15 in.) and a weight of 15.4 kg (34 lb.) per disc [68].

- Lightning current

The important parameters of a lightning impulse are its impulse crest value I_0, the front time to crest t_f, and the time to half settle on the tail t_t. In lightning voltage analysis of transmission lines, a front time, t_f, must be selected first. Voltages will be directly proportional to strike-current amplitude. The magnitude of the current impulse due to lightning discharge is a probability function [69]. As described earlier, low discharge levels may result in a higher tendency for the lightning strike to bypass the shield wires and directly hit the pole conductors. The larger lightning impulse currents may tend to strike the tower top and lead to a back flashover. Generally for back flashover studies the current ranges from 50kA-300kA, since beyond this peak value there is inadequate information [122]. These currents require a front time somewhere between 1.2 and 2.5μsec for the calculations. The decay time is of secondary importance in back flashover studies and can be assumed to be a fixed value for all scenarios since insulation failure occurs shortly after the lightning strike [122].

A variety of equations exist in the literature [122] to represent the lightning current impulse waveform, including the double ramp, double exponential and Heidler function current

waveforms, as shown in Figure 6-12. The double ramp and double exponential equation are widely used in lightning study analysis. However, the Heidler model reproduces the observed concave rising portion of a typical current waveform, as opposed to other wave-forms [122], [144]. Experiments show that the crest current and the rapidly rising frontal currents near the crest play the key role in back flashover occurrence [122]. Therefore, the Heidler model is used in this thesis for back flashover analysis.
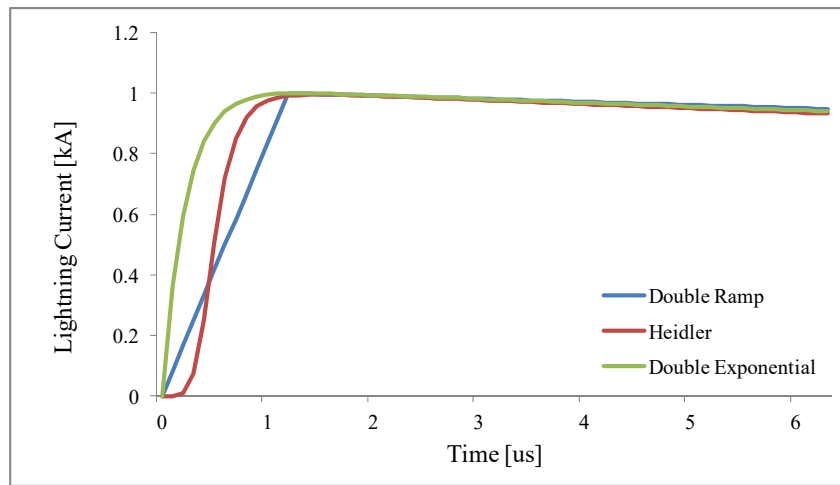
Figure 6-12 Different models of the lightning current waveform (1.2 us/50 us)

The Heidler function lightning current waveforms *i(t)* is expressed in equation 6.19 [122]:

$$i(t) = \frac{I_0}{\eta} \frac{(t/\tau_1)^n}{(t/\tau_1)^n + 1} e^{-t/\tau_2} \qquad\qquad 6.19$$

where I_0 is the peak of lightning, τ_1 is the rise time constant, τ_2 is the tail time constant, n is the concave factor, and η is the peak correction factor. Since most lightning currents are negative, only back flashovers for the positive pole are considered here.

Generally, the mean number of strikes per lightning flash is three, typically separated in time by 20 to 50 milliseconds. The time between strikes is sufficiently long, so that the fast

front transient effect is dissipated before the next strike arrives. The amplitude of the first

and second strike is independent in the recorded measurements. But the first strike-current

waveform in a flash tends to rise more gradually to crest than the waveforms in the subse-

quent strikes. The experiments [69] showed that for typical transmission lines, the subse-

quent strike is not likely to be dominant more than 20% of the time primarily because its

voltage generating effects are of fractional microsecond duration at a time when the volt-

time strength of an insulator string is extremely high. Therefore for practical lightning per-

formance calculations, the contribution of the second strikes to transmission lines can be

ignored. Generally the volt-time curves are obtained with a 1.5×50 μsec time constant

waveform [69].

6.4.2   Back Flashover Simulation Results

6.4.2.1. Impact of Different Tower Structures

The insulator voltage waveform resulting from lightning currents with different crest mag-

nitudes for compact and conventional towers are shown in Figure 6-13 and Figure 6-14

respectively. The minimum lightning current required to cause back flashover in compact

lines is 180 kA, whereas for conventional lines it is 100 kA. This means that the compact

tower is more resistant to back flashovers. Except for the tower design and shield wire and

conductor positions, all the other parameters, such as ground resistance (5 ohms), lightning

front time (1.2 us), insulator length and properties are assumed to be the same for both

simulation cases of the compact and conventional designs.
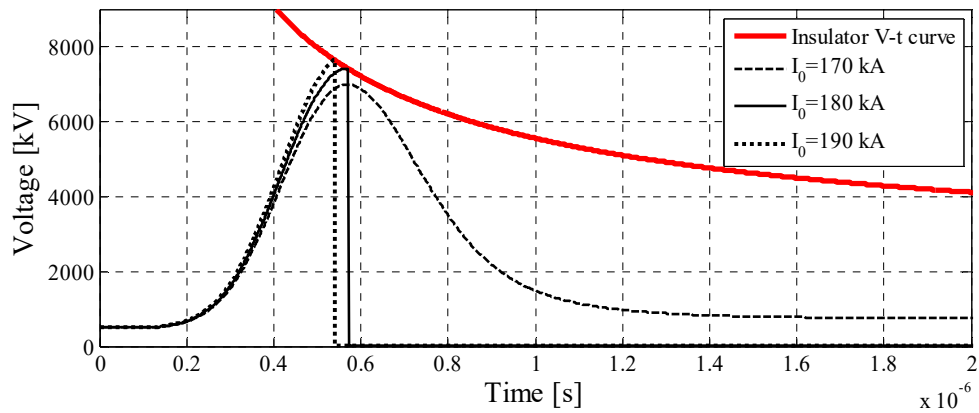
Figure 6-13 Insulator voltage for different magnitude of the lightning current for compact towers
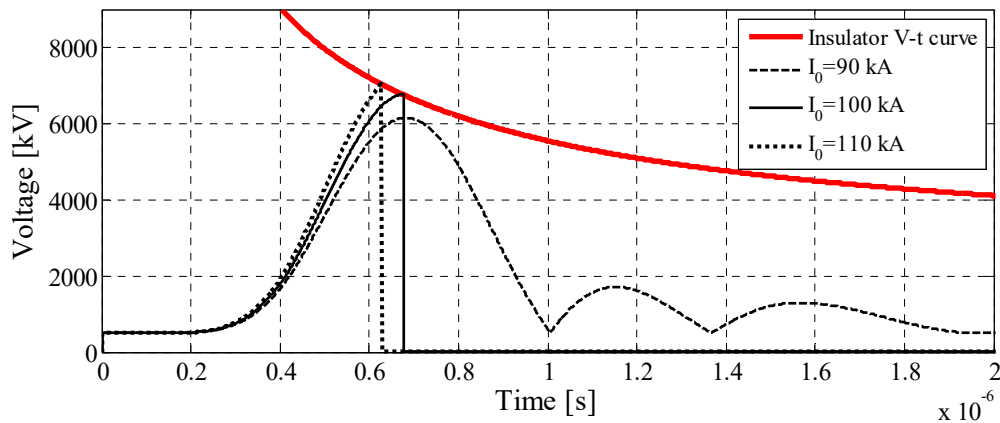
Figure 6-14 Insulator voltage for different magnitude of the lightning current for conventional towers

As explained earlier, the discharge speed of electrical charges to the ground increases as the impedance of the current path decreases and consequently causes the amplitude of surge voltage created on the tower top to decrease. Figure 6-15 shows the voltage stress on the insulator for conventional and compact lines for the lightning crest current of 100 kA that result in a back flashover in conventional line, but not in the compact line. This again demonstrating its superior performance of the proposed compact design in the face of lightning strikes.
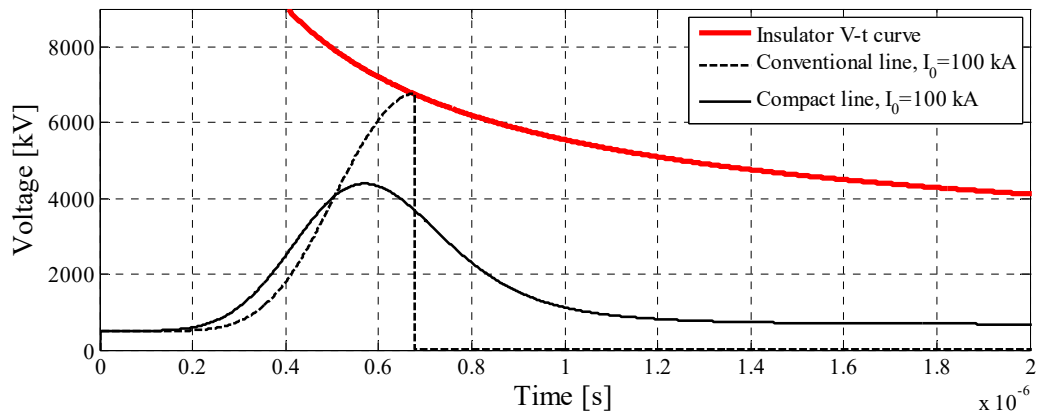
Figure 6-15 Insulator voltage for conventional and compact line when the lightning crest current is 100 kA

6.4.2.2. Impact of Shield Wires and Tower Height

In comparing compact and conventional designs, there are a number of variables that impact the generated voltage at the top of the tower, including the tower height and the number of shield wires. In other words, the compact design not only has shorter height that results in lower impedance and faster ground to tower top voltage reflections limiting tower top voltage build up, but also includes two shield wires. The shield wires provide more paths for current flow, therefore less current travels through the tower.

In order to consider only the impact of shield wires on back flashovers, this study was repeated for a conventional tower with two shield wires with the shielding angle of zero. Figure 6-16 shows that the minimum lightning current increases from 100 kA to 140 kA by using two shield wires in the latter design. Likewise, the study was also performed for the conventional lines with ±10% variations in their tower height. The impact of height on the minimum current for back flashover in the conventional design is shown in Figure 6-17.

These results show that using two shield wires decreases the chance of back flashover more

effectively than reducing the tower height by 10%.
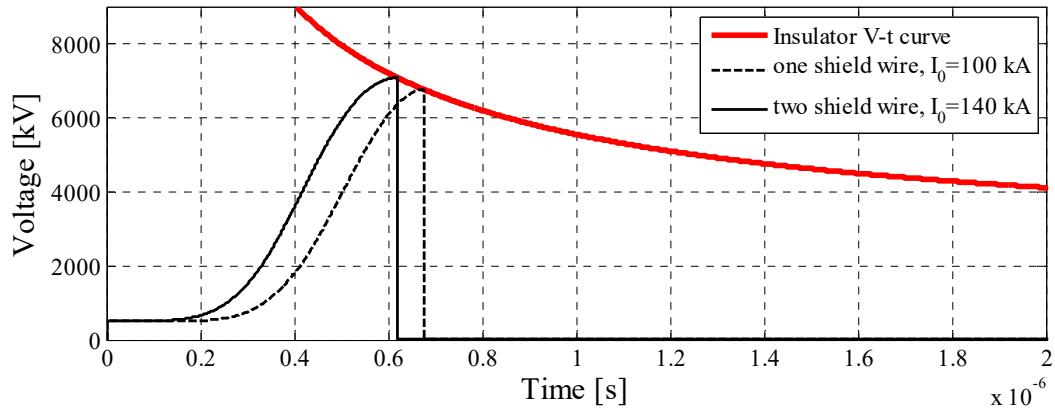
Figure 6-16 Minimum lightning currents that results in back flashover in conventional towers with one or two shield wires.
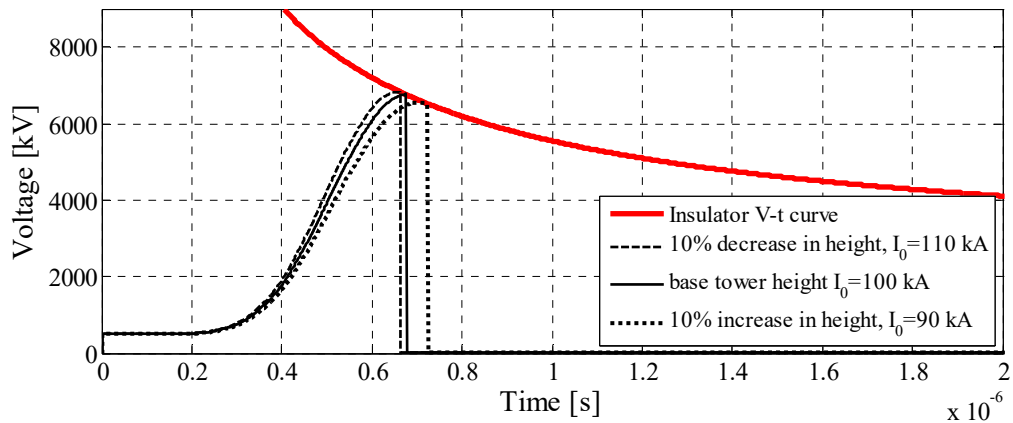
Figure 6-17 Minimum lightning currents that result in back flashover in conventional designs, ±10% variation in tower height

6.5   Conclusion

The lightning analysis of the low profile compact dc line, comparing to the conventional

line, was presented in this chapter. This study shows that:

- Compact transmission lines have a low profile and hence a smaller lightning shadow and are thus less prone to attract lightning strikes.

- It should be realized that as described in Chapter 3, the compact line has many more towers and hence more insulator strings. Although the probability of lightning induced flashover is reduced in the compact line for any individual insulator string, further reliability calculations should be conducted to investigate the corresponding fault risk considering the larger number of strings.

- Shielding angle and tower height are the main factors in maximum shielding failure current (I_{MSF}) calculations. Although there is a great variability in I_{MSF} among different electro-geometric lightning models, all of them showed that I_{MSF} increases with increase in the shielding angle and the conductor height.

- The most important parameter effecting back flashover rate is the impedance of the current path, including both the footing resistance and the tower structure impedance. Because smaller towers have lower overall impedance and shorter wave propagation travel times down the tower, compact transmission lines have less chance of back flashovers. Moreover, using two shield wires provides more paths for the current flow which will further increase the minimum lightning current required for the back flashover.

Chapter 7

Contributions, Conclusions and Future Research

This chapter presents the concluding remarks of this thesis, summarizes the main contributions, and provides a number of recommendations for future research in compact HVDC transmission.

7.1   Contributions

The main contributions of this thesis are as follows:

- Through a comprehensive literature review, the HVDC overhead transmission line design parameters and their interdependence were investigated to find out the components that have a major impact on the ROW width and tower height. Then, based on this discussion, a new compact dc overhead line was proposed.

- Detailed electromagnetic transient models of the MMC HVDC systems with two different transmission configurations (symmetrical monopole and bipole) and different transmission medium (purely overhead lines as well as the systems that

have both overhead lines and underground cables in the same circuit) were developed using PSCAD/EMTDC to perform electrical analysis of the proposed compact dc line.

- All the fault contingencies and associated overvoltages of those MMC HVDC systems were carried out using electromagnetic transients (EMT) simulation with the PSCAD/EMTDC software. A sensitivity analysis on the most important parameters, such as line length, fault time and location, etc., that may impact the magnitude and duration of overvoltages in the dc line has been also performed. The worst case scenario of each case, which is required for the insulation coordination of the dc line, was determined accordingly.

- A methodology for significantly reducing the dc overvoltage and consequently minimizing air clearances for maximum compaction was developed. This methodology uses a new control scheme for the MMC HVDC, which reduces pole-pole dc voltage, together with an appropriate arrangement of the dc line surge arresters.

- The lightning performance analysis of the proposed compact design was carried out with a focus on the evaluation of the critical lightning currents that results in fast front overvoltage stresses.

- In all the research steps, the results were compared with a conventional HVDC line design in order to assess the effectiveness and limitations of the proposed compact line design.

7.2   Conclusions

The thesis investigated the complex interdependencies of parameters affecting the behavior of compact dc lines. Compaction of HVDC overhead lines is achieved through reductions in tower height and required ROW width for a given power, voltage and conductor array so that it can improve the prospect of HVDC transmission siting on existing road, and rail ROW.

ROW width is driven by pole-to-pole spacing, conductor out-swing and lateral safety clearances. Tower height mainly consists of insulator length, conductor sag and minimum required ground clearance. It was shown in Chapter 3 that the parameters affecting tower height and ROW width are complex and interdependent. A number of design options that can serve to reduce both the height profile and ROW width requirements of dc lines and their relative effectiveness are shown in Table 3-4. In conclusion, the conductor sag was seen to be the principal factor affecting tower height for a given voltage and minimum ground clearance, and therefore also the major factor in conductor blow-out at high winds and the corresponding ROW width requirement. The main recourses for reducing sag are:

(1) Shortening spans, since sag is approximately proportional to the span length squared for a given conductor choice, stringing tension, electrical loading and weather context in a flat terrain.

(2) High-Temperature, Low Sag (HTLS) conductors which have a reduced sag for a given thermal loading.

The conductor surface voltage gradient is mainly a function of the number and diameter of sub conductors in the bundle and is much less affected by pole to pole spacing. Decreasing

pole to pole spacing can be compensated by marginally increasing the conductor size. However, an important factor in the pole to pole spacing of transmission lines is the required horizontal clearances between pole conductors and tower members, which depend on the maximum expected overvoltages on the dc line.

The main source of the slow-front overvoltages on MMC-HVDC transmission lines is the single dc pole to ground fault. The magnitude of these overvoltages depends primarily on the dc transmission system configuration. It was shown that in grounded bipole systems, the maximum peak value of slow front overvoltages are generally at most around 2.0 pu without any control actions or surge arresters; similar to the case for LCC HVDC systems. However these values in high resistance grounded symmetrical monopole configurations are about 3.0 pu, which is significantly larger than the grounded bipolar systems. In the high resistance grounded symmetrical monopole configuration, the peak overvoltage value on the unfaulted pole also depends on the damping ratio of the dc transmission line. As the damping ratio increases the voltage overshoot decreases. The damping ratio and the frequency of oscillations are a function of the system parameters such as line resistance, inductance and capacitance.

In dc lines with positive and negative poles, the line inductance and capacitance per unit length are a function of the distance between the conductor and a neutral and the conductor equivalent radius. Decreasing pole to neutral distance reduces the inductance and increases the capacitance of the line. Hence the capacitance to inductance ratio in the cable models is much larger than the transmission lines. Thus in dc transmission systems including cable, the voltage overshoot is generally less than in dc transmission systems with overhead lines. This also shows that reducing the pole to neutral spacing of the overhead lines decreases

the reactance and increases the capacitance of the dc line, which will result in a larger damping factor for transient overvoltages. Hence doing so can reduce slow front overvoltages, especially for symmetrical monopole configurations. In addition, as transmission line length increases the inductance and capacitance in the line increases. Therefore the system resonance frequency also decreases which increase the rise time of the voltage overshoot. In high resistance grounded symmetrical monopole systems, it is not possible to reduce these high overvoltages to below 2.0 pu just by using surge arresters without any further actions, since the pole to pole voltage remains constant at 2.0 pu. Hence, a modified control technique, which reduces pole to pole voltage, along with an appropriate fault detection method is required to minimize the overvoltage on the dc line and hence the required air clearances. The proposed control methods in this thesis can also reduce the required size of the surge arresters.

The study results showed that using larger values for the line smoothing reactors decreases the resonance frequency and hence delays the time of the voltage overshoot, which helps the controller system to reduce the overvoltage more effectively.

In the MMC with half-bridge sub-modules, the peak ac voltage cannot exceed the dc pole voltage. However the MMC with full-bridge sub-modules does not have this limitation. This feature of the full-bridge converters can be used to reduce the dc pole to pole voltage of the converter to essentially zero without impacting the ac side voltage. Although the dc voltage of half-bridge converters cannot be reduced as much as full-bridge converters, it can be reduced marginally to the point where the surge arresters reduce the excessive overvoltage. In each of these MMC-HVDC systems, it is possible to maintain partial power flow during temporary faults. However the alternative method of blocking the converter

and using ac breakers to protect the system will also result in power interruption for non-permanent faults.

Overhead transmission lines are subject to lightning strikes which are the main cause of fast front overvoltages that can cause flashovers and thus can also result in the disruption to power flows. Low profile transmission lines have smaller lightning shadow and are thus less prone to attracting lightning strikes. Increasing the conductor height also increases the maximum shielding failure current that eventually increases the chance of flashovers on the pole conductors.

The back flashover rate is mainly affected by the surge impedance of the current path, including the footing resistance as well as the tower structure and its height. It was shown that compact transmission lines have less chance of back flashovers due to their lower overall impedance and shorter wave propagation travel times down the tower. In addition, using two shield wires provides more paths for the current flow which will further increase the minimum lightning current required for the back flashover.

7.3   Recommendations for Future Research

Prior to this research, there was no comprehensive investigation on the methods for compaction of dc overhead lines. This thesis has created a foundation to make essential modifications in other aspects of dc line design that can help to maximize the compaction of the line while also enhancing the performance of the transmission system. Several recommendations for future work are listed below:

- From the civil engineering point of view, new low profile tower designs that are both economical and aesthetic.

- Developing a physical test line for further research on practical challenges of the compact dc line designs.

- Field measurements on the test line to assure the satisfaction in the field and corona performance of the line and also validate the results of software tools that predicts the ground level field effects.

- Performing a reliability study related to insulator requirements of the low profile compact transmission lines.

- Reassessment of criteria assigned to ground level field effect limits.

- Developing a multi-terminal, e.g. three- or four-terminal, dc grid model to investigate the overvoltages and fault clearing methods in a grid configuration.

Appendix A

An Approach to Find the Optimum Span Length Considering the Material and ROW Cost

The main capital cost components of any transmission line are conductor, tower and foundation material, labor cost, ROW clearance and access and also land used in some cases [47], [71]. Reducing the costs of minor items such as, conductor hardware, shield wires, dampers, etc. is not likely to result in any significant benefits for the total cost reduction [71].

In this approach, to find the optimum span length for a HVDC transmission line with a specific rated voltage and power, the cost is defined as a function of the span length. Since the details of the design are not available, a number of assumptions and reasonable approximations are considered as listed below:

1) Based on the electrical specification of the transmission line, such as rated voltage and power and field and corona effects, the conductor type and size is initially determined. Moreover, the minimum ground clearance of the conductor is also defined based on the standards. Therefore, conductor weight, *w*, and tension, *T,* are

assumed to be the same for all different tower designs. As expressed in equation 3.7, for a given conductor weight, w, and tension, T, sag is a function of the span length squared, i.e. $S = k \cdot l_s^2$, where $k = w/8T$, l_s is the span length, S is the conductor sag.

2) For this HVDC transmission line, a base tower is then designed which has a base span length l_{sb}, a base conductor sag, S_b, and a base tower height h_b. The tower cost including tower material, assembly and erection, foundation material and installation, is assumed to have a base value of P_b [*$/each*].

3) From this base case, the tower height variations (within a certain range considering the fixed minimum height requirement) are considered. This changes the sag and hence the span length, and thus impacts the numbers of towers required. It also affects conductor swing and hence the right of way (ROW) width. All these change the overall cost.

   Based on cost of towers of varying heights presented in [90], it is assumed that tower height variations will linearly change the required foundation and tower materials as well as the labor work for tower assembly and foundation structure. Therefore, based on the base case, the cost of each tower with height, h, is

$$P_t(h) = P_b + (h - h_b)P_{\Delta h} \quad [\$/each] \qquad\qquad \text{A.1}$$

   where $P_{\Delta h}$ [$/m] is the cost difference of the tower per meter. The impact of the wind loading on towers with different height is negligible here.

4) Shorter spans and less sag will reduce the required conductor length slightly. However, this difference is not a significant factor in overall cost vs. span [71].

Once a general tower top geometry is adopted and minimum horizontal and vertical con-

ductor clearances are specified, tower height and ROW width, as a function of sag and span

length, can be expressed as follows:

$$h(l_s) = H_{cnst} + S = H_{cnst} + k \cdot l_s^2 \qquad \text{A.2}$$

$$ROW(l_s) = Y_{cnst} + (2\sin(\phi)) \cdot S = Y_{cnst} + \beta \cdot l_s^2 \qquad \text{A.3}$$

where h is tower height, H_{cnst} is the height required for minimum ground clearance and

vertical distance between shield wire and the pole conductor, Y_{cnst} is the sum of the pole to

pole spacing and minimum horizontal clearances, ϕ is the conductor swing angle, and

$\beta = 2 \cdot k \cdot \sin(\phi)$.

The tower cost P_t, which is expressed in equation 3.6, can also be expressed as a function

of the span length for this specific design using equation 3.7:

$$P_t(l_s) = P_b + (k \cdot l_s^2 - S_b) \cdot P_{\Delta h} \quad [\$/each] \qquad \text{A.4}$$

Assuming the total overhead transmission line length is L, the number of towers used in

specific design of a point to point line is approximately $n = L/l_s$. Therefore the total tower

cost (*Towers_cost*) as a function of the span length is

$$TOWERS\_cost(l_s) = L \cdot [(P_b - S_b \cdot P_{\Delta h}) \cdot \frac{1}{l_s} + k \cdot P_{\Delta h} \cdot l_s] \qquad \text{A.5}$$

$$[\$/each]$$

The total cost of the land used is as follows if the unit price of the land is P_l [$\$/m^2$]

$$LAND(l_s) = (L \cdot ROW) \cdot P_l = L \cdot (Y_{cnst} + \beta \cdot l_s^2) \cdot P_l \qquad \text{A.6}$$

Therefore the total cost of the tower and the land is

$$COST\ (ls) = TOWER\ (ls) + LAND\ (ls)$$

$$COST(l_s) = a \cdot l_s^2 + b \cdot l_s + c \cdot \frac{1}{l_s} + d$$

Where   A.7

$$a = L \cdot \beta \cdot P_l$$
$$b = L \cdot k \cdot P_{\Delta h}$$
$$c = L \cdot (P_b - S \cdot P_{\Delta h})$$
$$d = L \cdot Y_{cnst} \cdot P_l$$

The minimum of this total cost function can be found by solving the first derivative of 3.16

as expressed in 3.17.

$$\frac{d(COST)}{dl_s} = a' \cdot l_s + b' + c' \cdot \frac{1}{l_s^2} = 0$$

$$a' = 2\beta \cdot P_l$$ A.8
$$b' = k \cdot P_{\Delta h}$$
$$c' = -P_b + S \cdot P_{\Delta h}$$

Hypothetically, the unit cost of this tubular base tower is \$150,000 for span length of 488

m, which is the optimum span length, without considering the land cost [90]. Based on

[90], the differences in the costs of towers with different heights is approximately \$3,000

per meter. Moreover, based on calculations in 1.2.1, it is assumed that the blow-out angles

for all different heights are 45^0. Figure A.1 shows the optimum span length as a function

of the land cost.
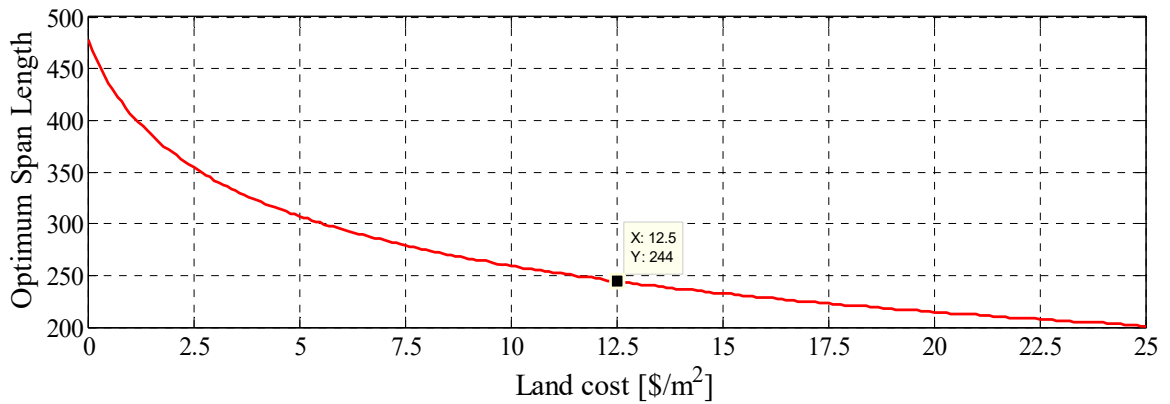
Figure A-1 Optimum Span length for different land costs

There is an additional less tangible cost factor representing the ROW permission and social

acceptance costs, also known as externalities of overhead lines [34], which is beyond the

scope of thesis. In some cases the land cost itself might not be significant; however, the

cost penalty associated with the failure to obtain ROW permission will clearly overwhelm

any difference in cost associated with shorter span designs, if they can facilitate to obtain

approval. Hence, it should be certainly considered separately and added to the above op-

timized cost.

Appendix B

Conductor Surface Gradient Calculation

The method of calculating the conductor surface electric field of transmission lines was first developed by Markt and Mengele. This method can be divided into two stages: the first stage consists of replacing each bundle by an equivalent single conductor (from the point of view of capacitance) and determining the total charge on each of them using the simple Maxwell potential coefficient method. The second stage consists of computing the electric field of the bundle, by assuming that it is located in free space, with the total charge obtained from the first stage distributed uniformly among the sub-conductors of the bundle. The details of these steps are as follows:

Step 1: Each conductor bundle is replaced by an equivalent conductor having a radius r_{eq} defined by:

$$r_{eq} = \left[n \cdot r \cdot A^{n-1} \right]^{1/n} \qquad\qquad \text{B.1}$$

where n is the number of the sub-conductors in the bundle, r is the sub-conductor radius and A is the bundle radius.

Step 2: The total charge on each of the equivalent conductors is calculated by the Maxwell

potential coefficient method, assuming appropriate potentials on the different poles. The

ground wires are also considered.

To do so, first assume the conductors are cylindrical and infinitely long with the radius of

$r_1, r_2, ..., r_n$. They are placed parallel to each other and the ground at the height of $h_1, h_2,$

..., h_n above the ground plane. The coordinates of the centers of each conductor with the

reference to an arbitrary coordinate system are $(x_1, y_1), (x_2, y_2), ..., (x_n, y_n)$ as shown in

Figure B.1. Assume further that $U_1, U_2, .., U_n$ are the voltages applied to the conductors

and $\lambda_1, \lambda_1, ..., \lambda_n$ are the line charges at the centers of the n conductors.
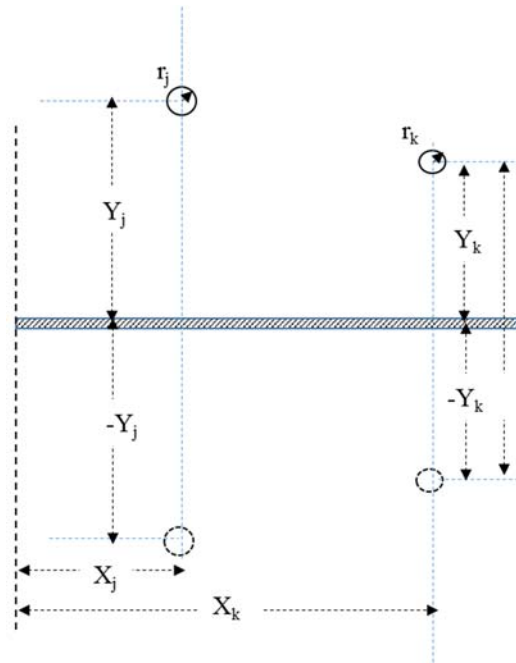
Figure B.1 Multi conductor Line configuration

Following the theory of the images, the ground plane can be replaced by the image of the

conductors. Then the line charges can be obtained from the known conductor potentials by

solving the following matrix equation:

$$[P][\lambda]=[U]$$

<div align="right">B.2</div>

where $[U]$ and $[\lambda]$ are the vectors of the potentials and line charges of the conductors

and $[P]$ is the $n \times n$ square Maxwell potential coefficient matrix, whose elements are given

by:

$$P_{kk} = \frac{1}{2\pi\varepsilon_0}\ln\frac{2h_k}{r_k} \qquad k = 1,2,...,n$$

<div align="right">B.3</div>

$$P_{km} = \frac{1}{2\pi\varepsilon_0}\ln\frac{2D_{km}}{d_{km}} \qquad k,m = 1,2,...,n \ \ k \neq m$$

where $D_{km} = \sqrt{(x_k - x_m)^2 + (y_k + y_m)^2}$ and $d_{km} = \sqrt{(x_k - x_m)^2 + (y_k - y_m)^2}$. In B.3

P_{kk} and P_{km} are the diagonal and off diagonal elements of $[P]$.

Step 3: Knowing the total charge on the bundle $[\lambda]$ from the preceding step, the average

bundle gradient is calculated as:

$$E_{av} = \frac{q_t}{2\pi\varepsilon_0} \cdot \frac{1}{nr}$$

<div align="right">B.4</div>

Step 4: The average maximum bundle conductor gradient is then obtained as:

$$E_m = E_{av}\left[1 + (n-1)\frac{r}{A}\right]$$

<div align="right">B.5</div>

Appendix C

Overview of Transmission Line Modeling

An overview of each modeling method [111] is provided here. Note that the detailed mathematical procedure of frequency dependent transmission line modeling is complicated and will not be discussed here.

- π-section model [111]

  The π-section model basically lumps the series-impedance and shunt-admittance of the transmission line. The total shunt-admittance is then divided in half and located at each end of the circuit with the series-impedance between the two ends to form the equivalent circuit, which is referred to as a π-section. This model is mostly a proper representation of the line when the wave propagation travel time is smaller than the simulation time step; therefore, it can only be suitable for very short lines. Moreover, it can be used correctly for the fundamental frequency, but cannot accurately represent other frequencies unless many sections are used, which is generally inefficient [111].

- Bergeron Model [111]

  The Bergeron model is based on travelling wave theory. It is a progression of the simple π-model, which represents the distributed inductance and capacitance of the circuit by

using an infinite number of series-connected π-sections. The line resistance is lumped, with a quarter of the resistance connected at the line terminations and half of the total resistance connected in the middle of the line. The Bergeron model does not consider the frequency dependence of the line's parameters arising from ground and conductor skin effects, and is therefore precise only at one frequency and therefore is suitable for studies where a single specified frequency is important. Thus its use in harmonics and fault transient studies will lead to approximation errors [111].

- Frequency Dependent Mode Model (FDMM) [112]

  Time domain equivalent circuit expressions for the Bergeron model can be solved in a relatively straightforward way, whereas these expressions for frequency dependent models are almost impossible to solve directly in time domain. Therefore, converting to frequency domain can facilitate to practically derive the solutions for each given frequency [112].

  FDMM technique can be described by considering the second derivative of the wave equations 4.9 and 4.10, as follows:

$$\frac{d^2V}{dx^2} = Z \cdot Y \cdot V \qquad\qquad\qquad \text{C.1}$$

$$\frac{d^2I}{dx^2} = Y \cdot Z \cdot I \qquad\qquad\qquad \text{C.2}$$

For multi-phase systems with n conductors, the voltage, V, and current, I, are n dimensional vectors. Z and Y are also $n \times n$ matrices for the series impedance and shunt admittance per unit length of the line respectively. Thus, it shows equations 4.11 and 4.12 each contain n mutually coupled equations.

By means of the modal analysis method, these mutually coupled equations in the phase domain can be transformed to decoupled linear equations in the modal domain, which allows them to be solved as several independent single modes. Each mode is then treated as a single-phase circuit. In terms of a system matrix, this means that the *YZ* and *ZY* matrices become diagonal, where all off-diagonal elements are zero.

To do so, constant modal transformation matrices, T_I and T_V, which is also frequency dependent, can be used to make the *YZ* and ZY matrices diagonalizable as

$$T_I^{-1} \cdot YZ \cdot T_I = D_{YZ} \qquad \text{C.3}$$

$$T_V^{-1} \cdot ZY \cdot T_V = D_{ZY} \qquad \text{C.4}$$

where D_{YZ} and D_{ZY} are the diagonal matrices whose diagonal elements are the eigenvalues of *YZ* and *ZY* respectively.

There are typically two main modes; the ground mode (also known as zero-sequence mode) and the metallic modes (similar to the *positive* and *negative* sequence modes). Each mode in unbalanced transmission lines has different characteristic impedance and travel time. The ground mode usually has larger characteristic impedance and resistance and a longer travel time than the metallic modes. FDMM is accurate only for geometrically balanced transmission systems, such as ideally transposed circuits, single conductors or any other systems where a naturally occurring constant modal transformation matrix can be derived. Therefore, it is often not reliable to accurately simulate systems with unbalanced line geometry.

- **Frequency Dependent Phase Model (FDPM) [113]**

  FDPM methods offer solutions for the voltage and current equations formulated directly in the phase domain without diagonalization in order to eliminate the problems associated with the frequency dependent transformation matrix for unbalanced systems [113]. For an *n*-phase transmission line, the solution of the traveling wave equations 4.9 and 4.10 can be derived directly in the frequency domain, as expressed in the following equations at each end-of the line:

$$I_k = Y_c V_k - A(Y_c V_m + I_m) \qquad\qquad \text{C.5}$$

$$I_m = Y_c V_m - A(Y_c V_k + I_k) \qquad\qquad \text{C.6}$$

  where *'k'* and *'m'* indicate sending-end and receiving-end of the line, *V* and *I* are *n* dimensional voltage and current vectors respectively. The $n \times n$ characteristic admittance matrix, Y_c, and the propagation matrix, *A,* are calculated as:

$$Y_c = \sqrt{(YZ)^{-1}} \cdot Y \qquad\qquad \text{C.7}$$

$$A = e^{-\sqrt{YZ}\,l} \qquad\qquad \text{C.8}$$

  where *Y* and *Z* are $n \times n$ shunt admittance and series impedance matrices per unit length of the line respectively. Finally in order to solve the transmission line in the time domain, the Y_c and *A* are approximated using an efficient robust technique for rational fitting of frequency-domain responses called *Vector Fitting*. In this curve fitting process, a set of frequency domain response points are considered first, then this data is fitted with a low order, rational function approximation of suitable orders that can be expressed as follows.

$$A_{i,j}(s) = \sum_{m=1}^{N_g} (\sum_{p=1}^{N} \frac{c_{p,m}}{s - a_{p,m}}) \cdot e^{-s\tau}$$ C.9

$$Yc_{i,j}(s) = \sum_{q=1}^{M} \frac{c_q}{s - a_q} + d$$ C.10

where all the coefficient are calculated by the Vector Fitting method, and the time delay

(τ) is estimated before the fitting procedure. These forms then are converted into differ-

ential equations and finally are numerically solved. For most practical transient simula-

tion studies, it is sufficient to consider frequencies from zero or near zero Hz to 1 MHz

for the fitting procedure.

Bibliography

[1]   L. R. Christensen and W. H. Greene, "Economies of Scale in U.S. Electric Power Generation," *The Journal of Poletical Economy,* vol. 84, no. 4, pp. 655-676, Agu., 1976.

[2]   L. O. Barthold, D. A. Woodford and M. Salimi, "DC Is Where We Started: Is It Also Where We are Going?," *IEEE Power and Energy Magazine,* vol. 14, no. 2, pp. 112-110, 2016.

[3]   M. Bladh, Electric Stories: Contributions to the history of electricity in Sweden, Linköping University Electronic Press, 2011.

[4]   J. Molburg, J. Kavicky and K. Picel, "The Design, Construction and Operation of High-Distance High-Voltage Electricity Transmission Technologies," Argonne National Laboratory, Argonne, Illinois, Nov. 2007.

[5]   H. Martensson, "History of High Voltage D. C. Transmission," *IEEE Power Engineering Review,* Vols. PER-4, no. 7, pp. 16-17, 1984.

[6]   A. M. Nekrasov and A. V. Posse, "Work Done in the Soviet Union on High-Voltage Long-Distance D-C Power Transmission," *Transactions of the American Institute of Electrical Engineers. Part III: Power Apparatus and Systems,* vol. 78, no. 3, pp. 515-521, 1959.

[7]   F. J. Ellert and N. G. Hingorani, " HVDC for the long run: High-voltage de transmission may be a viable alternative to ac transmission for long-distance routes," *IEEE Spectrum,* vol. 13, no. 8, pp. 37-44, Aug. 1976.

[8]   P. Esmeraldo, E. Araújo and D. Carvalho, "HVDC Madeira Transmission System – Planning Development and Final Design," in *CIGRÉ*, Paris, 2010.

[9]   "ABB Review Special Report," ABB Group R&D and Technology, Zurich, Switzerland, July 2014.

[10]   "HVDC Light, It's time to connect," ABB Grid Systems - HVDC, Ludvika, Sweden, December 2012.

[11]   "High Voltage Direct Current Transmission – Proven Technology for Power Exchange," Siemens AG, Energy Sector, Erlangen, Germany, 2011.

[12]   B. R. Andersen, "HVDC transmission-opportunities and challenges," in *The 8th IEE International Conference on AC and DC Power Transmission, 2006. ACDC 2006*, London, UK, March 2006.

[13]   B. Andersen, "The Path towards HVDC Grids," *ELECTRA,* vol. 14, no. 275, August 2014.

[14] M. MacLeod, M. Callavik, B. M., M. Dhesi, R. Huuva and F. Schettler, "A Technological Roadmap for the Development of the European Supergrid," in *CIGRÉ B4 Symposium*, Lund, Sweden, May, 2015.

[15] J. McCalley, W. Jewell, T. Mount, D. Osborn and J. Fleeman, "A Wider Horizon," *IEEE Power and Energy Magazine,* vol. 9, no. 3, pp. 42 - 54, 2011.

[16] D. Osborn, "Frequency Response, Load, Wind and Solar Diversity HVDC Network Sketch," MISO Policy and Economic Studies, June, 2013 .

[17] D. Osborn, "Potential value of HVDC overlays to provide a more reliable and economical power system," in *2011 IEEE Power and Energy Society General Meeting*, San Diego, CA, 2011.

[18] S. G. Johansson, G. Asplund, E. Jansson and R. Rudervall, "Power System Stability Benefits withVSC DC-Transmission Systems," in *CIGRÉ*, Paris, France, 2004.

[19] "List of major power outages," Wikipedia, Available: https://en.wikipedia.org/wiki/List_of_major_power_outages.

[20] M. Hayden, C. Hébert and S. Tierney, "Cybersecurity and the North American Electric Grid," Bipartisan Policy Center, Washington, DC, February 2014.

[21] Z. Zhou, "Co-ordination of Converter Controls and an Analysis of Converter Operating Limits in VSC-HVdc Grids," University of Manitoba, Winnipeg, Manitoba, Canada, 2013.

[22] O. Saksvik, "HVDC technology and Smart Grid.," in *9th IET International Conference onAdvances in Power System Control, Operation and Management (APSCOM 2012)*, Hong Kong, 2012.

[23] J. W. Feltes, B. D. Gemmell and D. Retzmann, "From Smart Grid to Super Grid: Solutions with HVDC and FACTS for grid access of renewable energy sources," in *2011 IEEE Power and Energy Society General Meeting*, San Diego, CA, 2011.

[24] M. Häusler, "Multiterminal HVDC for High Power Transmission in Europe," in *CEPEX99, Poznan*, Poland, 1999.

[25] B. Jacobson, "Developments in Multiterminal HVDC," in *IEEE EPEC 2011* , Winnipeg, Manitona, Canada, 2011.

[26] N. Flourentzou, V. Agelidis and G. Demetriades, "VSC-Based HVDC Power Transmission Systems: An Overview," *IEEE Transactions on Power Electronics,* vol. 24, no. 3, pp. 592-602, March 2009.

[27] R. Sellick and M. Åkerberg, "Comparison of HVDC Light (VSC) and HVDC Classic (LCC) site aspects, for a 500MW 400kV HVDC transmission scheme," in *10th IET International Conference onAC and DC Power Transmission (ACDC 2012)*, Birmingham, UK, Dec. 2012.

[28] CIGRÉ Working Group B4.52, "HVDC Grid Feasibility Study," CIGRÉ Technical Brochure 533, April 2013.

[29] CIGRÉ Working Group B4.57, "Guide for the Development of Models for HVDC Converters in a HVDC Grid," CIGRÉ Technical Brochure 604, December 2014.

[30] J. Sneath, "Grounded HVDC Grid Line Fault Protection Using Rate of Change of Voltage and Hybrid DC Breakers," University of Manitoba, Winnipeg, Manitoba, Canada, 2014.

[31] J. Häfner and B. Jacobson, "Proactive Hybrid HVDC Breakers - A key innovation for reliable," in *CIGRÉ* , Bologna, 2011.

[32] M. Saeedifard, M. Graovac, R. F. Dias and a. R. Iravani, "DC power systems: Challenges and opportunities," in *IEEE Power Energy Soc. General Meeting*, Minneapolis, Jul. 2010.

[33] J. Häfner and B. Jacobson, "Proactive Hybrid HVDC Breakers - A key innovation for reliable HVDC grids," in *CIGRÉ symposium*, Bologna, 2011.

[34] CIGRÉ Working Group C3.08, Externalities of Overhead High Voltage Power Lines, CIGRÉ Technical Brochure 616, April 2015.

[35] "List of HVDC projects," Wikipedia, 2016.
Available: https://en.wikipedia.org/wiki/List_of_HVDC_projects.

[36] "Overhead vs. Underground Information about Undergrounding High-Voltage Transmission Lines," Xcel Energy Inc., Colorado, 2011.

[37] E. C. Bascom and V. D. Antoniello, "Underground Power Cable Considerations: Alternatives to Overhead," in *47th Minnesota Power Systems Conference (MIPSYCON)* , Minnesota , November 2013.

[38] P. S. Maruvada, Corona Performance of High-Voltage Transmission Lines, Baldock, Hertfordshire, England,: Research Studies Press Ltd., 2000.

[39] "Clean Energy Projects; Requirements for Planning, Design and Construction to Protect Forest Roads or Timber Tenures," Ministry of Forests, Lands and Natural Resource Operations, British Colombia, 2013.

[40] "Aesthetic Tower Design Helps Danish Grid Operator Obtain Approvals for Important New 400 kV Line," *Independent T&D Information Resources (INMR),* October 2015.

[41] https://yougov.co.uk/news/2015/04/17/pylons/ .

[42] M. Salimi, L. Barthold, D. Woodford and A. Gole, "Prospects for Compaction of HVDC Transmission Lines," in *CIGRÉ,* Montreal, Canada, 2016.

[43] E. Bystrup, "Public Acceptance," in *3rd European Grid Conference, Royal Museum of Art and History*, Brussels, Belguim, December 2013.

[44] CIGRÉ Joing Working Group B4/C3/B2.5, "Electric Field and Ion Current Environment of HVDC overhead Transmission Lines," CIGRÉ Technical Brochure 473, August 2011.

[45] CIGRÉ Working Group 22-06, "Tower Top Geometry," CIGRÉ Technical Brochure 48, June 1995.

[46] CIGRÉ Working Group B4.37, "VSC Transmission," CIGRÉ Brochure 269, April 2005.

[47] CIGRÉ Join Working Group B2/B4/C.17, "Impacts of HVDC Lines on the Economics of HVDC Projects," CIGRÉ Technical Brochure 388, August 2009.

[48] T. Jonsson, P. Lundberg, S. Maiti and Y. Jiang-Häfner, "Converter Technologies and Functional Requirements for Reliable and Economical HVDC Grid Design," in *CIGRÉ Canada*, Calgary, September 2013.

[49] "IEEE Guide for Improving the Lightning Performance of Transmission Lines," IEEE Std 1243-1997, 1997.

[50] CIGRÉ Working Group 33.01, "Guide to procedures for estimating the lightning performance of transmission line," Technical Brochure no. 63, 1991.

[51] C. Adamson and N. G. Hingorani, High voltage direct current power transmission, London: Garraway, 1960.

[52] "HVDC Classic - Reference list Thyristor valve projects and upgrades," ABB AB Grid Systems - HVDC, Ludvika, Sweden, 2012.

[53] J. Arrillaga, High Voltage Direct Current Transmission, IEE Power and Energy series , 1998.

[54] K. Sadek, M. Pereira, D. P. Brandt, A. M. Gole and A. Daneshpooy, "Capacitor commutated converter circuit configurations for DC transmission," *EEE Transactions on Power Delivery,* vol. 13, no. 4, pp. 1257-1264, Oct 1998.

[55] CIGRÉ Join Working Group C4/B4/C1.604, "Influence of Embedded HVDC Transmission on System Security and AC Network Performance," CIGRÉ Technical Brochure 536, April 2013.

[56] F. Schettler, E. G. Siemens AG, H. Huang and N. Christl, "HVDC transmission systems using voltage sourced converters design and applications," in *Power Engineering Society Summer Meeting, 2000. IEEE* , Seattle, WA, 2000.

[57] N. Flourentzou, V. G. Agelidis and G. D. Demetriades, "VSC-Based HVDC Power Transmission Systems: An Overview," *IEEE Transactions on Power Electronics,* vol. 24, no. 3, pp. 592-602, March 2009.

[58] J. Holtz, "Pulsewidth modulation for electronic power conversion," *Proceedings of the IEEE,* vol. 82, no. 8, pp. 1194-1214, Aug 1994.

[59] C. Schauder and H. Mehta, "Vector analysis and control of advanced static VAr compensators," *IEE Proceedings C - Generation, Transmission and Distribution,* vol. 140, no. 4, pp. 299-306, July 1993.

[60] "VSC HVDC for Power Transmission – Economic Aspects and Comparison with other AC and DC Technologies," CIGRÉ Technical Brochure 492,, April 2012.

[61] CIGRÉ Working Group 14.03, "DC Side Harmonics and Filtering in HVDC Transmission Systems," CIGRÉ Technical Brouchure 92.

[62] M. Salimi, X. Chen, D. Woodford and A. Gole, "Fast Reduction of DC Voltage for Half-Bridge MMC HVDC Systems with Symmetrical Monopole during the Nonpermanent Pole to Earth DC Fault," in *CIGRÉ Symposium* , Lund, Sweden, May 2015.

[63] P. McGarry, "Bipole III Transmission Project: Ground Electrode Facilities," Manitoba Hydro, Winnipeg, Canada, March 2011.

[64] L. Brand, R. d. Silva, E. Bebbington and K. Chilukuri, "Grid West Project HVDC Technology Review," EirGrid, December 2014.

[65] D. Woodford, "Symmetrical Monopole VSC Transmission," Electranix Corporation, Winnipeg, Canada, 2014.

[66] A. Gustafsson, M. Saltzer, A. Farkas, H. Ghorbani, T. Quist and M. Jeroense, "The new 525 kV extruded HVDC cable system," ABB Grid Systems, Aug 2014.

[67] "Prysmian Group, P-Laser," Available:http://www.prysmiangroup.com/en/business_markets/markets/pd/downloads/brochures/P-Laser.pdf.

[68] "Bipole III Project; Chapter 3: Project Description," Manitoba Hydro Library, Winnipeg, Canada, 2013.

[69] HVDC Transmission Line Reference Book, 345 kV and Above/Second Edition, Palo Alto: Electric Power Research Institute (EPRI), 1982.

[70] CIGRÉ Working Group B2.51, "Guide to Overall Line Design," CIGRÉ Technical Brochure 638, December 2015.

[71] Overhead Conductor Manual, Carrallton, Goergia: SouthWire Company, 1994.

[72] The Planning, Design and Construction of Overhead Power Lines, Johannesburg, SA: Eskom, 2005.

[73] "Design Manual for High Voltage Transmission Lines," Bulletin 1724E-200, U.S. Department of Agriculture, May 2009.

[74] "Design Criteria of Overhead Transmission Lines," IEC/TR 60 826, 3rd edition, 2003.

[75] L. Barthold and H. Huang, "Conversion of AC Transmission Lines to HVDC using Current Modulation," in *IEEE Power Engineering Society Inaugural Conference and Exhibition*, Africa, 2005.

[76] CIGRÉ Working Group C4.303, "Outdoor Insulation in Polluted Conditions: Guidelines for Selection and Dimensioning, Part 2: The DC Case," CIGRÉ Technical Brochure 518, December 2012.

[77] X. Jiang, J. Yuan, L. Shu, Z. Zhang, J. Hu and F. Mao, "Comparison of DC Pollution Flashover Performances of Various Types of Porcelain, Glass, and Composite Insulators," *IEEE Transactions on Power Delivery,* vol. 23, no. 2, pp. 1183 - 1190, 2008.

[78] R. Matsuoka, J. Nagoya, H. Shinokubo, K. Kondo and Y. Mizuno, "Assessment of basic contamination withstand voltage characteristics of polymer insulators," *IEEE Transactions on Power Delivery ,* vol. 11, no. 4, pp. 1895 - 1900, 1996.

[79] "Polluted Insulators: A review of current knowledge," Technical Brochure 158, June 2000..

[80] F. Zhang, X. Wang, L. Wang and Z. Guan, "Effect of arcing on DC flashover performance of contaminated porcelain insulators for various suspension

patterns at high altitudes," *IEEE Transactions on Dielectrics and Electrical Insulation ,* vol. 15, no. 3, pp. 783 - 791, June 2008.

[81] "Insulation co-ordination – Part 5: Procedures for high-voltage direct current," IEC 60071-5, Ed. 1, 2014.

[82] S. Narain, V. Naidoo and R. Vajeth, "Upgrading the performance of the Apollo – Cahora Bassa 533kV links," in *CIGRÉ Session*, Paris, France, 2012.

[83] D. Wikström and C. Öhlen, "Composite Insulation for Reliability Centered Design of compact HVAC & HVDC," STRI, 2004.

[84] Z. Fuzeng, W. Xin, L. Biao, W. Liming and G. Zhicheng, "Influence of angles of V-strings on DC flashover characteristics of polluted insulators in high altitude areas," in *IEEE Conference on Electrical Insulation and Dielectric Phenomena*, Kansas City, MO, 2006.

[85] "IEEE Guide for the Application of Insulation Coordination," IEEE Std 1313.2-1999, June 1999.

[86] "IEEE guide for improving the lightning performance of transmission lines," IEEE Std 1243, 1997.

[87] C. Neumann, A. Wasserrab, G. Balzer, B. Rusek, S. Steevens and K. Kleinekorte, "Aspects of insulation coordination for DC links using hybrid lines," in *CIGRÉ-IEC Colloquium*, Montreal, Canada, 2015.

[88] "Design criteria of overhead transmission lines," IEC 60826, 2003.

[89] E. Thayer, Computing Tensions in Transmission Lines., Electrical World, Vol. 84., July 12, 1924.

[90] E. Ghannoum and Z. Kieloch, "Use of modern technologies and software to deliver efficient design and optimization of 1380 km long bipole III ±500 kV HVDC transmission line, Manitoba, Canada,," in *Transmission and Distribution Conference and Exposition (T&D), 2012 IEEE PES*, Orlando, FL, May 2012.

[91] Aluminum Electrical Conductor Handbook, 900, 19th Street, N.W., Washington, DC: The Aluminum Association, Third Edition, 1989.

[92] "High-Temperature, Low-Sag Transmission Conductors," EPRI, Palo Alto, CA, 2002.

[93] I. Zamora, A. J. Mazon, P. Eguia, R. Criado, C. Alonso, J. Iglesias and J. R. Saenz, "High-temperature conductors: a solution in the uprating of overhead transmission lines," in *IEEE Power Tech Proceedings*, Porto, 2001.

[94] G. Markt and B. Mengele, "Drehstromferntibertragung," *E und M,* vol. 20, pp. 293-298,, May 1932..

[95] W. J. Maruvada P. Sarma, "Electrostatic field of a system of parallel cylindrical conductors," *IEEE Trans. on Power Apparatus and Systems,* Vols. PAS-88, pp. 1069-1079, July 1969..

[96] S. P. Maruvada "Application of moment methods to the computation of electrostatic fields. Part I: Parallel cylindrical conductor systems," in *IEEE*, 1972 Conference paper No. C72 574-2.

[97] H. Singer, H. Stienbigler and P. Weiss, "A charge Simulation Method for the Calculation of High Voltage Fields," *IEEE Trans,* Vols. PAS-93, pp. 1660-1668, 1974.

[98] IEEE Radio Noise Working Group, "A Survey of Methods for Calculating Transmission Line Conductor Surface Voltage Gradients," *IEEE Transactions on Power Apparatus and Systems,* Vols. PAS-98, pp. 1996-2014, 1979.

[99] "Bipole III Transmission Project; Electromagnetic Fields (EMF) Technical Report," Inc., Exponent, November 2011.

[100] J. M. Charry, "Biological Effects of Air Ions: A Comperhansive Review of Laboratory and Clinical Data," *In J.M. Charry, R. Kavet, (editors), Air Ions: Physical and Biological Aspects, CRC Press, Boca Raton,* pp. 91-149, 1987.

[101] J. Blondin, D. Nguyen, J. Sbeghen, D. Goulet, C. Cardinal, P. Maruvada, M. Plante and W. Bailey, "Human Perception of Electric Fields and Ion Currents Associated With High-Voltage DC Transmission Lines," *Bioelectromagnetics,* vol. 17, pp. 230-241, 1996.

[102] CIGRÉ Join Working Group B4/C3/B2.50, "Electric Field and Ion Current Environment of HVDC Overhead Transmission Lines," CIGRÉ Technical Brochure 473, August 2011.

[103] U. Gnanarathna, A. Gole and R. Jayasinghe, "Efficient Modeling of Modular Multilevel HVDC Converters (MMC) on Electromagnetic Transient Simulation Programs," *IEEE Transactions on Power Delivery,* vol. 26, no. 1, pp. 316-324, Jan. 2011.

[104] J. Andres, M. P. de, J. Dorn, D. Retzmann and A. Zenkner, "Prospects of VSC Converters for Transmission System Enhancement," in *Presented at the PowerGrid Europe*, Madrid, Spain, Jun. 2007.

[105] C. Du, "VSC-HVDC for Industrial Power System," Ph.D. dissertation, Chalmers Uni-versity of Technology, G¨oteborg, Sweden, 2007.

[106] T. Nakajima and S. Irokawa, "A control system for HVDC transmission by voltage sourced converters," *IEEE Power Engineering Society Summer Meeting 1999 Proceedings,* vol. 2, pp. 1113-1119, 1999.

[107] Z. Zhou, "Co-ordination of Converter Controls and an Analysis of Converter Operating Limits in VSC-HVdc Grids," Ph.D. dissertation, The University of Manitoba, Winnipeg, Canada, 2013.

[108] A. Lesnicar and R. Marquardt, "An Innovative Modular Multilevel Converter Topology Suitable for a Wide Power Range," in *IEEE Power Tech Conf Proc.* , Bologna, Italy, Jun. 2003.

[109] U. N. Gnanarathna, A. M. Gole and a. S. K. Chaudhary, "Multilevel Modular Converter for VSC-HVDC Transmission Applications: Control and Operational Aspects," in *Proc. 16th National Power Systems Conf., NPSC 2010,*, Hyderabad, India, Dec. 2010, pp. 405-410..

[110] H. W. Dommel, "Digital Computer Solution of Electromagnetic Transients in Single and Multiphase Networks," *IEEE Transactions on Power Apparatus and Systems,* Vols. PAS-88, no. 4, pp. 388-399, April 1969.

[111] EMTDC manual, Winnipeg:: Manitoba HVDC Research Center,, 2003.

[112] J. R. Marti, "Accurate Modeling of Frequency Dependent Transmission Lines in Electromagnetic Transients Simulation," *IEEE Transactions on Power Apparatus and Systems,,* Vols. PAS-101, no. 1, pp. 147-155, Jan. 1982.

[113] B. Gustavsen, G. Irwin, R. Mangelrød, D. Brandt and K. Kent, "Transmission Line Models for the Simulation of Interaction Phenomena Between Parallel AC and DC Overhead Lines," IPST '99 Proceedings, pp. 61-67, 1999.

[114] R. Iravani and F. B. Ajaei, "Cable Surge Arrester Operation Due to Transient Overvoltages Under DC-Side Faults in the MMC–HVDC Link," *EEE Transactions on Power Delivery,* vol. 31, no. 3, pp. 1213-1222, June 2016.

[115] "National Electrical Safety Code 2007 Edition," IEEE Std C2-2007 , Aug. 1 2006.

[116] C. Neumann, A. Wasserrab, G. Balzer, B. Rusek, S. Steevens and K. Kleinekorte, "Aspects of insulation coordination for DC links using hybrid lines," in *2016 CIGRÉ-IEC Colloquium*, Montréal, QC, Canada, May, 2016.

[117] D. Ingemansson, J. D. Wheeler, N. M. MacLeod, F. Gallon and O. Ruiton, "The South — West scheme: A new HVAC and HVDC transmission system in Sweden," in *AC and DC Power Transmission (ACDC 2012), 10th IET International Conference on*, Birmingham, 2012.

[118] H. Saadat, Power System Analysis, PSA Publishing, 3rd edition, 2010.

[119] CIGRÉ Working Group B1.32, "Recommendations for Testing DC Extruded Cable Systems for Power Transmission at a Rated Voltage up to 500 kv," CIGRÉ Technical Brochure 496, April 2012.

[120] K. Steinfeld, R. Göhler and D. Pepper, "High Voltage Surge Arresters for Protection of Series Compensation and HVDC Converter Stations," in *The 4th International Conference on Power Transmission and Distribution Technology*, China, 2003.

[121] Q. Tu, Z. Xu and J. Zhang, "Circulating current suppressing controller in modular multilevel converter," in *Proc. 36th Annu. Conf. IEEE Industrial Electronics Society, IECON 2010,*, Glendale, AZ, 2010.

[122] CIGRÉ Working Group C4.407, "Lightning Parameters for Engineering Applications," CIGRÉ Technical Brochure no. 549, August 2013..

[123] R. B. Anderson and A. J. Eriksson., "Lightning parameters for engineering applica-tion Pretoria," Report ELEK 170, South Africa:CSIR, June, 1979.

[124] R. H. Golde, Lightning, New York: Academic Press, Vols 1 and 2, 1977.

[125] IEEE Working Group, "A simplified method for estimating lightning performance of transmission lines," *IEEE Trans. Power Appar. Syst.,* vol. 104, no. 4, p. 919–932, 1985.

[126] P.N.Mikropoulos, T.E Tsovilis "'Lightning attachment models and maximum shielding failure current: application to transmission lines," in *Proc. IEEE PowerTech, pp. 1–8*, Bu-charest, Romania, 2009.

[127] P.N.Mikropoulos, T.E Tsovili "Lightning attachment models and maximum shielding failure current of overhead transmission lines: implications in insulation coordination of substations. Generation," *Transmission Distribution, IET,* vol. 12, no. 4, p. 1299 – 1313, december 2010.

[128] D. Woodford, "Training Course and Workshop PSCAD/EMTDC," Electranix Corporation, Winnipeg, MB, Canada, 2007.

[129] W. R. Burrows and B. Kochtubajda, "Cloud to Ground Lightning in Canada 1999:2008," in *21st International Lightning Detect ion Conference*, Orlando, Florida, USA, April 2010.

[130] R. Silver, E. Orville and C. Alan, "Lightning Ground Flash Density in the Contiguous United States: 1992–95", Annual Summary," Cooperative Insti-tute for Applied Meteorological Studies and Department of Meteorology, Texas A&M University, College Station, Texas, April 1997.

[131] IEEE Working Group, "Estimating Lightning Performance of Tkansmission Lines II - Updates to Analytical Models," *IEEE Transactions on Power Delivery,,* vol. 8, no. 3, pp. 1254-1267, July 1993.

[132] E. Whitehead, Protection of transmission lines", Lightning, Vol. 2, Edited by R.H. Glode,, New York: : Acadamic Press, 1977, pp. 697-745 .

[133] A. J. Eriksson., "The incidence of lightning strikes to power lines," *IEEE Transactions on Power Delivery,,* vol. 2, no. 3, p. 859 –870, July 1987.

[134] EPRI HVDC Reference Book: Overhead Lines for HVDC Transmission, Technical Up-date, Palo Alto, CA: Electric Power Research Institute (EPRI), Inc, June 2008.

[135] C. F. Wagner, "A New Approach to the Calculation of the Lightning Performance of Transmission Lines," *AIEE Transactions on Power Apparatus and Systems,* vol. 75, p. 1233Ð1256, 1956.

[136] C. F. Wagner and A. and Hileman, "The Lightning Stroke-II," *IEE Transactions on Power Apparatus and Systems,* vol. 80, pp. 622-642, 1961.

[137] F.S. Young, J.M. Clayton, A.R. Hileman. "Shielding of transmission lines," *IEEE Trans. Power Appar. Syst.,* vol. 82, no. 4, p. 132–154, 1963.

[138] H.R. Armstrong, E.R. Whitehead, "Field and analytical studies of transmission line shielding," *IEEE Trans. Power Appar. Syst,* vol. 87, p. 270–281, 1968.

[139] G.W. Brown, E.R. Whitehead, "Field and analytical studies of transmission line shielding-II," *IEEE Trans. Power Appar. Syst,* vol. 88, p. 617–626, 1969.

[140] E.R. Love "Improvements in lightning strokemodeling and applications to design of EHV and UHV transmission lines," MSc dissertation, University of Colorado, Denver, CO, 1973.

[141] A. M. Mousa and K. D. Srivastava, "The Lightning Performance of Unshielded Steel-Structure Transmission Lines," *IEEE Transactions on Power Delivery,* vol. 4, pp. 437-445, 1989.

[142] A.J. Eriksson "An improved electrogeometric model for transmission line shielding analysis," *IEEE Trans. Power Deliv.,* vol. 2, no. 3, p. 871–886, 1987.

[143] D. R. Swatek and S. J. Shelemy, "Monte Carlo Simulation of Lightning Strikes to the Nelson River HVDC Transmission Lines," in *presented at the Int. Conf. Power Systems Transients (IPST)*, Brazil, Jun. 2001.

[144] Y. Han, L. Li, H. Chen and Y. Lu, "Influence of Modeling Methods on the Calculated Lightning Surge Overvoltages at a UHVDC Converter Station Due to Backflashover," *IEEE Transactions on Power Delivery,* vol. 27, no. 3, pp. 1090-1095, July 2012.